ON THE STABILIZATION OF ALUMINUM FOAMS BY TIN ADDITIONS AND IN SITU INTERMETALLIC FORMATION

Lydia Y. Aguirre Perales

Department of Mining and Materials Engineering

McGill University, Montreal, QC, Canada

August 2014

A thesis is submitted to McGill University in partial fulfillment of the

requirements of the degree of Doctor of Philosophy

Abstract

The powder metallurgy (PM) technique is one of the most promising means of producing metallic foams. In the case of Al foams, this technique requires the mixing of Al or Al-based alloy powders with a blowing agent (most commonly TiH_2) after which the mixture must be compacted to a high density to form a precursor. Heat-treating the precursor allows foam formation by simultaneously melting metal powders and releasing gas from blowing agent decomposition. Nevertheless, the mismatch between TiH_2's decomposition temperature (typically between 450–650 ^oC) and the melting point of Al or Al alloy (about 660 ^oC) the main drawback of this technique as it leads to the formation of crack-like pores and to hydrogen loss prior to foaming. In addition, if foaming occurs at an elevated temperature (~800 ^oC), it leads to problems such as pore coalescence, metal drainage and foam collapse.

The purpose of this study is to develop new Al alloys that when foamed will produce stable and highly expanding foams with superior mechanical properties.

In order to overcome the temperature mismatch between TiH_2's decomposition and Al's melting point, Al foam's chemistry was modified in this work by alloying it with small amounts of Sn ($\leq$ 5 wt.%). The roles of Sn in the foaming process of Al are found to be (i) improving integrity of the powder mixture during hot compaction due to Sn's low melting temperature, (ii) controlling of gradual decomposition of the TiH_2 and (iii) decreasing surface tension of liquid

Al, resulting in higher foam expansion even at lower foaming temperature (725 ^{o}C), and higher foam stability.

Foam expansion and stability were further controlled by in-situ formation of intermetallic phases. Thermodynamic calculations made using FactSage thermodynamic software were used extensively to design foam alloys, and the foam alloys were thermally analyzed to build an understanding of the selected alloys' evolution during the foaming process. Five alloying elements (Co, Mg, Mn, Ni and Ti) were selected to change the foaming behavior of Al-3wt.% Sn alloy. Alloys based on these were designed (i) to enhance foam expansion (reaching higher maximum expansion) and/or (ii) to stabilize the foam (regularizing pore size and distribution) by forming an intermetallic phase during the foaming process.

The mechanical properties of new Al-Sn based alloys are superior to conventional Al alloy foams. An improvement of energy absorption efficiency and capacity was observed with increasing amounts of alloying element (particularly at higher amounts of Ti, Mn or Ni). This is the result of the intermetallics formed by alloying elements in the cell walls. A model correlating stress-strain curves with the cell wall's fracture mode during compression testing was proposed.

Résumé

La technique de métallurgie des poudres (PM) s'est avéré être l'une des voies les plus prometteuses pour la production des mousses métalliques. Dans le cas des mousses d'aluminium, cette technique requiert le mélange d'Al ou de poudres d'alliages à base d'Al avec un agent moussant (le TiH_2 est le plus souvent utilisé) ; un précurseur est ensuite formé par la compaction du mélange à haute densité. Le traitement thermique du dit précurseur permet la formation de mousse par fusion simultanée des poudres métalliques et la libération de gaz provenant de la décomposition de l'agent moussant. Néanmoins, la disparité entre la température de décomposition de TiH_2 (généralement entre 450-650 °C) et le point de fusion d'Al ou d'alliage d'Al (environ 660 °C) sont les principaux inconvénients de cette technique, car ils conduisent au craquement de pores et à la perte d'hydrogène avant le moussage. De plus, si la formation de mousse se produit à une température élevée (~800 °C), d'autres problèmes tels que la coalescence des pores, le drainage du métal et l'écroulement de la mousse peuvent se produire.

L'objectif de cette étude est de développer des nouveaux alliages moussants à base d'aluminium susceptibles de doter la mousse d'une plus grande stabilité et expansion ainsi que des propriétés mécaniques supérieures.

Afin de pallier les différences entre la température de décomposition et celle de fusion, la chimie des mousses d'Al a été modifiée dans la présente recherche, en introduisant de petites quantités de Sn ($\leq$ 5% en poids).

Les rôles de Sn dans le processus de moussage d'Al sont (i) l'amélioration de l'intégrité du mélange de poudre pendant la compaction à chaud de Sn, compte tenue de sa faible température de fusion, (ii) le contrôle de la décomposition progressive du TiH_2 et (iii) l'amélioration de la tension superficielle d'Al liquide, ayant pour conséquence un plus haut niveau de contrôle de l'expansion, ainsi qu'une meilleure stabilité de la mousse, même sous une basse température de moussage (725 ° C).

L'expansion et la stabilité de la mousse sont plus contrôlées par la formation in-situ de phases intermétalliques. Les calculs thermodynamiques utilisant le logiciel thermodynamique FactSage ont été largement utilisés pour la conception d'alliages, et des analyses thermiques d'alliages ont été réalisées afin de comprendre l'évolution des alliages sélectionnés pendant le processus de moussage. Cinq éléments d'alliage (Co, Mg, Mn, Ni et Ti) ont été sélectionnés dans le but de changer le comportement de moussage d'Al-3% poids Sn. Ces alliages ont été conçus (i) pour améliorer l'expansion de la mousse (en atteignant une expansion maximale plus élevée) et/ou (ii) pour stabiliser la mousse (uniformisation de la taille et de la distribution des pores) par la formation des phases intermétalliques durant le processus de moussage.

Les propriétés mécaniques des nouveaux alliages à base d'Al-Sn sont supérieures à celles des mousses classiques d'alliage d'Al. L'amélioration de l'efficacité et de la capacité d'absorption d'énergie a été observée suite à une augmentation de quantité d'élément d'alliage (en particulier à de plus grandes quantités de Ti, Mn ou Ni). Ceci en résulte des composés intermétalliques formés par les éléments

d’alliage dans les parois cellulaires. Un modèle corrélant les courbes contrainte-déformation avec le mode de fracture de la paroi cellulaire au cours du test de compression a été proposé.

A mis padres, Marco y Lidia, bajo su ejemplo he forjado mi camino.

A Issam, por ser mi cómplice en esta aventura.

A Dante, eres la luz de mi vida.

ACKNOWLEDGEMENTS

I wish to acknowledge CONACyT (Consejo Nacional de Ciencia y Tecnología) Mexico for awarding me the scholarship that gave me the opportunity to pursue graduate studies. I would also like to acknowledge GM (General Motors), FQRNT (Fond Québécois de la Recherche sur la Nature et les Technologies), and NSERC (Natural Science and Engineering Research Council) in Canada, and KIM (Korean Institute of Metals) in Korea for their financial support.

I am deeply grateful to my thesis directors. Prof. Robin A. L. Drew introduced me to the world of foams, a subject which has become a passion for me. His support, modesty, and the generous way he shares his extensive knowledge have undoubtedly shaped both my skills and my taste for research. I thank Prof. In-Ho Jung, for his deep knowledge, excellent leadership and unwavering support throughout my doctoral studies. His unique way of seeing things, attention to detail, availability, and generosity have forever shaped me. Thank you Prof. Jung for all the education and guidance you have given me! It has been a great pleasure to have you as a supervisor during my studies.

I want to thank my colleagues on the foaming team, my officemates, and the high-temperature thermo chemistry group for making my stay at McGill an extraordinary experience and for their assistance at every step. Special thanks to my friends Javier Tavitas, Ramona Vintila, Deniz Aydin, Manas Paliwal, Paula

Proa and Yaneth Aguilar for their encouragement and support through all these years.

This research would not have been possible without the McGill staff and the doctoral program's management team, who helped me orient myself and have been essential to my academic journey. They welcomed me into their offices and laboratories, and showed me how things work.

Finally, I would like to express my deepest gratitude to my family, and especially to my son Dante. Thank you for your patience and love.

TABLE OF CONTENTS

LIST OF FIGURES

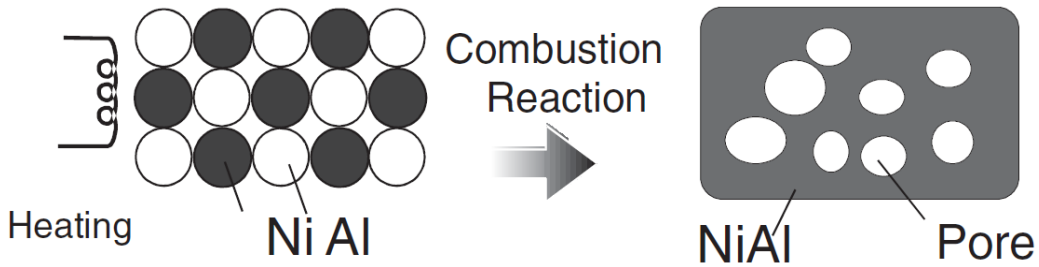

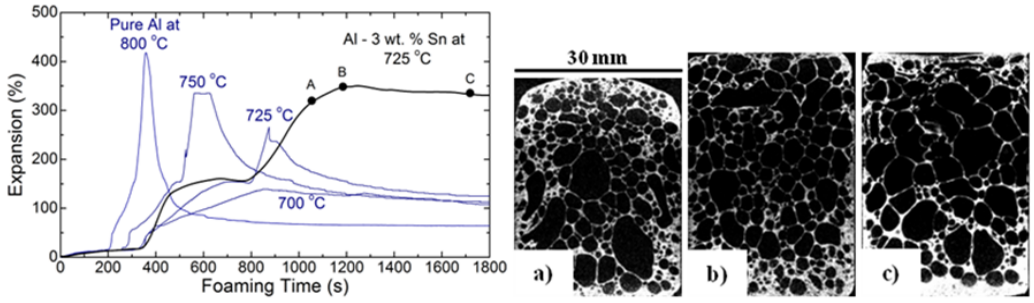

Figure 6.5: Expandometer curves for pure Al recorded at different foaming temperatures (800, 750, 725 and 700 ^{o}C) and Al–3wt.%Sn alloy foamed at 725

LIST OF TABLES

PREFACE

Contribution of Authors

This doctoral thesis is a collection of four sequential manuscripts. The first three manuscripts have already been published, while the last one has been submitted and is currently under consideration for publication. The references and logical sequence is as follows:

1. L. Y. Aguirre-Perales, I.-H. Jung, R. A. L. Drew, **"Foaming behavior of powder metallurgical Al–Sn foams"**, Acta Materialia. 2012; 60: 759-69.

2. L. Y. Aguirre-Perales, I.-H. Jung, R. A. L. Drew, **"Effect of Sn on the Dehydrogenation Process of TiH_2 in Al Foams"**, Metallurgical and Materials Transactions A. 2012;43:1-5.

3. L. Y. Aguirre-Perales, R. A. L. Drew, I.-H. Jung, **"The effect of in-situ intermetallic formation on Al-Sn foaming behavior"**, Metall. Mater. Trans. A, 2014:45:3714-3727

4. L. Y. Aguirre-Perales, Robin A. L. Drew, In-Ho Jung, **"Effect of Intermetallics on the Mechanical Behavior of Al-Sn Foams"**, submitted to Materials & Design Special Issue on "Lightweight Materials and Structural Solutions for Transport Applications". 2014.

All manuscripts were written by the candidate with the supervision, advice and revision of Prof. I-H. Jung and Prof. R. A. L. Drew.

The PhD candidate performed alloy selection using thermodynamic calculations for the first 3 manuscripts under the supervision of Prof. I-H. Jung.

The PhD candidate performed all experimental work on mixing, compaction and foaming either in a box furnace or in a mechanical expandometer.

Samples were prepared for scanning electron microscope by the PhD candidate, including mounting, polishing and image editing with Adobe® Photoshop® CS software for image analysis.

Non-destructive tests using the Skyscan 1172 scanner, including Skyscan™ CT-analyzer software, were all performed by the PhD candidate.

The PhD candidate performed compaction testing using an MTS compression machine under the supervision of Dr. P. Vo.

Prof. I-H. Jung and Prof. R. A. L. Drew contributed to the analysis and participated in extensive discussions.

Contribution to Original Knowledge

The powder metallurgy technique in the production of Al foams has been addressed in other works in different manners with the aim of reducing the mismatch between the blowing agent's decomposition temperature and the Al matrix's melting temperature. However, these attempts have only achieved limited foam stability.

The research done for this project has studied modifying Al foaming by alloying it with small amounts of Sn. Furthermore, tailoring of foaming characteristics and mechanical properties were examined by adding alloying elements that generated in-situ intermetallics.

The following points, derived from the information obtained in this study, are deemed to be contributions to original knowledge:

1. Al foaming was modified by the addition of small amounts of Sn. For the first time, Al foam stability was attained at about 300% expansion for more than 10 min.

2. TiH_2 decomposition was modified without heat treatment, coating or particle size selection of the powder prior to foaming. The Sn-rich liquid formation at low temperature allowed the gradual decomposition of TiH_2 prior to the melting of Al.

3. Sn additions improved foam stability by modifying Al surface tension, promoting energetically stable cell walls and the gradual decomposition of TiH_2.

4. A relationship between cell structure and expansion was proposed based on the derivative of the expansion curve. The optimum cell structure can be predicted using this method, particularly if foaming occurs in an expandometer. The foaming process at the optimum cell structure may be easily predicted and therefore interrupted.

5. A methodology for in-situ intermetallic formation during the foaming process was developed using the CALPHAD method. It is possible to predict the intermetallic phase type, amount, formation stage (during heating or cooling) and the amount of liquid present at any given temperature using this method. This information is essential to predicting the foaming process and further mechanical behaviour.

6. The foaming behaviour and stability of Al-3wt.%Sn was effectively controlled by adding an alloying element, forming in-situ intermetallic phases. The two typical plateaus on the expansion / time curve can be modified: the first plateau can be shortened due to the exothermic heat produced during the formation of the intermetallic phase, and the second can reach higher expansions, as the same exothermic heat will locally melt Al, promoting expansion. Alloying with 3wt.%Ni increased maximum expansion from 300% to 450% and maintained this expansion for 4 minutes.

7. Adding Sn improves the mechanical properties of Al foams. Furthermore, the foams' energy absorbtion capacity and efficiency can be controlled with intermetallics in the cell wall. In a metallic foam, increasing the amount of

intermetallics was found to promote the brittle bending of cell walls under compression. A model was proposed relating the amount and the type of intermetallic to the foams' compression behaviour.

8. Al-Sn-Mn foams showed great stability during the foaming process; their expansion was similar to that of the Al-3wt.%Sn base alloy, but with a shortened first plateau and homogeneous pore structure throughout foaming. Therefore, foam reproducibility and homogeneous mechanical properties can be achieved through easier process control that yields to homogeneous pore structure and cell wall thickness.

Chapter 1

Introduction

Industrial demand for metallic foams varies depending on their cell morphology: while structural applications require closed porosity, functional applications require open porosity [1]. Automotive, aerospace, building and even biomedical industries are mostly interested in structural applications, such as foams that can act as load bearing materials, whereas functional applications are used for filtering and separating, heat exchangers and cooling devices, acoustic control, etc.

Metallic foams are promising in a number of ways, but their multifunctional capabilities make them particularly attractive to the automotive industry. Increasing demands related to safety and environmental concerns have led car manufacturers to introduce safer, lighter, and greener vehicles. Metal foams can easily replace heavy parts, providing a high stiffness to weight ratio, reduced fuel consumption, diminish environmental impact, and provide safer vehicles for passengers in the event of an accident [2-4]. Foamed aluminum has been widely studied for its specific properties and possible applications in, for example, load-bearing components and energy absorbers [1, 5]. From a safety perspective, the automotive industry evaluates energy absorption capability as an impact behavior [6]. Filling components such as bumpers, crash boxes and A- and B- pillars with Al foam has been shown to improve these properties [3].

Even though the applications of metallic foam are continuously increasing, process shortfalls still exist. In the case of Al foaming using the powder metallurgy technique, the limits of its industrial applications are mainly based on process control. In the powder metallurgy technique, a mixture of Al and blowing agent powders (commonly TiH_2 in Al foaming) are compressed into a high-density precursor. This precursor is heat-treated at a temperature above the metal's melting temperature. As the temperature rises, the blowing agent decomposes, releasing gas that is trapped by the molten metal matrix, forming pores and cell walls. The resulting foam structure depends heavily on the time and temperature where the heat treatment is performed. The cell walls and overall foam structure change with the processing time. Once the heat treatment is interrupted, the metal solidifies and the foam is obtained [1]. Nevertheless, a mismatch between the blowing agent's decomposition temperature and the Al's melting point leads to problems such as pore coalescence, metal drainage, and ultimately foam collapse [7, 8]. In addition, Al foams expand during processing, reaching maximum expansion and collapse within a short time [9-11], leading to difficulties in foam reproducibility, which can be directly correlated to foam stability [12]. Foam stabilization in the powder metallurgy route was associated with the presence of solid oxide networks [13]. These oxides are naturally found covering the Al powders, but with additional heat treatments, they can be further thickened. In fact, small amounts of solid components were demonstrated to prevent cell walls from coalescing, while having very little influence on the viscosity of the metal matrix [12]. It is important to note that viscosity as well as the metal matrix's surface tension are key in pore nucleation and foam

stabilization [14]. While surface tension influences pore nucleation, viscosity determines pore coalescence during solidification. The governing mechanisms of foam stabilization have been extensively studied, but they are still not well understood [15].

In seeking solutions to the issues previously defined, two main approaches have been taken by other researchers: 1) increasing TiH_2's decomposition temperature, and 2) alloying Al to decrease its melting temperature.

To increase TiH_2's decomposition temperature several approaches have been studied:

- Oxidation of TiH_2 has been investigated in various atmospheres (air, argon and nitrogen). This entails creating an oxide layer on the surface of the hydride that acts as a diffusion barrier [8, 16-19].
- Additionally, applying a Ni coating to the oxidised hydride has been studied to avoid hydrogen loss during the dehydrogenation [20].
- Furthermore, isothermal x-ray diffraction and thermal analysis of different particle sizes have been performed to improve understanding of the dehydrogenation of TiH_2 [21, 22].

To decrease the Al matrix's melting temperature, the most viable option is to alloy Al with elements that act as melting point depressants. Wrought Al alloys from series 2xxx and 6xxx, alloyed with Mg and Cu or Mg and Si, respectively, are commonly used. Casting alloys with large solidification ranges employed for metal foams are often combinations of Al-Si-Mg-Cu-Zn. For example, Al–

7wt.%Si–Mg (A356) or Al–9wt.%Si–3wt.%Cu allows foaming at a lower temperature in the semi-solid state [9, 11].

Regardless of efforts to coordinate TiH_2's decomposition temperature and the Al matrix' melting temperature, the Al alloys' foaming behavior should be further improved, as these foams are still unstable. As Al foaming takes place in such a short period of time—30 seconds from expansion to collapse—foam reproducibility becomes very difficult in practice.

This thesis' aim is to develop new Al alloys for the powder metallurgy technique that will produce high expanding, stable foams with superior mechanical properties. Thermodynamic modeling was performed using FactSage software to design these alloys. First, the effects of alloying Al with small amounts of Sn were evaluated, and then further alloying with elements to create in-situ intermetallic phases during the foaming process was studied.

This is a manuscript-based thesis; therefore Chapter 2 presents a comprehensive literature review, emphasizing the powder metallurgy technique. The foaming process for Al and its underlying problems such as crack-like pore formation, pore coalescence, metal drainage and foam collapse, are also detailed along with other researchers' efforts in foam stabilization. Chapter 3 describes the experimental techniques used to characterize powders, precursors and foams in the present work. Sn's influence on the Al foaming process is presented in Chapters 4 and 5. The effect of Sn on Al surface tension is explained in Chapter 4, while Chapter 5 explains foam stabilization from the gradual decomposition of TiH_2. Chapter 6

presents in-situ intermetallic formation in Al-3wt.%Sn foams by adding a ternary alloying element. The mechanical properties of these new alloys were tested and demonstrated in Chapter 7. All contributions and conclusions can be found in Chapter 8.

References

1. Banhart, J., *Manufacture, characterisation and application of cellular metals and metal foams*. Progress in Materials Science, 2001. 46(6): p. 559-632.

2. Fuganti, A., et al., *Aluminium foam for automotive applications*. Advanced Engineering Materials, 2000. 2(4): p. 200-204.

3. Ito, K. and H. Kobayashi, *Production and Fabrication Technology Development of Aluminum Useful for Automobile Lightweighting*. Advanced Engineering Materials, 2006. 8(9): p. 828-835.

4. Delucchi, M.A., *Environmental Externalities of Motor-Vehicle Use in the U.S. Journal of Transport Economics and Policy.* 2000. 34 (2): p. 135 - 168.

5. Davies, G.J. and S. Zhen, *Metallic Foams: Their production, properties and applications*. Journal of Materials Science, 1983. 18(7): p. 1899-1911.

6. Kretz, R., K. Hausberger, and B. Götzinger, *Energy-Absorbing Behavior of Aluminum Foams: Head Impact Tests on the A-Pillar of a Car*. Advanced Engineering Materials, 2002. 4(10): p. 781-785.

7. Banhart, J., *Metal Foams: Production and Stability***. Advanced Engineering Materials, 2006. 8(9): p. 781-794.

8. Matijasevic, B. and J. Banhart, *Improvement of aluminium foam technology by tailoring of blowing agent*. Scripta Materialia, 2006. 54(4 SPEC ISS): p. 503-508.

9. Lehmhus, D. and M. Busse, *Potential new matrix alloys for production of PM aluminium foams*. Advanced Engineering Materials, 2004. 6(6): p. 391-396.

10. Duarte, I. and J. Banhart, *Study of aluminium foam formation - kinetics and microstructure.* Acta Materialia, 2000. 48(9): p. 2349-2362.

11. Baumgartner, F., I. Duarte, and J. Banhart, *Industrialization of Powder Compact Foaming Process.* Advanced Engineering Materials, 2000. 2(4): p. 168-174.

12. *Mechanical testing of metals— Ductility testing— Compression test for porous and cellular metals*, in ISO 133142011, International Standards: Switzerland. p. 7.

13. *Alloy Phase Diagrams*, in ASM Handbook ASM International. p. 322.

14. *Clemex Vision PE/Lite™ 3.5 User's Guide*, 2002, Clemex Technologies inc.: Longueuil.

15. Adachi, H., et al., *Microstructure and mechanical properties of ternary intermetallic compound dispersed P/M Al-Mn-X-Zr (x=Cu,Ni) alloys*. Transactions of the Indian Institute of Metals, 2009. 62(2): p. 163-167.

16. Matijasevic-Lux, B., et al., *Modification of titanium hydride for improved aluminium foam manufacture*. Acta Materialia, 2006. 54(7): p. 1887-1900.

17. Kennedy, A.R., *The effect of TiH_2 heat treatment on gas release and foaming in Al-TiH_2 preforms.* Scripta Materialia, 2002. 47(11): p. 763-767.

18. Lehmhus, D. and G. Rausch, *Tailoring titanium hydride decomposition kinetics by annealing in various atmospheres*. Advanced Engineering Materials, 2004. 6(5): p. 313-330.

19. von Zeppelin, F., et al., *Desorption of hydrogen from blowing agents used for foaming metals.* Composites Science and Technology, 2003. 63(16): p. 2293-2300.

20. Proa-Flores, P.M. and R.A.L. Drew, *Production of aluminum foams with Ni-coated TiH_2 powder.* Advanced Engineering Materials, 2008. 10(9): p. 830-834.

21. Bhosle, V., et al., *Dehydrogenation of TiH_2.* Materials and Engineering, 2003. A(356): p. 190-199.

22. Malachevsky, M.T. and C.A. D'Ovidio, *Thermal evolution of titanium hydride optimized for aluminium foam fabrication.* Scripta Materialia, 2009. 61(1): p. 1-4.

Chapter 2

Literature Review

This chapter summarizes the background in metallic foams, emphazising the powder metallurgy technique (known as the powder compact melting technique), foam formation, stabilization, and scenarios to avoid in order to achieve homogeneous foams. The measurement of some mechanical properties interesting in the context of the current research is presented as well.

2.1. **Metallic foams**

The general definition of "foam" is any material that can trap gas bubbles in a liquid state. Metallic foams are solid materials with a 40% to 98% volume of gas; they are generally classified according to either their applications or their processing route [3]. Banhart [2] classified the production methods according to the state in which the metal has been processed, whether as liquid metal, solid metal in powdered form, metal vapor, or electrochemical deposition, as can be seen in Table 2.1.

For aluminum foam production, the liquid metal route is the most usual. Molten aluminum is first prepared for the various processes, or else aluminum is melted at some point of the process. Then, as gas is introduced, molten aluminum solidifies, retaining gas bubbles. Gas can be introduced in various ways, either by using foaming agents or by injecting the gas directly into the melt. Since gas has a lower density than the molten metal, gas bubbles tend to rapidly reach the surface

of the liquid metal. In order to control bubble distribution in the liquid metal and produce sound metallic foams, the residence time of the bubbles must be long enough. To ensure this condition is met, various processing and material parameters can be changed. Depending on the processing route, these parameters include: increasing the viscosity of the molten metal, varying the temperature of the molten metal, changing the gas or system pressure, etc. [4]. In the following section, a brief description of each of these processes applied to the liquid state is presented in the order shown in Table 2.1. However, the focus is on the powder compact melting technique, as it is the one used in the present study. This technique is explained in detail in section 2.2.

Table 2.1. "Families" of production methods for cellular metallic materials [2]

Cellular metals			
Metal vapor	**Liquid metal**	**Powdered metal**	**Metal ions**
• Vapor deposition	• Direct foaming with gas • Direct foaming with blowing agents • Gasars • **Powder compact melting** • Casting • Spray forming	• Sintering of hollow spheres • Gas entrapment • Slurry foaming • Pressing around fillers • Extrusion of polymer/metal mixtures • Reaction sintering	• Electrochemical deposition

2.1.1. Liquid State Processing of Metallic Foams

The most common method of producing metallic foams is by injecting gas bubbles into liquid metals. Although this may seem simple, it is extremely

difficult to control the homogeneity of the final solidified product's structure, as gas bubbles tend to rise in the liquid metal, coalesce, and when reaching the surface of the liquid metal, collapse. To prevent bubbles from escaping to the surface, the melt's viscosity must be increased. This has been achieved primarily by adding ceramic particles or alloying elements that produce stabilizing particles in the melt, increasing the melt's viscosity and surface tension [4].

2.1.1.1. Direct foaming with gas

This method is used by Hydro Aluminium (Norway) and Cymat Technologies Ltd (Canada) to mass-produce aluminum and aluminum alloy foams. To increase liquid aluminum's viscosity, up to 10 – 20 wt.% silicon carbide, aluminum oxide or magnesium oxide particles 5 to 20 μm in size are added.

Next, the mixture of liquid aluminum and ceramic particles is transferred into a tundish where gas (air, nitrogen or argon) is injected. As can be seen in Figure 2.1, an impeller can produce homogenous distribution of fine gas bubbles in the melt [1]. Stable metallic foam is then produced on the melt's surface, which is pushed by new bubbles that are constantly injected from the bottom. When the metallic foam reaches the surface, a conveyor belt pulls it out still in a semi-solid state. This process can theoretically produce an endless length of metallic foam, reducing production costs. However, the solid foam has a heterogeneous structure, its width is controlled by the vessel and the conveyor belts, and it has an approximate thickness of 10 cm. The density of the metallic foam produced by this method varies between 0.069 and 0.54 g/cm^3 [1, 2].

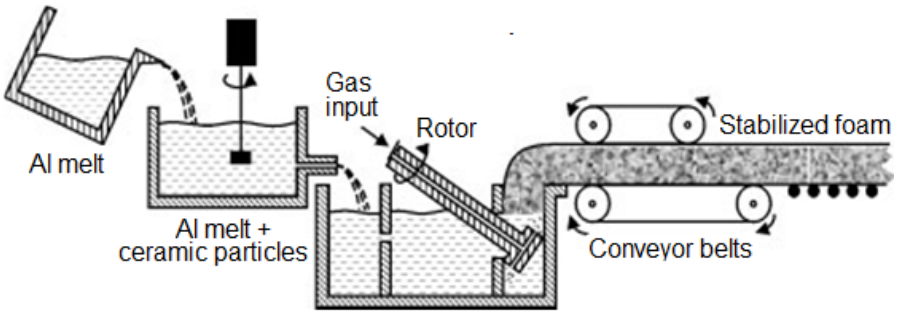

Figure 2.1: Schematic diagram for producing aluminium foam using Cymat's route [1, 2].

2.1.1.2. Direct foaming with blowing agents: Alporas process

Shinko Wire in Japan has used direct foaming with blowing agents, also called the Alporas process. The key to this method (Figure 2.2) is mixing TiH_2 with aluminum powders at a temperature near the melting point of aluminum (when the metal is in a semi-solid state), so that the mixture has the viscosity necessary to keep bubbles trapped [5]. Adding calcium metal can produce calcium oxide or calcium-aluminum oxide, which increases viscosity [6]. Gas bubbles are created when the TiH_2 begins to decompose at ~450 ^{o}C. To control bubble growth, the press is kept at a constant pressure and hydrogen is injected at the mixture's surface. This method is very efficient, because the size and shape of the pores in the metallic foam can be controlled relatively early. Furthermore, it is possible to control the foam's shape, as it takes the shape of the containment vessel. The foam's density is typically between 0.18 and 0.24 g/cm^3 [2].

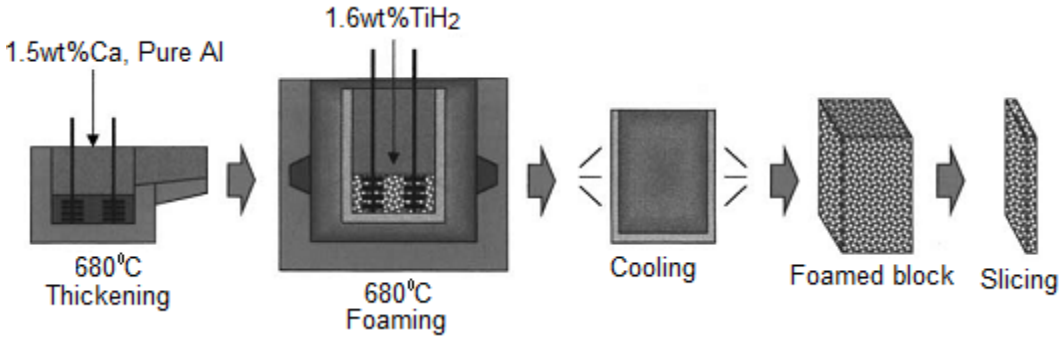

Figure 2.2: Alporas manufacturing process [1, 2].

2.1.1.3. Gasars: Solid-gas eutectic solidification

A method called "*Gasars*" (solid-gas eutectic solidification) was developed in the mid-1970s, though it only became popular in the 1990s. This process uses metals such as Cu, Fe, Ni, Co, Mg, Al, etc., which can form a eutectic system with hydrogen gas at high pressure in its liquid state. The melt is held in a high-pressure hydrogen atmosphere, then by lowering the temperature, it turns into a two-phase system of solid and gas. Keeping the pressure constant and reducing the temperature leads to directional solidification, which advances the solidification plane front where the hydrogen bubbles are formed. The pore size, morphology and porosity percentage (5-75%) are primarily determined by the hydrogen content pressure and the direction and rate of heat removal [7].

Figure 2.3 shows the setup employed in producing Gasar foams. Hydrogen is constantly injected into an autoclave that contains the melt. Finally, the melt charged with hydrogen passes to a mould where heat removal is regulated.

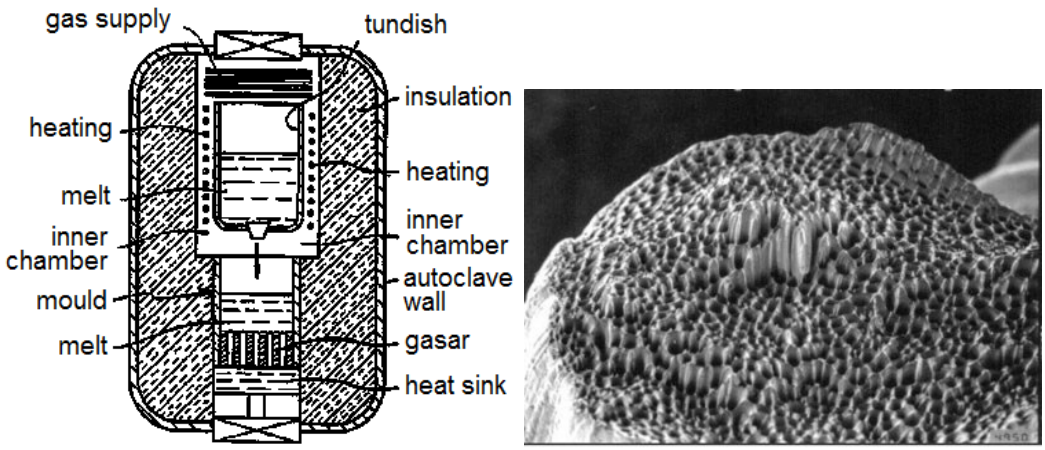

Figure 2.3: Apparatus used to fabricate aluminum foams by the gasar method, and view of the fracture surface on a cupper gasar [7].

2.1.1.4. Casting

An alternative foam production without involving gas injection is through casting methods as used by ERG, the manufacturer of DUOCEL. One of these casting methods involves fabricating a mould from polymeric foam with the desired cell size and relative density. First, the polymeric foam is infiltrated with a slurry (a mixture of mullite, phenolic resin and calcium carbonate) and dried. Next, it is heated to harden the cast material and decompose the polymer template. The residual structure (negative image of the foam) is filled with the liquid metal and finally removed, leaving a porous structure. Figure 2.4 depicts the steps necessary to produce a cellular material by this method, also known as *investment casting* [1, 2].

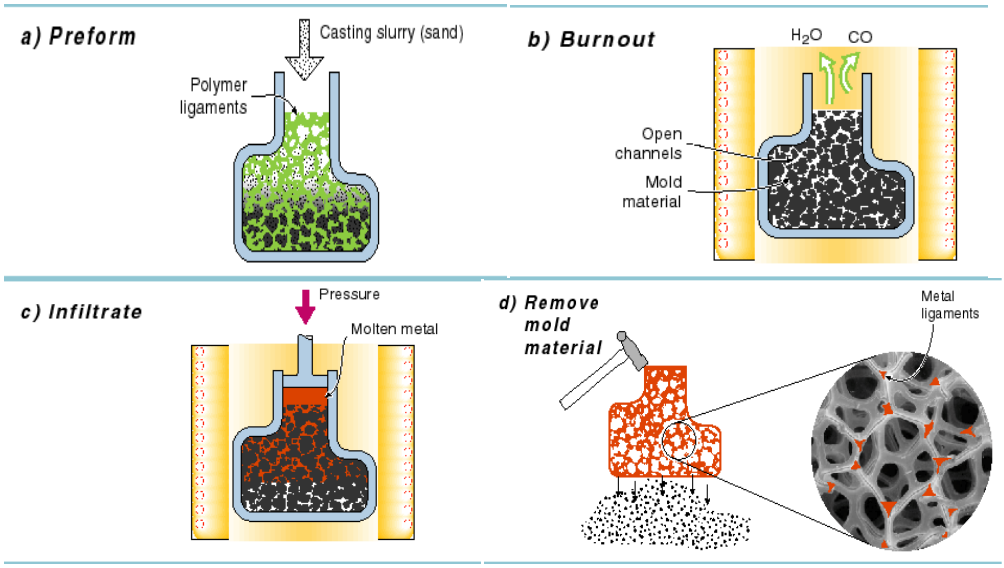

Figure 2.4: Investment casting process for the fabrication of open cell structures [8]

Another casting method uses inorganic or organic granules. Liquid metal can be poured into a mould that contains these granules. The granules can be removed by leaching after casting. When pouring the melt on the granules, it is important to create a vacuum between the granules or to pressurize the melt to ensure the liquid metal fills the mould properly. This technique is known as "casting around space holding materials" and the pore size and morphology can be easily controlled by choosing the size and distribution of the space holders [9].

"Lattice block materials" (LBMs) is another casting method, in which straight beams are connected by nodes. The structure can be very regular and is commonly produced with a prefabricated injection-molded polymer. Foams produced by this technique are easily reproduced, which is an advantage.

2.1.1.5. Spray Forming (Osprey process)

In this process, molten metal is atomized under an inert gas where a stream of droplets is propelled away from the spray zone and collected on a substrate. There, it solidifies in a variety of geometries with high density and low oxide content. Another characteristic of this process is the possibility of producing metal matrix composites if oxides and carbide particles are added to the sprayed metal [10]. When the injected powders react or decompose with the molten material, pores are created, producing a foam of up to 60% porosity [2].

2.2. **Powder Compact Melting Technique**

Also called powder metallurgy technique, this method also involves liquid state processing, and is the one used in this research. It was first developed at the Fraunhofer Institute in Bremen and the Bratislava University in collaboration with the Karmann Society. This technique is described in the schematic drawing in Figure 2.5 [2]. First, a foaming agent (hydride or carbonate) is mixed with metal powder. For aluminum, the blowing agent used most commonly is TiH_2 (1 wt.%) [11]. To obtain foams, a well-compacted precursor (above 99% of its theoretical density) made up of metallic powders combined with the foaming agent is required. Compaction is carried out using any technique that ensures low porosity (rolling, rod extrusion, hot uniaxial or isostatic pressing), but the most common compaction technique involves cold pressing [12]. Regular machining operations can then shape this semi-finished product.

For aluminum foams, the foaming process starts by heating the compacted precursor, which begins to foam above 500^{o}C. Actual foaming begins with the decomposition of the foaming agent, which releases gas [13]. Simultaneously, the metal begins to melt as the temperature is increased. There is a point (a temperature near the melting point of the metal powder) when the metal's viscosity and the internal gas pressure are in equilibrium. At this point, the gas creates bubbles, which either begin to coalesce, leading to larger bubbles, or which are pushed to the surface. Since the melt's surface tension is so low, the gas pressure can finally pop the bubbles, causing the foam to collapse.

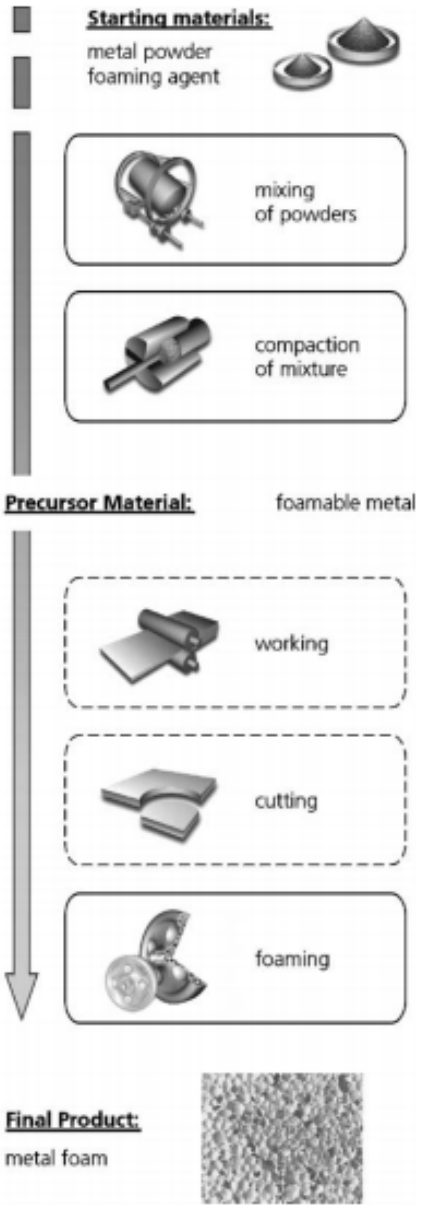

Figure 2.5: Powder metallurgical process for foam production [1, 2]

One advantage of the powder metallurgical precursor is the possibility of foaming inside a mould to create a variety of shapes. As the foaming happens inside the mould, an almost finished product is obtained, requiring little machining. This mould can even be made from aluminum sheet that will become part of the final

product. In this case, the foaming precursor has very good adherence to the aluminum sheet [14]. Figure 2.6 shows examples of mould filling of complex shapes using multiple precursors. Nevertheless, a relevant aspect when producing elaborated parts is to study the cooling or heating profile of the required part. A solidification front is created (starting at the walls of the mould and moving towards the center) so smaller pores can be found adjacent to the mould (the colder area), and if the foam is held for longer periods of time, pore coalescence will occur within the un-solidified areas. This is the reason companies primarily produce aluminum foam core sandwiches; where solidification occurs faster and pore structure can be better controlled. In producing foam core sandwiches, sheets of steel or titanium can also be employed, as long as good adhesion of the sheet to the foam is ensured [15].

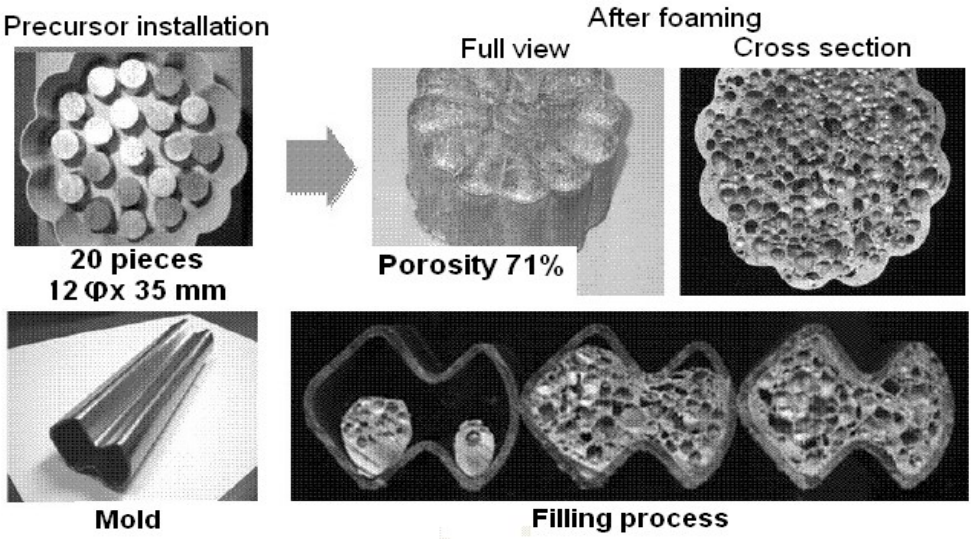

Figure 2.6: Mould foaming examples by powder metallurgy technique: mould filling with multiple precursors [14]

2.3. **Foaming Process**

The powder compact melting technique consists of 3 main stages (Figure 2.5*)*:

- Homogeneous mixing of the starting powders: metallic powder and blowing agent.
- Compaction of the mixture: reaching 99% of its theoretical density.
- Heat treatment of the foamable precursor: above the melting point of the metallic matrix.

Foam properties can be changed at this stage by modifying parameters such as: foaming temperature, heating rate, furnace size, constrained foaming or free foaming (with or without a mould or crucible), etc.

2.3.1. Foam Formation

Fine adjustments of the process's parameters are required for the formation of homogeneous foam. However, metallic foam production is still an expensive process, and foam properties are not always sufficient for selected applications.

The metallic system's melting behavior must be coordinated with the blowing agent's decomposition characteristics. If the matrix's temperature is below the solidus temperature, the gas evolving from the blowing agent will create cracks and escape [16]. Ideally, as gas begins to evolve, partial melting of the matrix produces enough liquid to start the formation of spherical pores [17, 18].

Graphs like the one presented in Figure 2.7 can be built to match the blowing agent's decomposition to the metal or alloy used for the matrix [17]. Solidus and liquidus temperatures of aluminum and two alloys are shown on the left side,

while the onset of the maximum gas evolution for titanium hydride (as loose powder or in a compact) is shown on the right side. This graph provides corroboration for the hypothesis that the solidus and liquidus temperatures of Al6Si4Cu alloy correspond to the onset and maximum of hydrogen released from TiH_2 heat-treated at 480 ^oC for 180 min. Therefore this alloy with the heat-treated hydride would be expected to produce homogeneous foams.

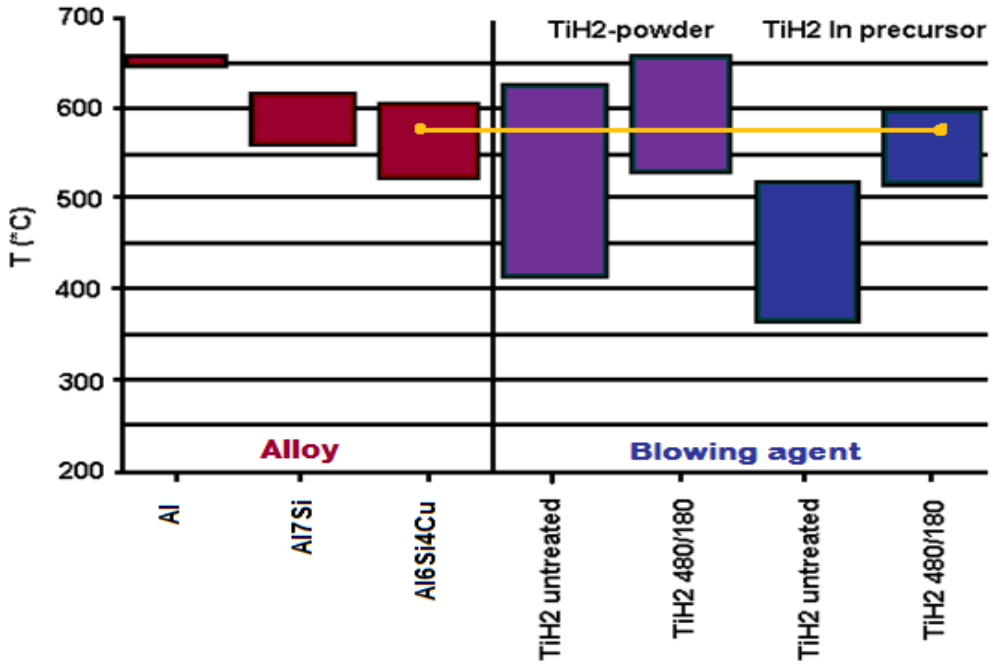

Figure 2.7: Temperatures governing the foaming process of metals[17]
Left: range between solidus and liquidus for three commercial Al alloys (‘‘Al’’ = AW-1050, ‘‘Al7Si = A356, ‘‘Al6Si4Cu’’ = A319).
Right: range between the onset and maximum of hydrogen release from TiH_2-powder and pure Al precursor containing this TiH_2. Heat treatment “480/180” stands for 480°C during 180 min

Figure 2.8 shows an aluminum foam expansion curve as a function of time [2]. At a time zero, the precursor is placed inside a crucible (which acts as a mould). After 7 minutes at 750 ^oC, a crack-like pore begins to form (the liquid fraction of aluminum is still small). Next, there is a sudden rise in expansion at about minute 10. This is the moment when optimal cell structure is attained. After this maximum expansion, metal drainage and pore coalescence can take place [2, 19].

To obtain high-quality foams, a careful selection of the heating condition during foaming is essential. Nevertheless, as foaming happens at temperatures above the melting point of aluminum or the aluminum alloy, the foam must be cooled down below the metal's melting point. Otherwise, pore coalescence and metal drainage will occur and destroy optimum cell structure [2].

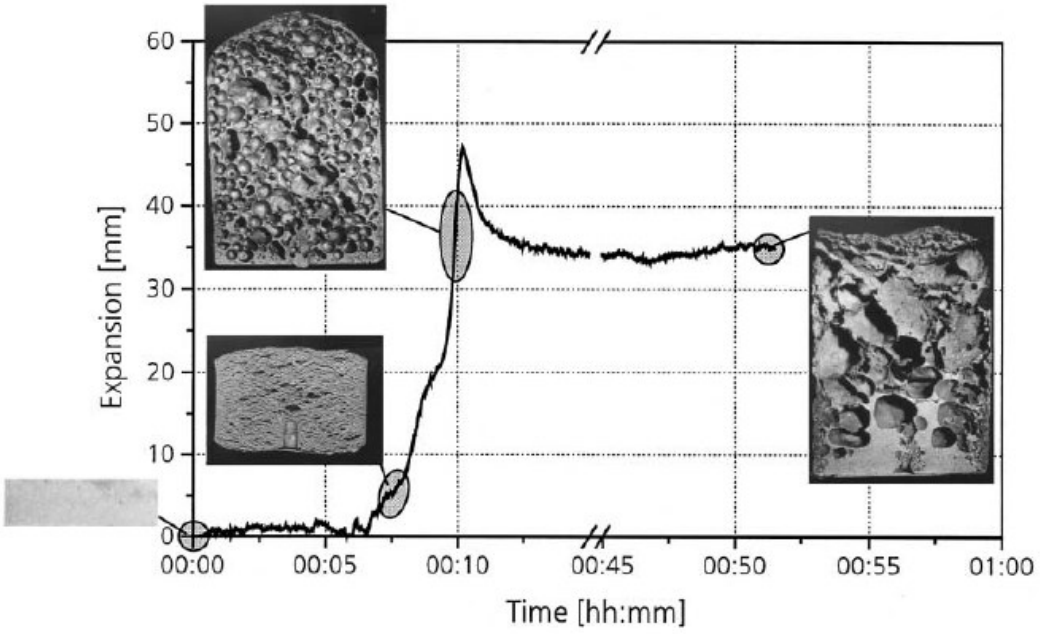

Figure 2.8: Expansion behaviour as a function of time for Al/TiH_2 precursors foamed at 750 ºC [2].

Since metallic foams change continuously throughout the foaming process they are considered unstable. In order to obtain stable foam, the foaming process should not change drastically over long periods of time (between completion of the release of gas from the blowing agent to its solidification). During this time the forces acting on the foam are: gravity, external atmospheric and internal gas pressure, mechanical forces, and forces from within the metallic phase (surface

tension, capillarity forces, etc.) [20]. Any change in these forces will change the foam morphology by:

- Flow: bubble movement due to internal gas pressure or mechanical forces.
- Drainage: liquid metal being dragged to the bottom of the foam through Plateau borders by gravitational and capillary forces.
- Coalescence or cell wall rupture: irreversible binding of 2 or more bubbles.
- Coarsening or Ostwald ripening: gas diffuses from smaller bubbles to bigger ones due to pressure differences.

Some of the resulting phenomena are identified in the cross section of aluminum foam analyzed with x-ray tomography as seen in Figure 2.9.

2.3.2. Foam Stabilization

Even though some processes are now being industrialized, foams show many deficiencies, which make it difficult to control their final mechanical properties. To improve metallic foams, stabilization mechanisms must be understood. The term *foam stability* for different foaming methods refers to whether those methods successfully minimize drainage and avoid bubble rupture and collapse of cell walls [21, 22].

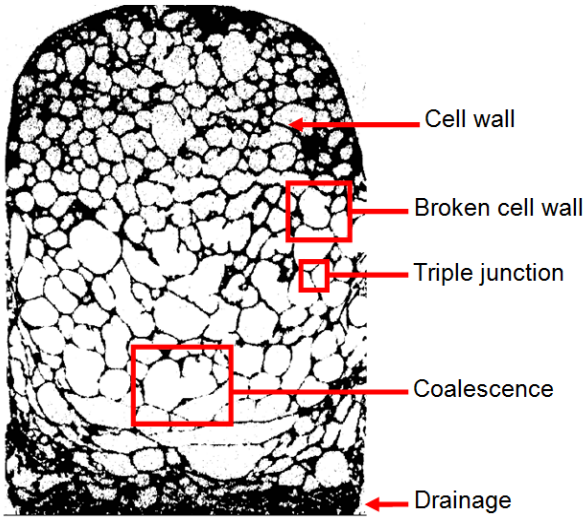

Figure 2.9: Cross section of Al foam from tomography

These phenomena are linked to the liquid being drained through the cell walls by gravity and surface tension forces that leave positive pressure at the cell walls compared to the triple junctions. At some points, cell walls become very thin, and as pressure differences increase they begin to rupture, resulting in coarsening of pores and collapse of the foam. Figure 2.9 shows details of these effects in an aluminum foam cross section. Therefore, many researchers have tried to strengthen the cell walls and inhibit these phenomena. Different solutions to this problem have been attempted; for example, enhancing the melt's viscosity, using different alloying elements in the melt, employing ex- or in-situ particles that stabilize the cell wall, etc. [4]. Some of these solutions will be explained in the following sections.

2.3.2.1. Ceramic Particle Addition

After aqueous foams and emulsions were stabilized using particles, great interest arose in trying to stabilize metallic foams in a similar manner. The distribution of the particles and the forces in an emulsion are well known (van der Waals and repulsive electrostatic interactions) [23]. However, research on metal foam stabilization is still ongoing, despite the fact that many theories have been proposed on how particle additions stabilize metallic foams. Table 2.2 lists several theories.

Table 2.2: Theories on mechanisms affecting particle-stabilized foams

Authors	**Particle Stabilization and other methods**	**Stabilizing Mechanism**
Gergely et al. [24]	• Increasing viscosity • Higher particle content • Reducing temperature to semi-liquid state	Damping vertical motion of liquid
Ip et al. [25]	Solid particle addition flattens curvatures around plateau borders	Reduced suction of metal from cell wall into the border
Kaptay [26]	Optimum wetting angle between solid particles-gas-liquid	Stabilize the gas/liquid-bubble interface

A comparison of stabilization models by particles was also done schematically (Figure 2.10) by Haibel et al. [27]. These authors compared their observations on Al-10wt.%Si-1wt.%Mg alloy stabilized by 10wt.%SiC (Figure 2.10-f) to previous models. Figure 2.10-a represents a film (cell-wall) connected to Plateau borders. The radius of the film (R_F) and the Plateau (R_{PB}) along with surface tension create a difference in pressure (Δp). With gravitational and pressure differences, metal starts to drain unless a stabilizing mechanism is present. Adding particles changes

the radius of the Plateau and the film; this is expected to reduce capillary suction and slow drainage. Nevertheless, the schematic shown in Figure 2.10-b is not observed in metal foam structures. To reduce capillary suction, Figure 2.10-c considers the settling of the particles along the liquid-gas interface, which will also change the radius, while Figure 2.10-d assumes particle bridges across the film, providing repulsive mechanical forces that keep the liquid-gas interfaces apart. Figure 2.10-e postulates an increase in viscosity resulting in partial immobilization of the melt.

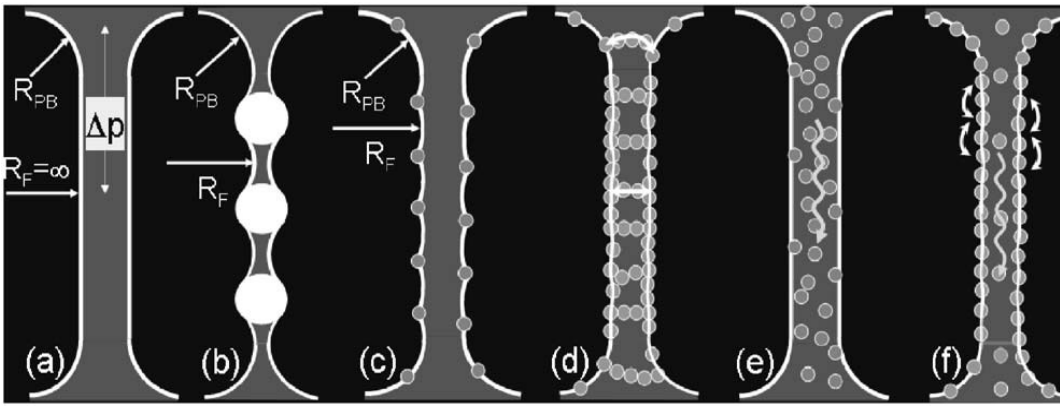

Figure 2.10: Schematic representation of particle stabilization[27]
(a) Liquid film in a foam, (b) adsorbed particles bridged by film, (c) interfaces modulated by adsorbed particles, (d) particle layers on interfaces mechanically connected by bridges, (e) drainage reduction by particles, and (f) model proposed by Haibel et al.

The model proposed by the Haibel et al. shows particle interaction on the cell wall surface (creating surface elasticity and thus avoiding rupture); meanwhile particles within the film increase the apparent viscosity. Therefore, an improvement of particle interactions is proposed rather than increasing particle content [27].

As summarized by Kaptay [26], the particle interaction or position in the metallic film is associated with the metal-particle contact angle[1] and the interface with the gas bubble (see Figure 2.11). Contact angle measurement has been widely used to characterize interfacial phenomena, wetting/dewetting of solid surfaces, capillary penetration into porous media, etc [28]. It is important to note that wetting a solid with a liquid and spreading a liquid on a solid are closely related. Wetting is a surface phenomenon in which the solid surface is covered by the liquid placed on it. Spreading is the physical process by which the liquid wets the solid. Therefore, wetting or spreading can be classified in a similar manner into two main categories: non-reactive and reactive wetting. Non-reactive wetting is governed first by surface tension, then gravity and finally any viscous forces. Reactive wetting is more complicated as diffusion, reaction, absorption, solidification, and many other phenomena can change the contact angle making it difficult to reach a state of equilibrium[28].

In metal foams containing ceramic particles as the stabilization method, wetting is considered to be non-reactive in most cases (depending on the system). It is well known that particles only stabilize if they have a contact angle between 20 and 90°; being 90° the angle at which maximum energy is required to remove a particle from the interface. Experimentally, foam stability varies from 40 to 110°. The expected optimum contact angle to stabilize aluminum with alumina is 85°, when clusters are presented in the cell walls [26]. Also, metal foams exhibit particle aggregation in restricted volumes [27].

[1] Contact angle is the measurement between the tangent drawn at the triple point among the three phases (solid, liquid and vapor) and the substrate surface.

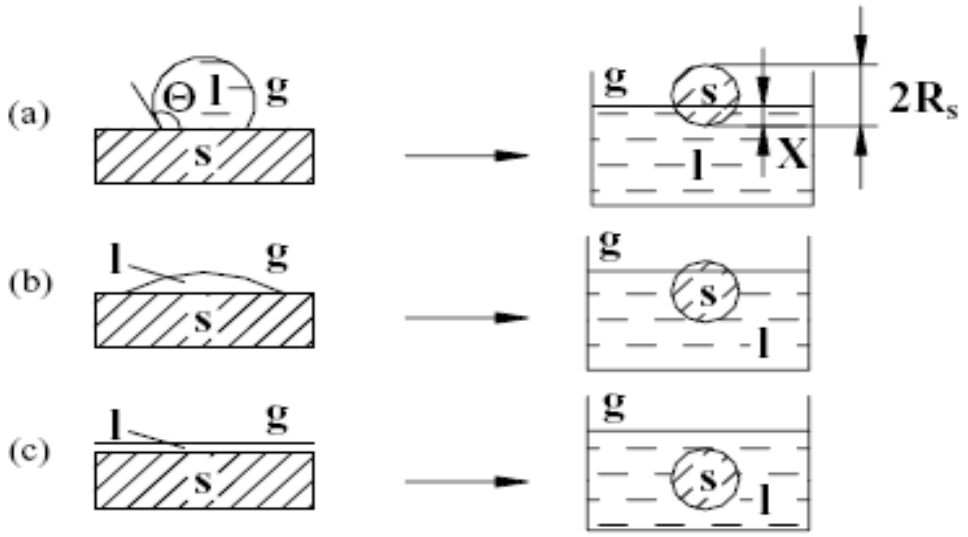

Figure 2.11: Immersion of a solid spherical particle into a liquid as a function of contact angle: (a) non-wetting, 180 ° > Θ > 90 °, (b) wetting, 90 ° > Θ > 0 ° and (c) perfect wetting, Θ = 0 °. The left column represents experimental observation during a sessile drop experiment while the right column shows the equilibrium position of a small particle at the liquid-gas interface. [26]

Rs represents the radius of the solid and X the depth of immersion of a spherical particle. S, l and g stand for solid, liquid and gas phase.

When ceramic particles are added to metallic foams (i.e. TiB_2 in aluminum foam [29]), the cell wall thickness is reduced, allowing larger expansions before the cell wall ruptures and collapse occurs.

Metal foams can be stabilized by adding ceramic particle (as seen in the Cymat process), or in situ formation of stabilizing particles (like conditioning with calcium, belonging to a reactive wetting system in the Alporas process). For powder metallurgy foams, heat treating aluminum powders to increase the thickness of the oxide layer covering each powder is another stabilization mechanism [30]. Likewise, foaming in the semisolid state (endogenous stabilization) produces very stable foams, as α-grains present in the solid behave

as particles [20]. Micrographs from the cell-walls of the previous examples are seen in Figure 2.12 [31].

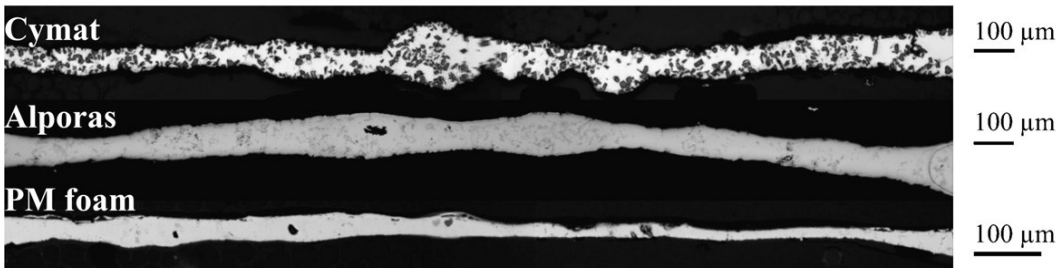

Figure 2.12: Cell walls of aluminum foams produced by Cymat (SiC-particle reinforced melt by gas injection), Alporas (melt conditioning with calcium and TiH_2 as blowing agent) and powder metallurgy process (powder compacts with TiH_2 as blowing agent) [31]

2.3.2.2. Oxidized Powders

Aluminum has the property of oxidizing readily, therefore aluminum powders are surrounded by an oxide layer (melting point of alumina is 2072°C) with a nanometric thickness that will contain molten aluminum [20]. As modeled in Figure 2.13, the oxide shell can form a skeleton in the cell wall, maintaining the structure. Nevertheless, there is a limit to how thoroughly powders can be oxidized.

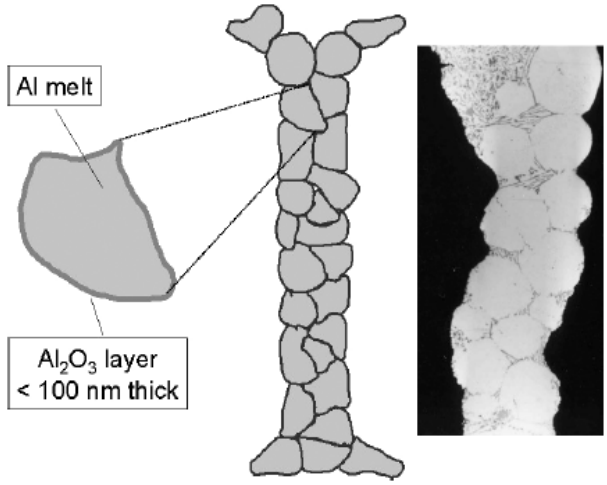

Figure 2.13: Model and cell wall of a Al-7wt.%Si foam produced by powder metallurgy technique using 0.6wt.%TiH_2 [20].

Asavavisithchai et al. [30] oxidized aluminum powders to different oxygen contents (low < 0.3wt.%, moderate 0.3-0.6wt.% and excessive > 0.6wt.%) and found that as the oxygen content increases, stability increases, but maximum expansion can be achieved at moderate oxygen levels. As the oxygen content increased, they observed that the crumpled oxide film clusters restricting the drainage effect also inhibited foam expansion. This agrees with Körner et al. [32], who proposed stabilization using a network of oxides penetrated by liquid metal, which behave similarly to particles and which they called "oxide network particle stabilization".

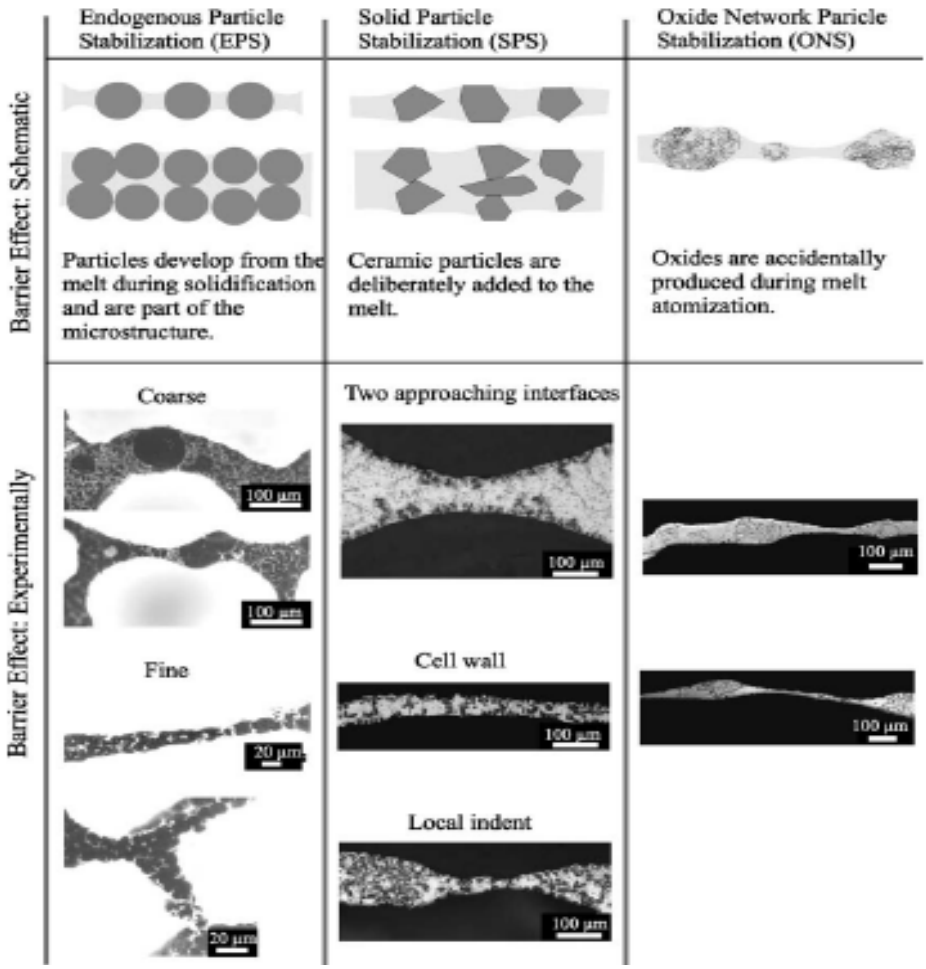

Figure 2.14: Particle stabilization. Top: schematic diagrams. Bottom: light microscopy showing particles as dark phases. Left: AZ91, middle: Al with SiC and right:Al99.9 [32]

The particle network develops from the oxide in the precursor material, forming a gel-like network that can withstand elastic forces. This particle network remains in the melt as long as the metal wets the oxide. Körner et al. [32] compared particle stabilization both by oxide network and by solid ceramic to endogenous particle stabilization (see Figure 2.14).

2.4. **Effect of Alloying Elements in Aluminum**

Another technique for attaining homogeneous foams consists of the tailoring of the metal matrix that will contain the gas. Adding some metallic elements to aluminum can lead to the formation of intermetallics or eutectic phases with lower melting points than pure aluminum.

Maximum solid solubility in aluminum alloys occurs at the eutectic, peritectic, or monotectic temperature. The solid solubility limit can be extended through quenching or by adding other elements to the alloy. Additions of elements that are especially susceptible to solubility extension in binary alloys (for example, manganese) can be used in ternary alloys to increase the solubility limits of less susceptible elements such as iron, cobalt and nickel [33]. Nine elements show sufficient solid solubility (more than 1% at.) with Al, but only five of them have been exploited commercially. Table 2.3 summarizes these alloys and their properties.

Table 2.3: Main alloying elements for aluminium and the final property [34]

Aluminum +				
Magnesium	Silicon	Iron	Copper	Zinc
Increased strength, hardness and weldability. Good corrosion resistance.	Results in heat treatable alloys when combined with magnesium. Good corrosion resistance.	Most common impurity found in aluminum. Reduces grain size.	Results in heat treatable alloys. Increased strength and hardness. Reduced corrosion resistance.	Increased strength and hardness. Possibility of stress corrosion. Results in heat-treatable alloys when combined with Mg.

In the process of foaming an aluminum alloy, the presence of silicon decreases the eutectic temperature, shortening the period of time to initiate pore nucleation. For Al-Si alloys, Si determines the fraction of the solid α-phase. Under higher Si contents, this fraction decreases. The α-phase is believed to hinder pore growth during foaming since it solidifies adjacent to the pore's perimeter, serving as stabilizer for cell formation and preventing pore coalescence [35].

Aluminum alloys containing Cu, Mg, Si and Zn have been widely studied using the powder metallurgy technique. For these alloys, expansion was entirely shifted to the semi-solid-liquid phase, due to the presence of a eutectic solid [36]. Other studies [35] with the same type of alloys (Al-Si-Cu-Mg) showed a sequence during foaming of:

1. crack-like pore nucleation occurring in the direction of the extrusion,
2. spherical pore growth,
3. coalescence of the neighboring pores,
4. collapse of the pores adjacent to the specimen's free surface.

Adding elemental Mn and Ni to Al forms intermetallics such as Al_6Mn and Al_3Ni, respectively. When Mn is added, intermetallics other than Al_6Mn can occur. It is well-known that Ti forms the stable $TiAl_3$ intermetallic, which aids in refining the cast grain size and enables recovery and recrystalization to be controlled [37].

Intermetallic foams have been fabricated by a combustion reaction process. This process is listed under the powdered metal category in Table 2.1. Using a foaming agent is optional, since porosity can be generated by moisture linked to the original powders. The ratio in which the powders are mixed is important in determining the final intermetallic foam. Figure 2.15 illustrates the combustion synthesis of aluminum nickel foam [38, 39].

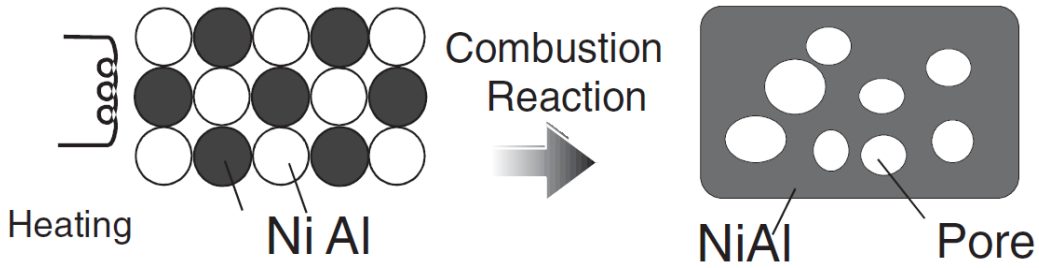

Figure 2.15: Schematic illustration of combustion synthesis of nickel aluminum [38, 39]

2.4.1. Interest in Tin Additions to the Aluminum Foams

Decreasing aluminum's melting point by using eutectic compositions is common practice. Therefore, in this research the production of Al alloy foams via powder metallurgy is proposed using a mixture of powders succeptible to form an Al-alloy. During foaming, these novel alloys are expected to generate intermetallics, resulting in isothermal stabilization of the foam, thus avoiding problems of coalescence and drainage while maintaining a stable structure.

Diffusion in the liquid state is several orders of magnitude higher than in the solid state. Therefore, any element in the liquid state will be useful for incorporating other alloying elements faster into the aluminum [40]. Additionally, the crack-like pore nucleation that occurs during the initial foaming stages can be avoided if one of the metallic elements liquifies at low foaming temperature.

Even when aluminum-tin interaction does not produce intermetallics, molten tin can generate a diffusion layer allowing other elements to react with aluminum. In another scenario, a ternary element addition can also react with tin, removing the liquid phase from the foaming system. In both cases, tin can unify the mixture as the foaming process occurs.

The presence of liquid Sn during hot pressing of Al would be similar to the initial stages of persistent liquid phase sintering, while alloying with additional elements to produce intermetallics could be considered in the reactive sintering process.

Trace elements can induce activated sintering in Al. Schaffer and Huo [41] reported that additions between 0.05wt.% and 0.5wt.% Pb or Sn activates

sintering in the Al-Zn-Mg-Cu system. Pd had the greatiest effect on sintering followed by Sn. Other elements such as Se had no effect while Bi and Sb were detrimental to sintering,

The binary Al-Sn phase diagram is perhaps the only phase diagram with Al which exhibits almost all of the features of an ideal system. The melting point of Sn is considerably lower than that of Al (232 °C vs. 660 °C) and there are no intermetallic phases. Sn is barely soluble in solid Al while Al is completely soluble in liquid Sn and no immiscible liquids form [42]. In addition, the diffusivity of Al in liquid Sn is about five times greater than the self diffusivity of liquid Sn [43].

Persistent liquid phase sintering implies the liquid remains in existence as long as a heat treatment is maintained. The process begins with mixed powders and pores between the particles. During heating the particles sinter, but when a melt forms wetting induces liquid spreading to fill pores and penetration of grain boundaries to enable grain rearrangement. Subsequent densification is accompanied by coarsening [44].

The most common scenario for liquid phase sintering has the following characteristics [44]:

1. Newly formed liquid wets the solid grains due to solid solubility in the liquid. Pore filling preferentially follows capillarity; therefore, the smaller pores will be filled first.

2. Solid grains partly dissolve into the liquid to reach the solubility limit. The solid dissolves from the grain surface into the liquid, preferentially from higher energy asperities, convex points, or areas under compression; the dissolution of small grains is preferred [45]

3. Liquid is low in solubility in the solid; low solubility for the liquid species in the solid.

4. Solid alloying with the liquid causes a decrease in solidus and liquidus; liquid segregation to interparticle bonding.

Persistent liquid phase sintering and reactive sintering (based on the joining approach) could be extrapolated to the foaming process of Al-Sn-X (X being an additional metallic element that will form in situ intermetallics) as follows: elemental powders are mixed, during hot compaction one of the elements melts first (Sn) while the applied pressure will disrrupt the surface oxide on Al powders allowing fresh metallic contact that can bond. During the foaming process, the foam is in expansion, the Al matrix reacts with X element generating in situ intermetallics. The intermetallic presence in the cell walls will thicken the melt as in the Cymat's process, counterballancing the gas pressure from the hydrogen release of TiH_2. In turn, the pore coalescence and metal drainage could be avoided.

2.4.2. Literature of Tin with Aluminum

Bishop et al. [37] modified a standard powder metallurgy procedure to analyze trace element additions commonly processed by ingot metallurgy. In this procedure, a previously pressed alloy substrate is cold isostatic pressed, sintered and cold extruded, worked with a thin alloy-mineral outer shell, and then normal sintering and extrusion is performed. The same authors suggested tin and silver as promising elements for microalloying an aluminum alloy. Silver was found homogeneously throughout the alloy microstructure, while tin was concentrated at intergranular regions only. When sintering at 600 ^{o}C, the trace left by the liquid alloying element (Sn and Ag) on Al was easily formed, reaching the mushy alloy core.

Evans et al. [46] reported that for complete wetting of all grain boundaries in aluminum, a minimum of 5wt.%Sn was necessary. If there is less than 5wt.%, the liquid tin film breaks up into separate particles.

Eisenmenger-Sittner et al. [47] investigated solid state wetting and spreading of tin on aluminum interfaces. Their results show that metallic tin wets every type of polycrystalline aluminum interface. Also, they found that oxygen decreases the wetting and spreading of tin. Further research on this type of Al/Sn/Al sandwich layer system showed that grain boundary volume and temperature influence the wetting speed. This change in speed is the result of tin permeation through the grain boundaries and the increase in temperature [48].

Interactions of Al-Ti with Sn were reported by Wang et al. [49]. In their work, Sn was added to binary TiAl alloys to improve their room temperature ductility. The

ternary diagram was studied in the Ti-rich corner where Ti_3Al and Ti_3Sn intermetallics were found to be completely soluble in each other. In a different study [50], the formation of a single intermetallic ($TiMnSn_4$) at 497 ^oC was found in a Ti-Mn-Sn system.

Sercombe and Schaffer used tin to infiltrate aluminum in aluminum nitride skeletons for rapid prototyping applications. Due to its low melting point and low surface tension, tin controlled nitride growth and increased the infiltration rate. Also, because of its low surface tension, tin segregates in the molten aluminum, reducing aluminum's effective surface tension and improving its sintering response. In a more recent study, the authors explained how tin is incorporated into the growing nitride and, once consumed, increases the rate of nitridation [51, 52].

Alumina was successfully brazed using tin-based active metal brazing [53]. Ti and Mg were the active metals added to the base alloy, which consisted of 93.6wt.%Sn, 1.7wt.%Cu and 4.7wt.%Ag, but only Ti additions joined the alumina. Calorimetric analysis done in the brazing alloys containing Ti showed a solidus peak around 220 ^oC and a liquidus peak around 450 ^oC (depending on Ti wt.%). The brazing was carried out at 900 ^oC for 15 min. It was found that a temperature of 725 to 900 ^oC was critical to wet the alumina.

Other studies showed that adding tin to PM aluminum alloys enhanced wear resistance and lowered metal to metal contact, but decreased hardness and tensile properties [54].

2.5. **Metallic Foam Properties**

The properties of metallic foams depend on their geometric structure, such as distribution, size and shape of the cells [55], as well as their relative density, ρ/ρ_s (foam density divided by the density of the solid material in the cell wall) [9].

One of the advantages of foams is the possibility of targeting a desired profile of properties by selecting appropriate materials with the correct density [56, 57]. Different properties can be engineered through foaming: density, thermal conductivity, Young's modulus, compressive strength, etc. [55].

2.5.1. Mechanical properties

After considering foam density and porosity type (open or closed cells), the factor with the most influence on foam properties is defects: buckled, broken or missing cell walls, major differences in cell size or shape, and so on [58]. Therefore, metal foams have different properties compared to the materials from which they are made.

For instance, a metal foam's stress-strain behavior during compression and tension is compared with that of the metal itself, as seen in Figure 2.16 [1]. The elastic limit (σ_D) during tension and compression, the tensile strength (σ_{UTS}), the plateau stress under compression (σ_{pl}), the densification strain (ε_D), the ultimate tensile strain (ε_{UTS}) and the fracture strain (ε_f) of a metal foam can be completely different from the metal itself.

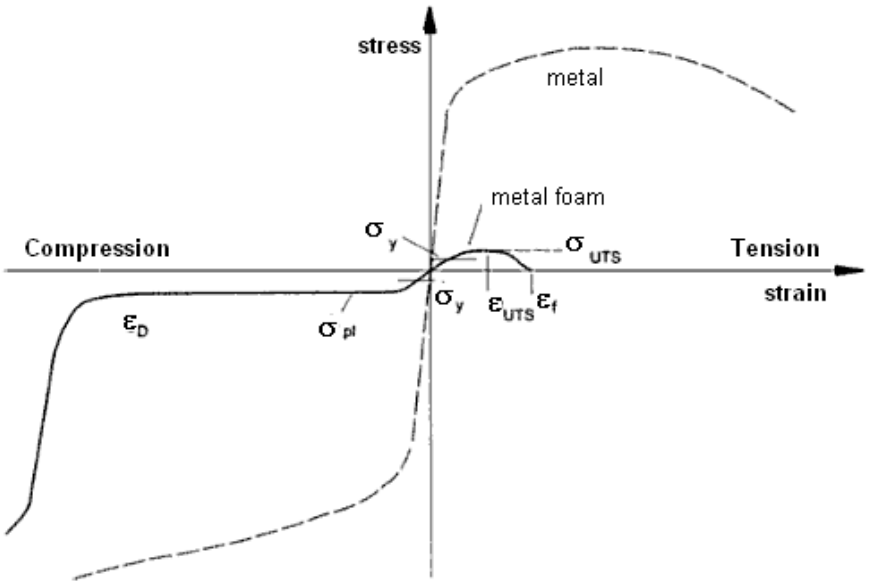

Figure 2.16: Comparison of the behaviour of a metal vs. a metal foam under compression and tension [1]

2.5.1.1. Compression behavior

The most common way of determining metallic foams' mechanical properties is to describe their stress-strain behavior. Figure 2.17 shows the stress-strain curve for compression. Young's modulus (E) is determined by the slope of the elastic region, and the plateau stress (σ_{pl}) is set by the yield point's distance from the strain axis. Once the foam is fully densified (ε_D), the applied stress rises steeply [9]. To describe the linear elastic behavior, isotropic materials need at least two moduli: Young's modulus, E, and the shear modulus, G. Some foams are non isotropic and more than two modulus are needed to describe their linear elastic behavior.

Young's modulus (E) and shear modulus (G) scale with density as:

$$E \approx \alpha_2 E_s \left(\frac{\rho}{\rho_s} \right)^n \qquad G \approx \frac{3}{8} \alpha_2 G_s \left(\frac{\rho}{\rho_s} \right)^n$$

where the constants vary with the foam structure: *n* ranges between 1.8 and 2.2 and α_2 between 0.1 and 4; E_S and G_S stand for Young's modulus and the shear modulus of the solid, respectively [59].

Also plateau stress (σ_{pl}) and densification strain (ε_D) scale with density as:

$$\sigma_{pl} \approx (0.25.to.0.35).\sigma_{y,s}\left(\frac{\rho}{\rho_s}\right)^m$$

$$\varepsilon_D \approx \left(1-\alpha_2\frac{\rho}{\rho_s}\right)$$

where *m* lies between 1.5 and 2.0 and α_2 between 1.4 and 2 [58].

A remarkable difference in the behavior of close cell foams and open cell foams can be seen in plateau stress. Open cell foams have a well-defined region while the behaviour of closed cell foams is unstable, due to the fact that the cell faces carry membrane stresses (tensile).

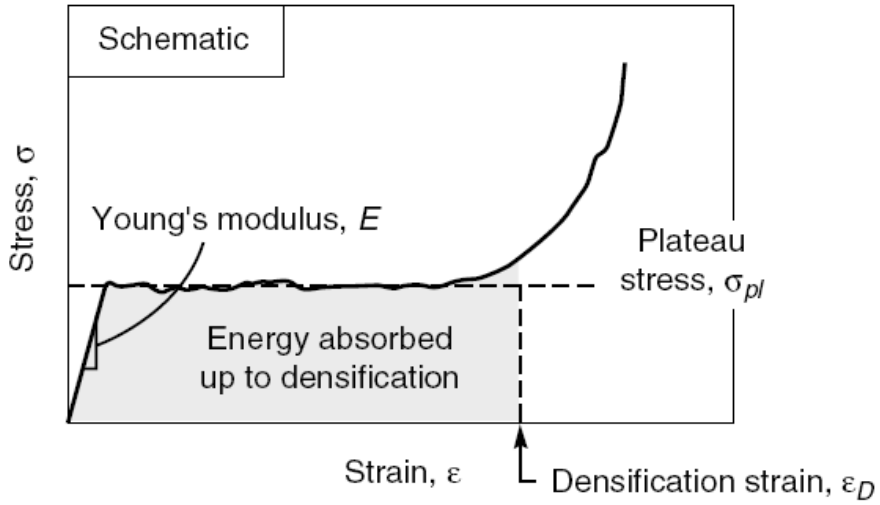

Figure 2.17: Stress-strain curve of a metallic foam under compression [9]

In metal foams, the tensile modulus (E_t) is often greater than the modulus under compression by 10%. The curve's slope before general yield is less than E, implying micro-plasticity even at very small strains, typically 1-4% [1]. Beyond yield (σ_y), metal foams harden up to their ultimate tensile strength (σ_{uts}), beyond which they fail, at tensile ductility (ε_t) [9].

2.5.1.2. Energy Absorbing

By definition, an energy absorber element is a system that totally or partially converts kinetic energy into another form of energy. Energy converted is either reversible (like elastic strain energy in solids) or irreversible (plastic deformation energy). In the transportation industry (crushable elements in cars, high speed rail passenger equipment, airplane fuselage, etc.) main focus is in obtaining of parts that will convert most of the kinetic energy into plastic deformation to minimize any danger to humans and other. Many factors come into play when designing a good energy absorber component, such as load magnitude and method of application, transmission rates, deformation patterns, and, most importantly, the properties of the material. Depending on the material the foam is made from, cell walls will bend plastically, buckle, or fracture [60].

Metallic foams are excellent energy absorbers, since they can support large strains at relatively low constant stress levels. Furthermore, the advantage of the tailoring of its plateau stress level (σ_{pl}) makes them more attractive for the applications as energy absorbers in the automotive industry, since they can take passenger safety

into account, as well as decreasing vehicle weight and therefore reducing fuel consumption [61].

The energy absorbtion capacity per unit volume (E_v) is determined by the area under a strain-stress curve during a certain strain interval (ε_1, ε_2) (see Figure 2.18) and can be calculated by [1]:

$$E_v = \int_{\varepsilon_1}^{\varepsilon_2} \sigma(\varepsilon) d\varepsilon$$

Comparing the two energy absorbers in Figure 2.18, both samples can absorb the same amount of energy; nevertheless, the second sample can absorb it at lower σ^*_{pl}, making it the more suitable absorber.

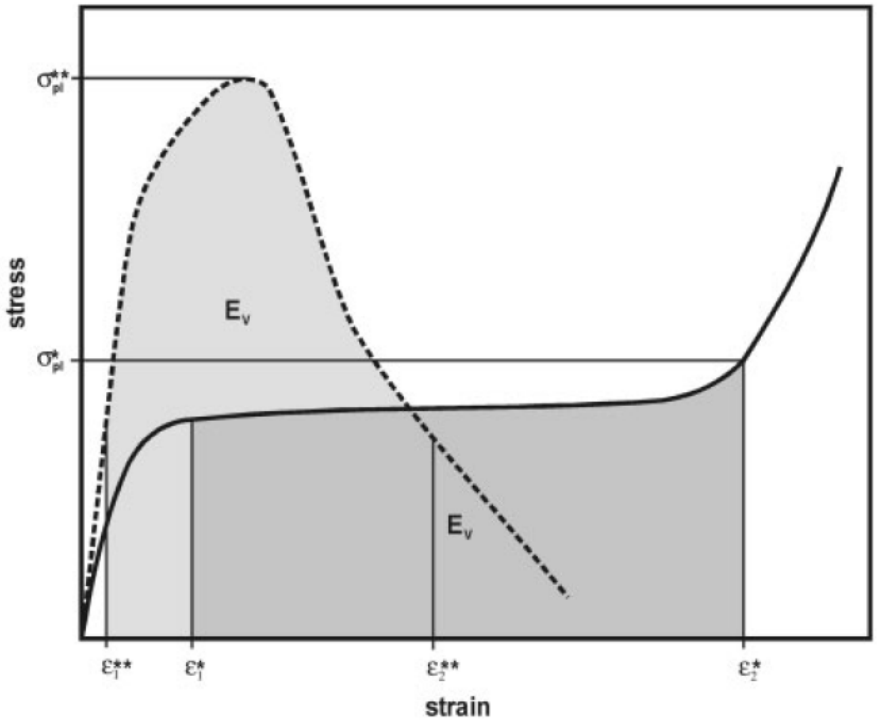

Figure 2.18: Stress- strain curves for 2 different energy absorbers with similar energy absorbed per unit volume [1]

The energy absorption efficiency (η) is a ratio between the energy absorbed by the real material and that absorbed by an ideal plastic material (Figure 2.18), and can be calculated by [1]:

$$\eta = \frac{\int_{\varepsilon_1}^{\varepsilon_2} \sigma(\varepsilon) d\varepsilon}{\sigma_0(\varepsilon_2 - \varepsilon_1)}$$

where σ_0 is the strain when the foam densification begins.

2.5.1.3. Impact Behavior

Transport industries, in particular the automotive industry, have to evaluate energy absorption capability as an impact behavior, since foam properties change at high deformation rates. One example is the evaluation of the head injury criterion (HIC), which involves the impact of a "dummy head" against a foam component inside a car and to determine if it meets vehicle safety standards [62]. Also, many shapes have been evaluated during compression (also called collapse), where the cell morphology and the alloy the foam is made from play an important role (Figure 2.19) [63].

Figure 2.19: Progressive collapse for a) hollow and Al-foam-filled steel tubes, Seitzberger et al. b) Al-foam-filled tubes, Fraunhofer-USA report 1 and c) Al-foam at the location of tube instability, Toksoy et al. [63]

For closed cell foams, two points that must be considered are: 1) the inertial mass of the cell edges and walls, and 2) the gas pressure and gas flow inside the cells, as the effects of these can change the strain rate. Since closed cell foams are not completely closed due to defects generated during its manufacturing process or as it is being deformed (increasing the number of cracks and hence increasing the gas flow between cells). The local strain rate is much higher than the global. As a result, plateau stress is increased when the strain rate increases [1].

2.5.2. Damping insulation

2.5.2.1. Sound Absorption Properties

Under certain conditions foams can damp vibrations and absorb sound. These qualities, combined with their lightweight and good mechanical properties make aluminum foams an attractive candidate for applications in automobile floors and bulkheads [9, 64].

A sound absorbing material is the one that does not reflect or transmit a sound wave; instead it absorbs its energy. Open cell metallic foams are better sound absorbers than closed cell ones [9]. To optimize this property in closed cell foams, rolling or drilling holes through the foam is necessary to break the cells and foam skin so the sound wave can enter and be absorbed instead of being reflected.

Metallic foams' sound absorption capability is also a function of foam thickness, pore size and density; for example the smaller the pores, the greater the absorption efficiency [3]. Although closed-cell metallic foams do not absorb sound as well as

glass wool, sound absorption can be greatly improved at a low cost by just rolling a foam, and their other properties make them attractive for multi-functional applications [1].

2.5.2.2. Structural Damping

Sound waves or mechanical vibrations generate vibrational energy. Aluminum foams have a relatively high damping capacity, since foams are able to convert this energy into thermal energy by internal friction (energy turns into heat and is expelled into the surrounding area). The vibrational energy is dissipated by friction between cracks and vibration of the cell walls, therefore, the thinner the cell walls, the higher the damping [1, 65, 66].

2.5.3. Thermal and Electrical Properties

Once again, the properties of the metallic foam are dependent on its structure. In closed cell foams, heat transport is dominated by solid conduction along the cell walls, so the apparent thermal conductivity depends on cell shape, connectivity, and topology. Heat transport decreases with imperfections such as plateau borders, fractured cell walls, missing cells, cell size variations, solid inclusions, etc. The thermal conductivity of closed cell foams is lower than that of fully dense parts. This is because 90% of the heat is transferred by conduction through gas in the cells while the remaining heat passes through the solid. The metal's contribution to the cellular structure's thermal conductivity (λ_S) can be described by:

$$\lambda_S = \lambda_0 \left(\frac{\rho}{\rho_0} \right)^t$$

where λ_0 represents the solid metal's thermal conductivity, ρ/ρ_0 the foam's relative density, and *t* is a constant that varies from 1.65 to 1.8 depending on the foam structure [1, 67].

A similar scenario is presented for electrical properties, where the metal foam's electrical resistivity varies with its density. The electrical conductivity (σ) and density (ρ) of the foam itself are related to those (σ_0, ρ_0) of the cell wall material as follows:

$$\frac{\sigma}{\sigma_0} = z \left(\frac{\rho}{\rho_0} \right)^t$$

where *t* can vary between 1 and 1.85 (depending on the foam structure) and the constant z is likely to be 1 [1].

2.6. **Industrial Interest**

Industrial requirements for cellular metals vary according to the presented cell morphology (open to close), the material from which it is produced, and its processing cost. Taking these into consideration, it is possible to classify cellular metals according to their porosity and their application as shown in Figure 2.20 [2]. Automotive, aerospace, building, and even biomedical industries are more focused on structural applications. Functional applications include filtering, use in heat exchangers, acoustic control and some electrochemical applications.

Metal foams have numerous promising properties, but their multifunctional capabilities is what makes them most attractive; for example, they can be used for sound absorption in rooms where inflammability is vital, or as car body parts that deform to protect passengers as well as reducing fuel consumption due to decreased weight, etc.

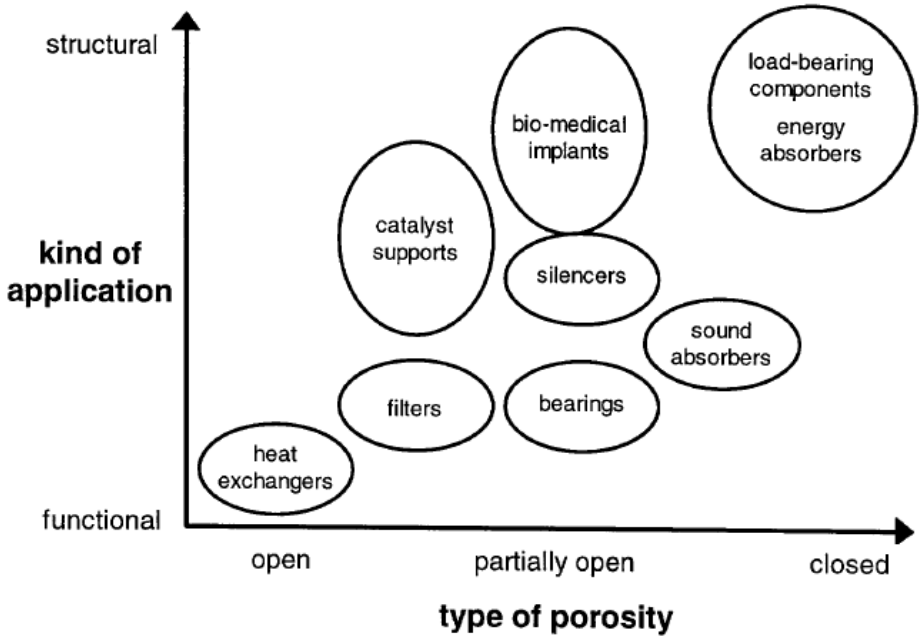

Figure 2.20: Application of cellular metals according to their porosity [2]

2.6.1. Automotive Industry

The automotive industry has a special interest in using metallic foams, because they can substitute heavy parts with light metallic foam, which has a high stiffness to weight ratio, consequently reducing fuel consumption. Aluminum foam structures or foam sandwich panels can be potentially incorporated into car frames, hoods and sliding roofs. Parts requiring energy absorption and impact energy dissipation include bumpers, crash boxes and A- and B- pillars. These

make the car safer for the driver in case of accident. Also, most car parts are required to damp sound and vibration while being heat resistant [68]. Some part applications are illustrated in Figure 2.21 [14].

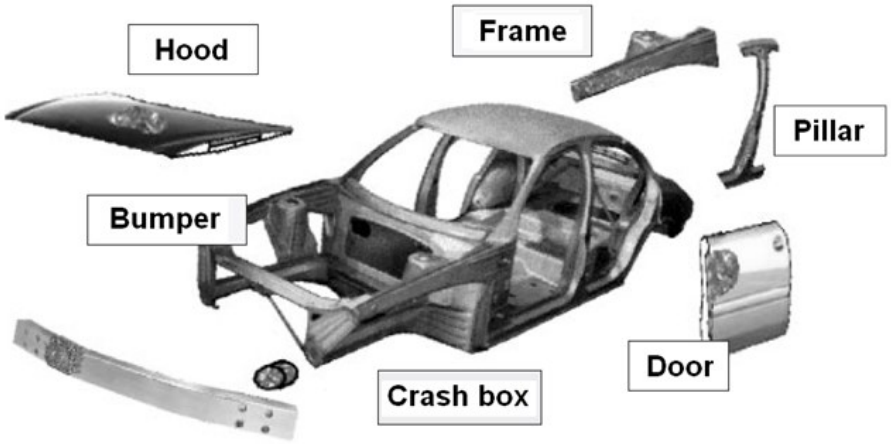

Figure 2.21: Anticipated applications of aluminium foams in the automotive industry

2.6.2. Aerospace Industry and Others

In the aerospace industry, honeycomb structures can be replaced by metallic foams (which cost less), offering properties such as improved fire retardation and structural integrity. Also, these foams can be fabricated with curvatures, in contrast to the generally flat honeycomb. High stiffness and damping are important in structural parts such as turbines. Space technology has evaluated aluminum foams for different applications, such as energy absorbing crash elements for space vehicle landing pads and reinforcement for load bearing structures in satellites. Boeing has evaluated the use of titanium foam sandwich parts and aluminum sandwiches with aluminum foam core for tail booms of helicopters [2].

The different applications of foams depend on the matrix material and its properties. For example, while gold and silver may be used in batteries, nickel and titanium may be used for biomedical purposes [69].

References

1. Degishcher, H.-P. and B. Kriszt, eds. *Handbook of Cellular Metals: Production, Processing and Applications*. 2002, WILEY-VCH Verlag Gmbh.

2. Banhart, J., *Manufacture, characterisation and application of cellular metals and metal foams.* Progress in Materials Science, 2001. **46**(6): p. 559-632.

3. Davies, G.J. and S. Zhen, *Metallic Foams: Their Production, Properties and Applications.* Journal of Materials Science, 1983. **18**(7): p. 1899-1911.

4. Srivastava, V.C. and K.L. Sahoo, *Processing, stabilization and applications of metallic foams. Art of science.* Materials Science, 2007. **25**(3): p. 733-753.

5. Miyoshi, T., et al., *ALPORAS Aluminium Foam: Production Process, Properties and Applications.* Advanced Engineering Materials, 2002. **2**(4): p. 179-183.

6. Onck, P.R., et al., *Fracture of open- and closed-cell metal foams.* Journal of Materials Science, 2005. **40**(22): p. 5821-8.

7. Shapovalov, V. and L. Boyko, *Gasar-- A new Class of Porous Materials.* Advanced Engineering Materials, 2004. **6**(6): p. 407-410.

8. Amjad, S., *Thermal Conductivity and Noise Attenuation in Aluminum Foams*, 2001, University of Cambridge.

9. Ashby, M.F., et al., eds. *Metal Foams: A Design Guide*. 2000, Butterworth-Heinenann: Boston.

10. Grant, P.S., *Spray Forming.* Progress in Materials Science, 1995. **39**: p. 497-545.

11. Kennedy, A.R., *The effect of compaction on expansion and gas release in Al-TiH_2 powder compacts.* Materials Science Forum, 2003. **416-418**(1): p. 299-304.

12. Asavavisithchai, S. and A.R. Kennedy, *The effect of compaction method on the expansion and stability of aluminium foams.* Advanced Engineering Materials, 2006. **8**(9): p. 810-815.

13. Bhosle, V., et al., *Dehydrogenation of TiH_2.* Materials and Engineering, 2003. **A**(356): p. 190-199.

14. Ito, K. and H. Kobayashi, *Production and Fabrication Technology Development of Aluminum Useful for Automobile Lightweighting.* Advanced Engineering Materials, 2006. **8**(9): p. 828-835.

15. Banhart, J., *Manufacturing Routes for Metallic Foams.* Journal of Metals, 2000. **52**(12): p. 22-27.

16. Ibrahim, A., C. Körner, and R.F. Singer, *The Effect of TiH_2 Particle Size on the Morphology of Al-Foam Produced by PM Process.* Advanced Engineering Materials, 2008. **10**(9): p. 845-848.

17. Matijasevic, B. and J. Banhart, *Improvement of aluminium foam technology by tailoring of blowing agent.* Scripta Materialia, 2006. **54**(4 SPEC ISS): p. 503-508.

18. Matijasevic-Lux, B., et al., *Modification of titanium hydride for improved aluminium foam manufacture.* Acta Materialia, 2006. **54**(7): p. 1887-1900.

19. Baumgartner, F., I. Duarte, and J. Banhart, *Industrialization of Powder Compact Foaming Process.* Advanced Engineering Materials, 2000. **2**(4): p. 168-174.

20. Banhart, J., *Metal Foams: Production and Stability***.* Advanced Engineering Materials, 2006. **8**(9): p. 781-794.

21. Babcsan, N., D. Leitlmeier, and J. Banhart, *Metal Foams---high temperature colloids Part I. Ex situ analysis of metal foams.* Colloids and Surfaces A: Physicochemical and Engineering Aspects, 2005. **261**: p. 123-130.

22. Babcsan, N., D. Leitlmeier, and H.P. Degischer, *Foamability of Particle Reinforced Aluminum Melt.* Mat.-wiss. u. Werkstofftech., 2003. **34**: p. 22-29.

23. Hunter, T.N., et al., *The role of particles in stabilising foams and emulsions.* Advances in Colloid and Interface Science, 2008. **137**: p. 57-81.

24. Gergely, V., R.L. Jones, and T.W. Clyne, *The effect of capillarity-driven melt flow and size of particles in cell faces on metal foam structure evolution.* Transactions of JWRI, 2001. **30**(Special Issue): p. 371-376.

25. Ip, S.W., Y. Wang, and J.M. Toguri, *Aluminum foam stabilization by solid particles.* Canadian Metallurgical Quaterly, 1999. **38**.

26. Kaptay, G., *Interfacial criteria for stabilization of liquid foams by solid particles.* Colloids and Surfaces A: Physicochemical and Engineering Aspects, 2004. **230**(1-3): p. 67-80.

27. Haibel, A., A. Rack, and J. Banhart, *Why are metal foams stable?* Applied Physics Letters, 2006. **89**(154102): p. 1-3.

28. Kumar, G. and K.N. Prabhu, *Review of non-reactive and reactive wetting of liquids on surfaces.* Advances in Colloid and Interface Science, 2007. **133**(2): p. 61-89.

29. Kennedy, A.R. and S. Asavavisitchai, *Effects of TiB_2 particle adddition on the expansion, structure and mechanical properties of PM Al foams.* Scripta Materialia, 2004. **50**: p. 115-119.

30. Asavavisithchai, S. and A.R. Kennedy, *Effect of powder oxide content on the expansion and stability of PM-route Al foams.* Journal of Colloid and Interface Science, 2006. **297**(2): p. 715-723.

31. Korner, C., *Foam formation mechanisms in particle suspensions applied to metal foams.* Materials Science and Engineering: A (Structural Materials: Properties, Microstructure and Processing), 2008. **495**(1-2): p. 227-35.

32. Korner, C., M. Arnold, and R.F. Singer, *Metal foam stabilization by oxide network particles.* Materials Science & Engineering A (Structural Materials: Properties, Microstructure and Processing), 2005. **396**(1-2): p. 28-40.

33. Hatch, J.E., *Aluminum : properties and physical metallurgy* ed. M. Park1984, Ohio: American Society for Metals. 274.

34. Dobrazanski, L.A., K. Labisz, and A. Olsen, *Microstructure and mechanical properties of the Al-Ti alloy with calcium addition.* Journal of

Achivements in Materials and Manufacturing Engineering, 2008. **26**(2): p. 183-186.

35. Kim, A., S.-S. Cho, and H.-J. Lee, *Foaming behaviour of Al-Si-Cu-Mg alloys.* Materials Science and Technology, 2004. **20**(12): p. 1615-1620.

36. Lehmhus, D. and M. Busse, *Potential new matrix alloys for production of PM aluminium foams.* Advanced Engineering Materials, 2004. **6**(6): p. 391-396.

37. Bishop, D.P., et al., *Diffusion-based microalloying of aluminium alloys by powder metallurgy and reaction sintering.* Journal of Materials Science, 1998. **33**: p. 3927-3934.

38. Kanetake, N. and M. Kobashi, *Innovative processing of porous and cellular materials by chemical reaction.* Scripta Materialia, 2006. **54**(4): p. 521-525.

39. Kobashi, M. and N. Kanetake, *Processing of intermetallic foam by combustion reaction.* Advanced Engineering Materials, 2002. **4**(10): p. 745-7.

40. Gupta, D., *Diffusion Processes inAdvanced Technological Materials*2005, New York: William Andrew publishing. 532.

41. Schaffer, G.B., et al., *The effect of trace elements on the sintering of an Al–Zn–Mg–Cu ALLOY.* Acta Materialia, 2001. **49**(14): p. 2671-2678.

42. Schaffer, G.B., T.B. Sercombe, and R.N. Lumley, *Liquid phase sintering of aluminium alloys.* Materials Chemistry and Physics, 2001. **67**(1–3): p. 85-91.

43. Ma, C.H. and R.A. Swalin, *A study of solute diffusion in liquid tin.* Acta Metallurgica, 1960. **8**(6): p. 388-395.

44. German, R.M., *Chapter Nine - Sintering With a Liquid Phase*, in *Sintering: from Empirical Observations to Scientific Principles*, R.M. German, Editor 2014, Butterworth-Heinemann: Boston. p. 247-303.

45. Greenwood, G.W., *The growth of dispersed precipitates in solutions.* Acta Metallurgica, 1956. **4**(3): p. 243-248.

46. Evans, E.B., et al., *Effect of Inclusion Size on Grain Boundary Wetting in Al-Sn Alloys.* Applied Physics A: Solids and Surfaces, 1987. **42**(4): p. 269-272.

47. Eisenmenger-Sittner, C., et al., *Solid-state wetting and spreading of tin (Sn) on aluminium interfaces.* Vacuum, 2003. **71**: p. 253-259.

48. Eisenmenger-Sittner, C., et al., *Experimental studies of solid state surface wetting of tin (Sn) on aluminium.* Applied Surface Science, 2006. **252**: p. 5466-5469.

49. Wang, D.N., et al., *Effects of Sn additions on the microstructures and tensile properties of two-phase TiAl alloys.* Intermetallics, 1996. **4**(3): p. 191-200.

50. Tkachuk, A.V., et al., *Isothermal section of the Ti-Mn-Sn system and crystal structure of the TiMnSn4 compound.* Journal of Alloys and Compounds, 2000. **312**(1-2): p. 284-287.

51. Sercombe, T.B. and G.B. Schaffer, *On the role of tin in the infiltration of aluminium by aluminium for rapid prototyping applications.* Scripta Materialia, 2004. **51**: p. 905-908.

52. Sercombe, T.B. and G.B. Schaffer, *On the role of tin in the nitridation of aluminium powder.* Scripta Materialia, 2006. **55**: p. 323-326.

53. Schwilm, T., O.T. Inal, and F.G. Yost. *Tin-based active metal brazes for the joining of alumina*. 1997. Orlando, FL, USA: Minerals, Metals & Materials Soc (TMS), Warrendale, PA, USA.

54. Kipouros, G.J., W.F. Caley, and D.P. Bishop, *On the Advantages of Using Powder Metallurgy in New Light Metal Alloy Design.* Metallurgical and Materials Transactions A, 2006. **37A**: p. 3429-3437.

55. Gibson, L.J., ed. *Cellular solids: structure and properties*. ed. L.J. Gibson and M.F. Ashby1997, Cambridge University Press: New York.

56. Feng, Y., et al., *Strain rate effects on the compressive property and the energy-absorbing capacity of aluminum alloy foams.* Materials Characterization, 2001. **47**(5): p. 417-22.

57. Beals, J.T. and M.S. Thompson, *Density gradient effects on aluminium foam compression behaviour.* Journal of Materials Science, 1997. **32**(13): p. 3595-600.

58. Ashby, M.F. and L.U. Tianjian, *Metal Foams: A Survey.* Science in China (Series B), 2003. **46**(6): p. 521-532.

59. Papadopolus, D.P., et al., *Mechanical Properties of Al Metal Foams.* Materials Letters, 2004. **58**(21): p. 2574-2578.

60. Alghamdi, A.A.A., *Collapsible Impact Energy Absorbers: An Overview.* Thin-Walled Structures, 2001. **39**: p. 189-213.

61. Baumeister, J., J. Banhart, and M. Weber, *Aluminum Foams for Transport Industry.* Materials and Design, 1997. **18**(4/6): p. 217-220.

62. Kretz, R., K. Hausberger, and B. Götzinger, *Energy-Absorbing Behavior of Aluminum Foams: Head Impact Tests on the A-Pillar of a Car.* Advanced Engineering Materials, 2002. **4**(10): p. 781-785.

63. Lopatnikov, S.L., B.A. Gama, and J.J.W. Gillespie, *Modeling the progressive collapse behavior of metal foams.* International Journal of Impact Engineering, 2007. **34**(3): p. 587-595.

64. Lu, T.J., A. Hess, and M.F. Ashby, *Sound absorption in metallic foams.* Journal of Applied Physics, 1999. **85**(11): p. 7528-7539.

65. Simancik, F., H.P. Degischer, and H. Worz, *Foamed Aluminum- Light structural and Insulation Material*, in *Euromat '95, Assozizzione Italiana di Metallurgica, Milano*1995: Venice/Padua.

66. Han, F., et al., *Damping Behaviour of Foamed Aluminum.* Metallurgical and Materials Transactions A, 1999. **30A**: p. 771-776.

67. J.lu, T. and C. Chen, *Thermal Transport and Fire Retardance Properties of Cellular Alluminum Alloys.* Acta mater., 1999. **47**(5): p. 1469-1485.

68. Fuganti, A., et al., *Aluminium foam for automotive applications.* Advanced Engineering Materials, 2000. **2**(4): p. 200-204.

69. Yu, C.J., et al., *Metal foaming by a powder metallurgy method: production, properties and applications.* Materials Research Innovations, 1998. **2**(3): p. 181-8.

Chapter 3

Experimental Procedure

Initial thermodynamic calculations were used to identify Sn as a suitable alloying element for stabilizing Al foams, and then third element additions were included in the selection process and alloy design. The third element was added to Al-Sn foams with the objective of creating in situ intermetallics. These intermetallics would play a role in the foam's micro and macro structure. Subsequently, foam characterization was performed using destructive and non-destructive methods. Finally, foams were tested mechanically under compression.

3.1. **Material Selection**

3.1.1. Thermodynamic calculations (FactSage analysis)

A large variety of elements that react with aluminum or tin can be identified from phase diagrams. In this work, the aim is to stabilize the metallic foam by forming in situ intermetallics. Therefore, thermodynamic modeling was done using FactSage™ 6.0 software to evaluate a series of powders that could form intermetallics either with aluminum or with tin during the foaming process.

Intermetallics can have different shapes, sizes and distribution through the metal foam's cell-walls. These variations are primarily consequences of foaming temperature and time (in order to reach equilibrium conditions) and the diffusion coefficient of the different alloying elements at the processing temperature.

All thermodynamic calculations were done under the "Equilibrium" module of the FactSage software. The reactants were added as 1 gram (100%) of the total metallic mixture plus 0.01 grams (1%) of TiH_2. The databases applied were Fact53 and FTlite. For the products, selected solids and ideal gas species were checked. The simulation was run from room temperature to 750 °C every 5 °C at a pressure of 1 atm. These results were plotted to analyze the amount of liquid and solid compounds formed after each interaction.

To verify whether the formation of the intermetallic occurs during heating or cooling, the liquid remaining from the last heating step (750 °C) can be saved as a stream file and reloaded in the reactant box. Simulating Scheil cooling with a step of 25 °C and plotting these results gives the amount of intermetallics that form as the temperature decreases.

3.2. **Powder Compact Melting Technique**

As described in the powder compact melting technique (Chapter 2, section 2.2), there are 3 main steps involved in obtaining metallic foams from powders: powder mixing, compaction, and foaming.

3.2.1. Powder mixing

A variety of high purity (>99.5%) metal powders with a -325 mesh were used as raw materials. Titanium hydride (99.0% purity, -325 mesh) was added as a foaming agent for all metal mixtures, and lithium stearate was applied directly to the die for lubrication. All powders were purchased from Alfa-Aesar. Each powder's characteristics as given by the supplier are listed in Table 3.1.

Table 3.1. Characteristics of powders used in the present study.

Powder	Al	Sn	Ni	Co	Ti	Mg	TiH_2
Metal basis, %	99.5	99.8	99.5	99.5	99.5	99.5	99
Particle size	----------Less than 45 microns----------						

* The oxygen amount in Al powder was analyzed using a LECO TCH600 simultaneous nitrogen/oxygen/hydrogen analyzer. The oxygen content of the Al powders in this study was 0.41wt.%.

First, the desired metal powder or combination of powders were weighted along with 1wt.% of TiH_2. Then, the powder mixture was loaded into a plastic container with alumina balls (3:1 ball to powder ratio) and filling the container volume up to 50% in order to ensure homogeneous mixing. The container was put on a tumbler mixer for 20 min. Finally, powders were separated from the alumina balls using a metal grid.

3.2.2. Compaction

The size of the compact was determined applying the rule of mixtures. With this formula it is possible to know the required weight of powder mixture in order to reach a standardized volume, depending on the test performed.

$$\frac{1}{\rho_m} = x_a \frac{1}{\rho_a} + x_b \frac{1}{\rho_b} + x_c \frac{1}{\rho_c} \qquad \text{Rule of mixtures}$$

where ρ_m is the theoretical density of the mixture, ρ_a, ρ_b and ρ_c are the densities and x_a, x_b and x_c are the weight fraction of the different powders.

The powders were cold and/or hot uniaxially pressed depending on the test. Time, pressure and temperature were varied to obtain the optimum conditions. As known from previous studies, precursors with theoretical densities above 94% are

required for powder metallurgy foams [1] but optimum foaming is achieved with compacts >99% of their theoretical density [1, 2].

3.2.3. Foaming

Depending on the composition of the precursor, different heat treatments were applied; always at a temperature slightly above the melting point of the alloy. The foaming configuration was another variable:

-Free foaming: the precursor was placed on an alumina plate and heat-treated in a Lindberg/Blue M box furnace

-Constrained foaming: the precursor was placed in an alumina crucible and heat-treated in a box furnace. Multiple precursors were also tested simultaneously under this configuration.

-Expandometer: At McGill's mechanical expandometer, the precursor was placed in a preheated stainless steel crucible coated with boron nitride (to facilitate sample removal) that is suspended inside a vertical tube furnace. A counterweighted piston lays on top of the precursor as a laser records its displacement registering foam expansion versus foaming time. Two 1° tapered crucibles were used: one with a 2 cm and one with a 3 cm internal bottom diameter. The 15 cm height was chosen for both crucibles so the compact could sit on the hottest part of the tube furnace. A schematic representation of this equipment is shown in Figure 3.1 [3].

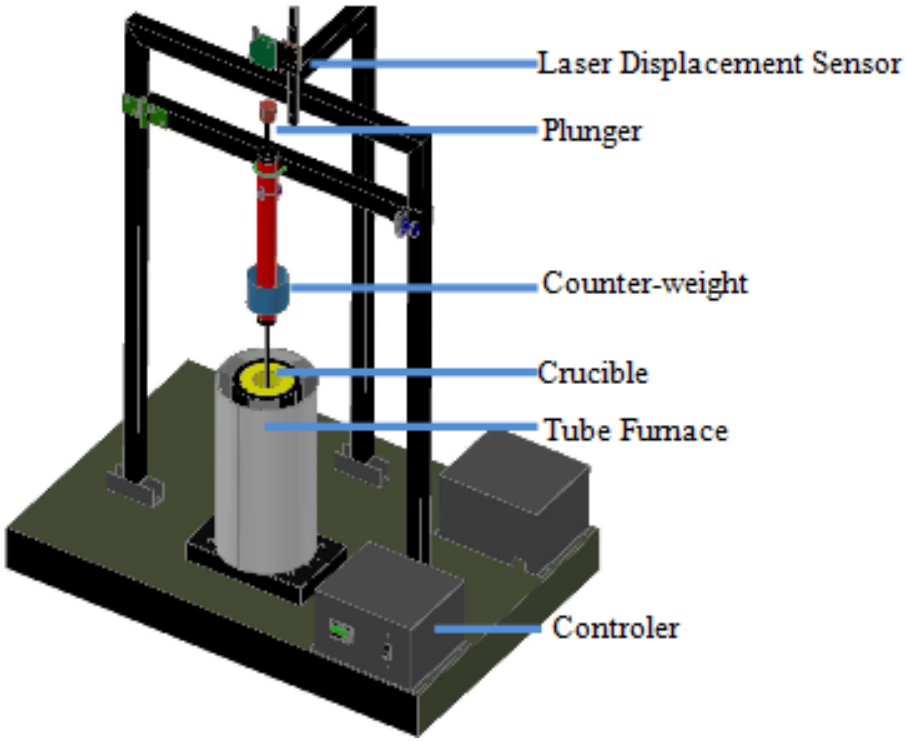

Figure 3.1: Schematic of the mechanical expandometer

3.3. **Compression test**

Foams with diameters of 3.4 cm were machined, removing the top, bottom and/or skin (external layer). The cylinder height was chosen according to each alloy's optimal expansion, and to minimize density gradients. The machined cylinders were crushed uniaxially on an MTS[2] compression machine at a constant strain rate up to 100kN. A layer of mica coated with boron nitride between the anvils (7.5cm diameter) and the sample was used to prevent friction or sample sticking. For each alloy's optimal condition, 3 samples were tested.

[2] MTS is a trademark of MTS systems corporation, Eden Prairie MN

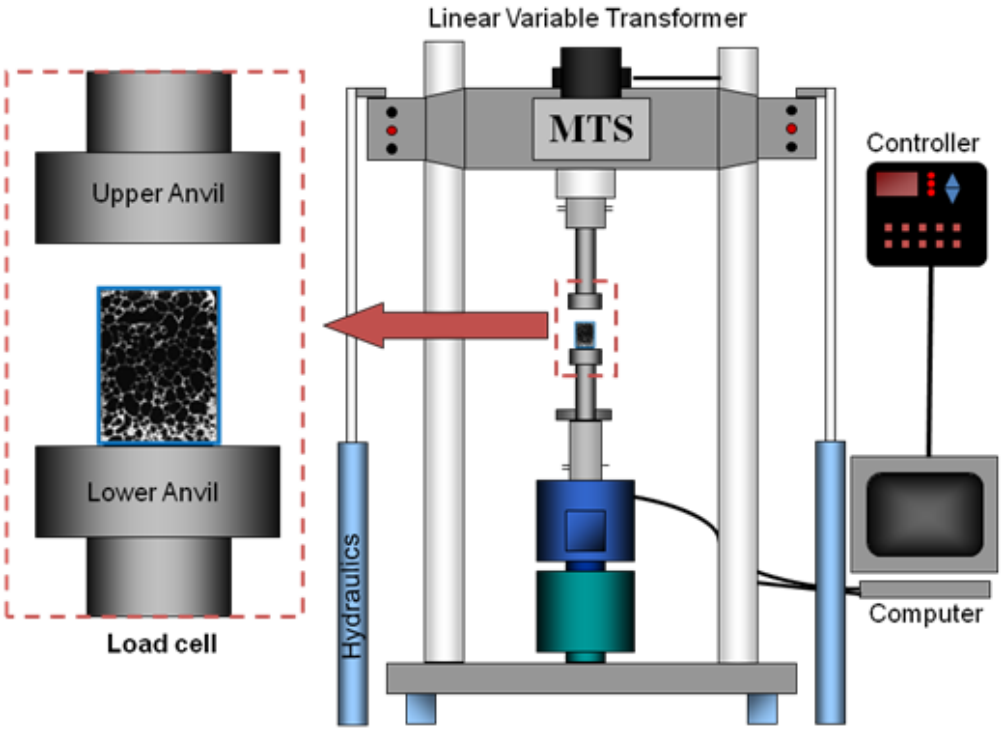

Figure 3.2: Schematic of MTS compression machine

3.4. **Characterization techniques**

Characterizations of the different powders (as received) as well as the resulting foams were achieved as follows.

3.4.1. Differential Scanning Calorimetric Analysis

The powder mixtures were characterized using a differential scanning calorimetric analysis (DSC) done in a Setaram Evolution 24 thermo-gravimetric analyzer to corroborate the melting point of the powders used in the powder metallurgy technique, and to establish whether any reaction occurred. The scanning rate and sample mass were kept constant at 10 °C/min and 20mg, respectively. Samples were placed in alumina crucibles and run under a high purity argon flow.

3.4.2. Optical Microscopy

For optical image analysis, foam cross sections were obtained using an Isomet diamond saw cutting machine. The samples' pores were spray painted black to increase contrast from the cell walls that were ground with SiC paper (400 to 1200 mesh), polished with diamond paste (down to 1 micron) and cleaned in an ultrasonic bath. Digital pictures were taken and edited in Adobe®Photoshop®CS software to improve the pores' contrast with the cell walls and background. To analyze pore shape, size and distribution, an image analysis program was designed using Clemex Vision® software (Professional Edition 5.0).

3.4.3. Scanning Electron Microscopy

Microstructural analysis of foamable precursors and foams' transverse sections were observed using a variable pressure scanning electron microscope (VP-SEM, Hitachi S-3000N). The tests were done under vacuum where a maximum resolution of 3 nm can be attained at 25 kV. Samples were prepared in a similar manner to those used for the optical microscopy. No etching was required since the elements involved in the process have different atomic numbers and can be easily identified by SEM. The VP-SEM is equipped with an energy dispersive spectroscopy (EDS) detector connected to the Oxford INCA system for spot analysis, line scan, and mapping. The operating voltage was 15 kV. The elemental distribution and compounds can be identified easily. A JEOL 8900 electron probe microscope (EPMA) was also used for more accurate compound composition and mapping.

3.4.4. X-Ray Diffraction

Powder composition was studied using an XRD Rigaku Rotaflex Ru-200B with a $CuK\alpha_1$ radiation source (λ=1.54 Å), and operated at 4.8 kW. The acquisition time was 0.5 s per step at $0.01°s^{-1}$ from 10 to 110°.

3.4.5. Density Measurments and Foam Expansion

Density measurements were performed using Archimedes' principle. In this method the porous material's weight is measured and its volume is obtained by measuring its buoyancy in a liquid of a given density. The metallic foam presents primarily closed porosity, but some pores are opened during the cooling stage. Therefore, the foam was coated with a polymer to prevent liquid from entering the pores.

Foam expansion can be calculated by correlating the precursor's initial volume and the foam's final volume. These data are given using Archimedes' principle (when foaming happened in a box furnace as free foaming) or directly recorded from the expandometer. In the latter case, the foaming process can be interrupted at any point as the laser registers the foam's height; the foam takes the shape of the crucible, whose shape and volume are known.

3.4.6. X-Ray Tomographer

Non destructive analysis was performed using a Skyscan 1172 scanner, including the Skyscan™ CT-analyzer software, which calculates morphometric parameters from binarised cross-section images (2D), or the addition of these images, resulting in 3D data. For the foams, 2D cross-sections (region of interest) were done first, followed by 3D measurements (volume of interest) such as porosity.

References

1. Kennedy, A.R., *The effect of compaction on expansion and gas release in Al-TiH_2 powder compacts*. Materials Science Forum, 2003. 416-418(1): p. 299-304.

2. Asavavisithchai, S. and A.R. Kennedy, *The effect of compaction method on the expansion and stability of aluminium foams*. Advanced Engineering Materials, 2006. 8(9): p. 810-815.

3. LaFrance, M., Isothermal *stabilization of Al-Zn foams*, in Mining and Materials Engineering. 2010, PhD Thesis. McGill University: Montreal.

Chapter 4

Foaming Behavior of Powder Metallurgical Al-Sn Foams

Lydia Y. Aguirre-Perales[a], In-Ho Jung[a*], Robin A. L. Drew[a,b]

[a] Department of Mining and Materials Engineering, McGill University, 3610 University Street, Montreal, Qc, H3A 2B2, Canada

[b] Departament of Mechanical and Industrial Engineering, Concordia University, 1455 de Maisonneuve Blvd. W., Montreal, Qc, H3G 1M8, Canada

Corresponding author:
Prof. In-Ho JUNG
E-mail: in-ho.jung@mcgill.ca
Tel: 1-514- 398-2608 Fax: 1-514-398-4492

Published in:

Acta Materialia 2012, vol. 60 (2), pp. 759-69.

As the first author of this manuscript, the Ph.D. candidate performed the experiments, analysis and calculations calculations and wrote the manuscript. Prof. Robin A. L. Drew and Prof. In-Ho Jung as thesis directors contributed to critical analysis and supervision of this work.

In this chapter the influence of Sn on Al foam processing is reported. The effect of Sn on Al surface tension and solid solution is explained. Process parameter optimization of Al-Sn foams was carried out to obtain an Al-Sn optimum foam.

Abstract

Foaming Al by the powder metallurgy technique was investigated with Sn additions (≤5wt.%). The low melting point of Sn and its immiscibility with Al creates integrity of the powder mixture during hot compaction and foaming. Furthermore, it decreases the surface tension of Al, reducing pore coalescence. Different alloying compositions, pressing and foaming parameters were evaluated. The materials were characterized using differential scanning calorimetry and thermodynamic simulation. Foam expansion and pore shape were studied by the construction of expansion maps and image analysis on foam cross-sections. It was established that with Sn additions, not only is foaming possible at lower temperatures, but also the Sn stabilizes the foam preventing collapse. The number of pores and sphericity values increased with increasing Sn concentrations. Optimized process parameters leading to an expansion of 375% for up to 10 min were achieved with 2–3wt.% Sn additions, hot pressing at 300 ^{o}C followed by foaming at 725 ^{o}C.

4.1. **Introduction**

Aluminum foams offer excellent strength and stiffness to weight ratios, high mechanical energy absorption, and good acoustic and thermal insulating properties [1]. These excellent properties have attracted and maintained the interest of automotive industry for applications such as crash boxes, frames, bumpers, and hoods [2].

Among a variety of routes used to fabricate aluminum foams, powder metallurgy has proven to be one of the most promising techniques for the production of net-

shape foams. In this method, pure Al or Al-based alloy powders are mixed with a blowing agent and then compacted to high density (>94%) [3, 4].

In the powder metallurgy process, foaming usually happens above the melting temperature of the alloy [3]. The major drawback with the process is the mismatch between the decomposition temperature of the blowing agent (typically about 450–650 ^{o}C for titanium hydride) and the melting point of Al (660 ^{o}C) or Al alloy, which can lead to crack-like pore formation and hydrogen loss prior to foaming [5]. Foaming of Al at a high temperature (~800 ^{o}C) also causes other problems such as pore coalescence and metal drainage [3].

In order to overcome the large mismatch between the blowing agent decomposition and the melting of the Al matrix temperatures, many researchers have focused either on increasing the decomposition temperature of the blowing agent or decreasing the melting temperature of the alloy employed. To increase the decomposition temperature of TiH_2, the as received powders are heat-treated under an air atmosphere, which causes a delay in decomposition due to the formation of layered Ti oxides around TiH_2 [5-9]. To decrease the melting temperature of Al matrix, Cu, Si, Mg or Zn are commonly alloyed [10], and the alloys with larger two phase region (semisolid, or solid + liquid region), e.g. Al-9wt.%Si-3wt.%Cu with a two-phase region ranging between 490 and 600 ^{o}C are better for foaming, as the decomposition of TiH_2 can occur in the semisolid state [10, 11].

In the present study, the influence of Sn on Al foam processing was investigated. Sn has proven to be beneficial in the extrusion of Pb–Sn powder mixtures at the melting temperature of Sn (232 ^{o}C) during the production of Pb–Sn foams [12]. Previously, the present authors found an improvement during the dehydrogenation process of TiH_2 in Al foams containing Sn [13] In the present study, the influence of Sn on the processing temperature, foam expansion and foam stability of Al foam are investigated, in detail, with Sn contents of 1, 3 and 5wt.%.

4.2. **Experimental procedures**

Al–Sn foams were produced using Al, Sn and TiH_2 powders (provided by Alfa Aesar) with purities of 99.5, 99.8 and 99%, respectively, and with particle sizes all less than 44 μm. The oxygen content of Al powders was determined with a LECO TCH600 simultaneous nitrogen/oxygen/hydrogen analyzer. It is known that a moderate oxide content (O = 0.3–0.6wt.%) can improve foam stability and produce a homogeneous cell structure [14]. The oxygen content of the Al powders in this study was 0.41wt.% which falls into this range.

The TiH_2 used was previously characterized by a thermo-gravimetric (TG) analysis which recorded a weight loss in the range of 460 and 700 ^{o}C; the derivative of the TG (DTG) curve showed dehydrogenation occurring in two steps with main peaks at 508 and 540 ^{o}C, the last one having the highest desorption [15].

For the powder metallurgy technique, first, the mixtures of powders were prepared using a tumbler mixer for 20 minutes. Next, a compaction of the powder was performed to prepare precursors with identical dimensions for all

compositions (Al–1wt.%TiH_2 with 0, 1, 3 and 5wt.%Sn). Finally, the precursors were heat treated at different temperatures (700, 725 and 750 ^oC) inside a box furnace.

4.2.1. Differential scanning calorimetry (DSC) experiments

The powder mixture characterization of loose powders and precursors (compacted powders) were carried out using a Setaram Evolution 24 differential scanning calorimeter, to corroborate the powders' melting points and other reaction temperatures. The temperature cycle was run twice with a scanning rate of 10 ^oC per min in an argon atmosphere, and 20 mg of samples was used employing alumina crucibles.

4.2.2. Foaming Experiments

Initially, Al powders were combined with 0 (reference), 1, 3 and 5wt.%Sn along with 1wt.% of TiH_2. To obtain precursors with a constant volume (0.71 cm in height and 2 cm in diameter), the amount of powders necessary was calculated using the theoretical density (ρ_{theo} in g/cc) of each component. Then, the powder mixtures were loaded into a steel die and kept in a hot press (200 and 300 ^oC) for 20 min to ensure the homogenization of temperature through the die and powders, and a uniaxial load of 550 MPa was applied for an additional 10 min to densify the powders. Finally, the precursors were unloaded and cooled in air.

For the foaming tests, the precursors were placed individually on an alumina plate and put into a preheated Lindberg/Blue M furnace. The furnace temperature was set at 700, 725 or 750 ^oC and the foaming time was established immediately after loading the sample in the furnace. Although it was not possible to measure the

sample temperature directly, from our experience, we estimated that it took about 12 min to reach the target temperature [13]. The precursors were foamed for given times and removed immediately to cool in air. Experiments for each condition were repeated three times to confirm the reproducibility.

4.2.3. Characterization

The density of the precursor was calculated from its weight and volume measurements. For the foam, the density was obtained using the Archimedes principle: the foam was coated with an impervious polymer film prior to its submersion in water. The volume expansion from precursor to foam was calculated based on the measured densities.

For optical image analysis and scanning electron microscopy, foams were cut using an Isomet diamond saw. The sample preparation consisted of grinding, polishing and cleaning in an ultrasonic bath. To measure the shape and number of pores, image analysis with Clemex Vision PE/Lite™ 3.5 system was employed. Pictures taken from the foam cross sections were edited before the image analysis to accurately measure the pore characteristics.

4.2.4. Thermodynamic Calculations

Thermodynamic calculations were performed using the FactSage™ 6.1 software [16] with FTlite and FACT53 databases in order to investigate the chemical reactions occurring for different alloys. FTlite database contains the optimized model parameters for all solid and liquid phases of binary Al–Sn, Al–Ti and Sn–Ti systems. The database also contains thermodynamic data for the Al–H system. All possible gas species and solid stoichiometric TiH_2 were selected from

FACT53 database. These databases are adequate to simulate the chemical reactions in the present study.

4.3. **Results and discussion**

4.3.1. Thermodynamic and DSC analyses

One of the key technologies to produce highly porous Al foams is to synchronize the melting of the Al matrix with the decomposition of TiH_2. In addition, if there is sufficient amount of liquid available during the release of $H_2(g)$, H_2 will form spherical pores rather than crack-like pores and more H_2 can be retained in the Al foam [8, 17]. In order to realize this idea, Sn was chosen as an alloying element for the present study and the thermodynamic calculations were first performed to understand the influence of Sn in the Al foaming behavior.

Figure 4.1 presents the calculated Al–Sn phase diagram from FTlite database [16]. Al–Sn system is a simple binary with solid Al (fcc), solid Sn (bct) and liquid phase with eutectic at 232 ^{o}C. The mutual solubilities of Al and Sn in the solid state are insignificant. Therefore, solid mixture of Al and 1 to 5wt.% of Sn powders will melt in the sequence of Al (fcc) + Sn (bct) → liquid + Al (fcc) → liquid. The liquid formed just above the eutectic temperature can be enriched with Sn, and the Al concentration in the liquid will increase with temperature.

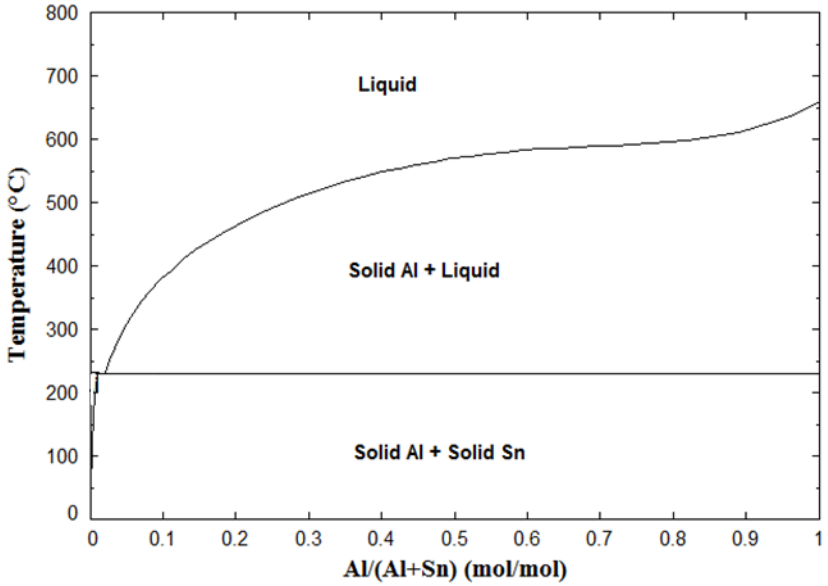

Figure 4.1**:** Calculated Al–Sn phase diagram.

Thermodynamic calculations of Al + 1wt.%TiH_2 + 0, 1, 3 or 5wt.%Sn are shown in Figure 4.2. In the case of Al + 1wt.%TiH_2 powder (Figure 4.2a), the Al melts at 660 ^oC. As $TiAl_3$ is thermodynamically more stable than TiH_2, the calculation shows the formation of $TiAl_3$ across the entire temperature range. In reality, this does not occur at low temperature due to the slow kinetics of $TiAl_3$ formation in the solid Al matrix [13]. The abrupt change of $TiAl_3$ content at about 655 ^oC is due to the peritectic solidification of fcc Al in the binary Al–Ti system.

The influences of Sn additions in the Al foam are calculated in Figure 4.2b-d. Liquid Sn begins to appear at 231 ^oC and the amount of liquid increases slowly up to ~580 ^oC because a relatively small amount of Al can be dissolved in liquid Sn. Then, the amount of liquid is drastically increased above 580 ^oC as a large content of Al can dissolve in the liquid phase (see relatively flat liquidus in Figure 4.1). On the other hand, the liquidus temperatures of Al–Sn decreases slightly with

increasing Sn additions: 654, 642 and 632 ^{o}C for 1, 3 and 5wt.%Sn, respectively. The amounts of liquid Al–Sn alloys formed at 500 ^{o}C are 1.04, 3.23, 5.49wt.% for 1, 3, and 5wt.%Sn alloys, respectively. This liquid can help retain a large volume of H_2 gas in the Al foam [10, 11, 13] decomposed from TiH_2 at about 505–545 ^{o}C. This is one of the fundamental reasons to use Sn as an alloying element in the present study.

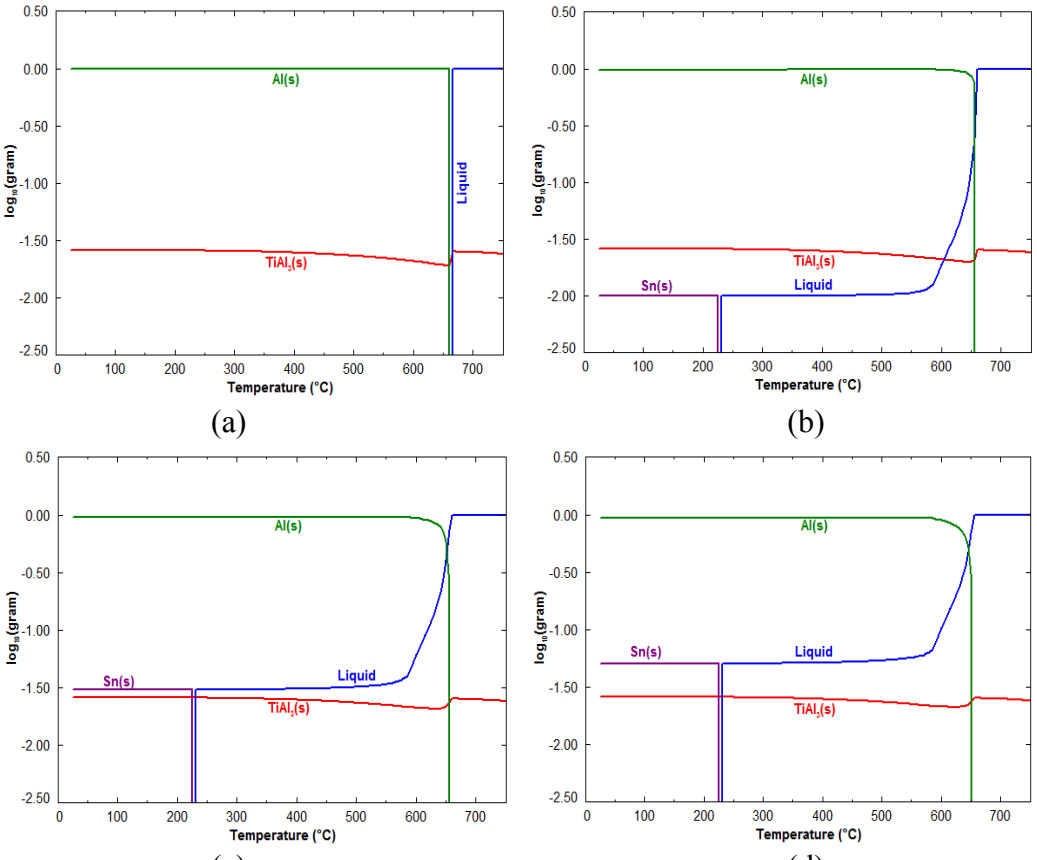

Figure 4.2: Thermodynamic calculations for foaming process of Al-Sn-1%TiH_2: (a) Sn = 0, (b) Sn = 1wt.%, (c) Sn = 3wt.%, and (d) Sn = 5wt.%.

To establish whether powder compaction at 300 ^{o}C influences the foaming behavior of Al, DSC analyses were performed for loose powders and precursors. Figure 4.3 shows the DSC results for loose powders mixtures of Al and Al–Sn with 1wt.%TiH_2. Two consecutive runs were performed from 25 to 750 °C with a heating rate of 10 °C per min. The DSC curves for Al + 1wt.%TiH_2 are presented in Figure 4.3a. There are only two peaks observed during the first heating: namely, the decomposition of the titanium hydride in a temperature range of 505-545 ^{o}C and the melting of Al at 660 ^{o}C. During the cooling stages and second heating stage, the decomposition peak disappeared and only a peak associated with Al solidification was observed. This is because no active TiH_2 remains after the first heating. The TiH_2 decomposition at 505–545 ^{o}C is in good agreement with the dehydrogenation behavior obtained by TG analysis of the same TiH_2 powders without Al [15].

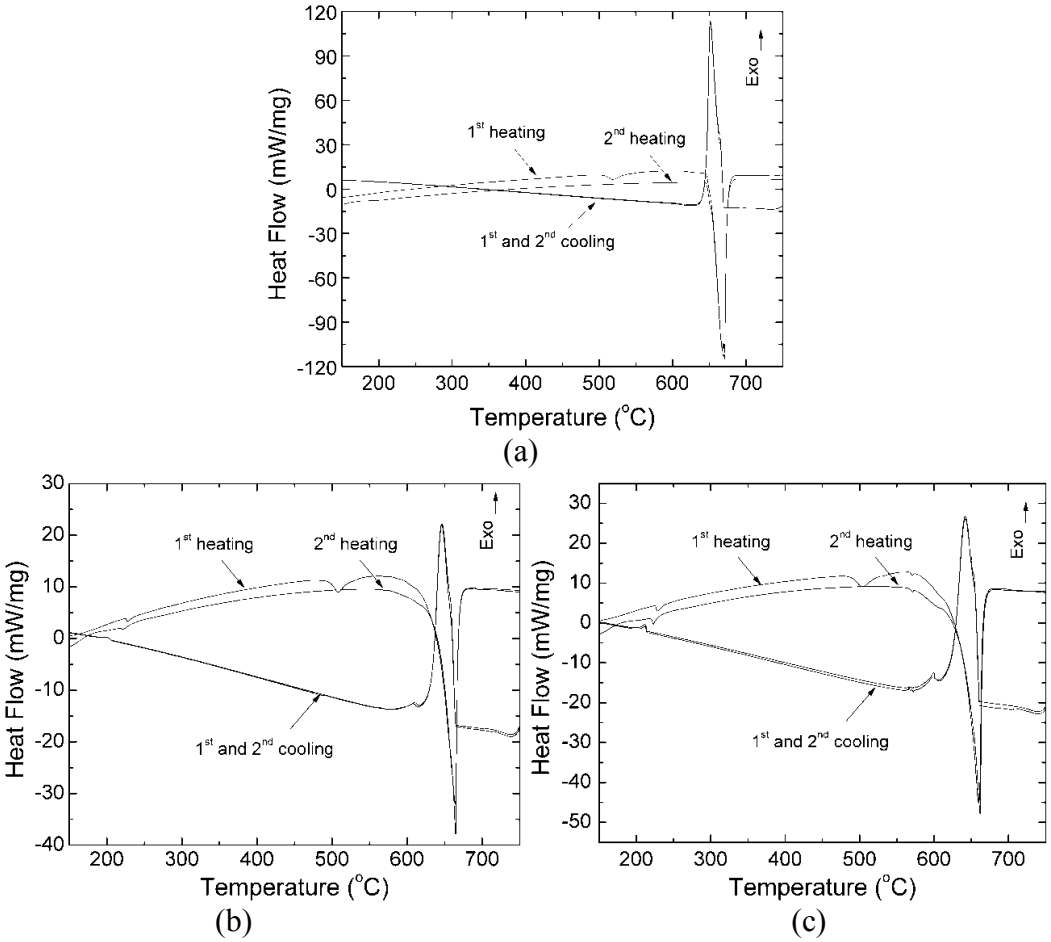

Figure 4.3: DSC results for Al–Sn–1 wt.%TiH_2 loose powder mixtures: (a) pure Al, (b) Sn = 3wt.%, and (c) Sn = 5wt.%.

Figure 4.3b and c present the DSC runs for the mixtures of Al–3 and 5wt.%Sn with 1wt.%TiH_2, respectively. The shape of heat flows is somewhat different from that of Al + 1wt.%TiH_2 because of early liquid formation with Sn addition. The beginning of a large endothermic heat flow for heating curves at 580 ^{o}C can be readily explained by the abrupt increase of the liquid content as shown in Figure 4.2. Two more peaks besides the decomposition of TiH_2 and melting of Al matrix were observed. The peak at about 231 ^{o}C is for the melting of pure Sn. Although it is not noticeable in the first heating run for 3wt.%Sn mixture, there

was an additional peak just below 590 ^{o}C as seen clearly on the heating curves of 5wt.%Sn mixture. The same peak was reversible and more visible in the cooling curves for both 3 and 5wt.%Sn mixtures. The peak at about 590 ^{o}C is reproduced by thermodynamic calculations in Figure 4.4. According to the calculations, the peak is associated with the drastic change in Al and Sn compositions in the liquid phase rather than new phase formation.

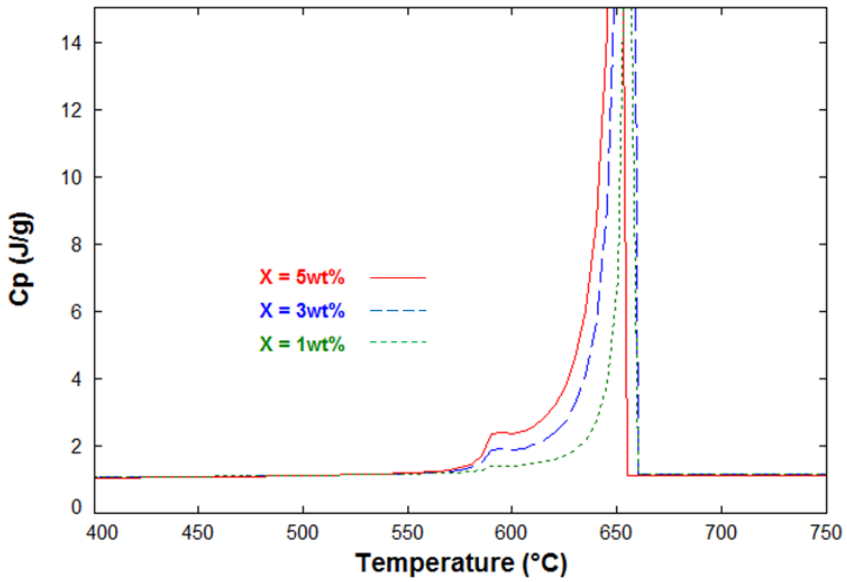

Figure 4.4: Calculated C_p curves with temperature for Al–Xwt.%Sn alloys.

The DSC runs for the Al and Al–Sn precursors are presented in Figure 4.5. The DSC curves did not register any of the hydride decomposition peaks observed for loose powders in Figure 4.3, although the other exothermic and endothermic peaks are similar to the latter. The disappearance of the TiH_2 decomposition peak at about 505–545 ^{o}C is a very interesting phenomenon similar to what Baumgärtner et al. [10] reported. It is believed that the reason for the disappearance of decomposition peaks for pure Al precursor and Al–Sn precursors are different. In our previous study [13] in the microstructural analyses

of Al and Al–Sn precursors during the foaming process, we found that no significant decomposition of TiH_2 occurs in the Al precursor until the melting of Al (660 ^{o}C), whereas the gradual decomposition of TiH_2 occurs in Al–Sn precursors much earlier and below the melting temperature of Al. Thus, the decomposition peaks of TiH_2 in the Al precursor seem to overlap with the Al melting peak, and those in Al–Sn precursors seem insignificant due to the gradual decomposition reaction. It should be noted that the densification can certainly influence the decomposition behavior of TiH_2 and foaming behavior of Al and Al– Sn powders.

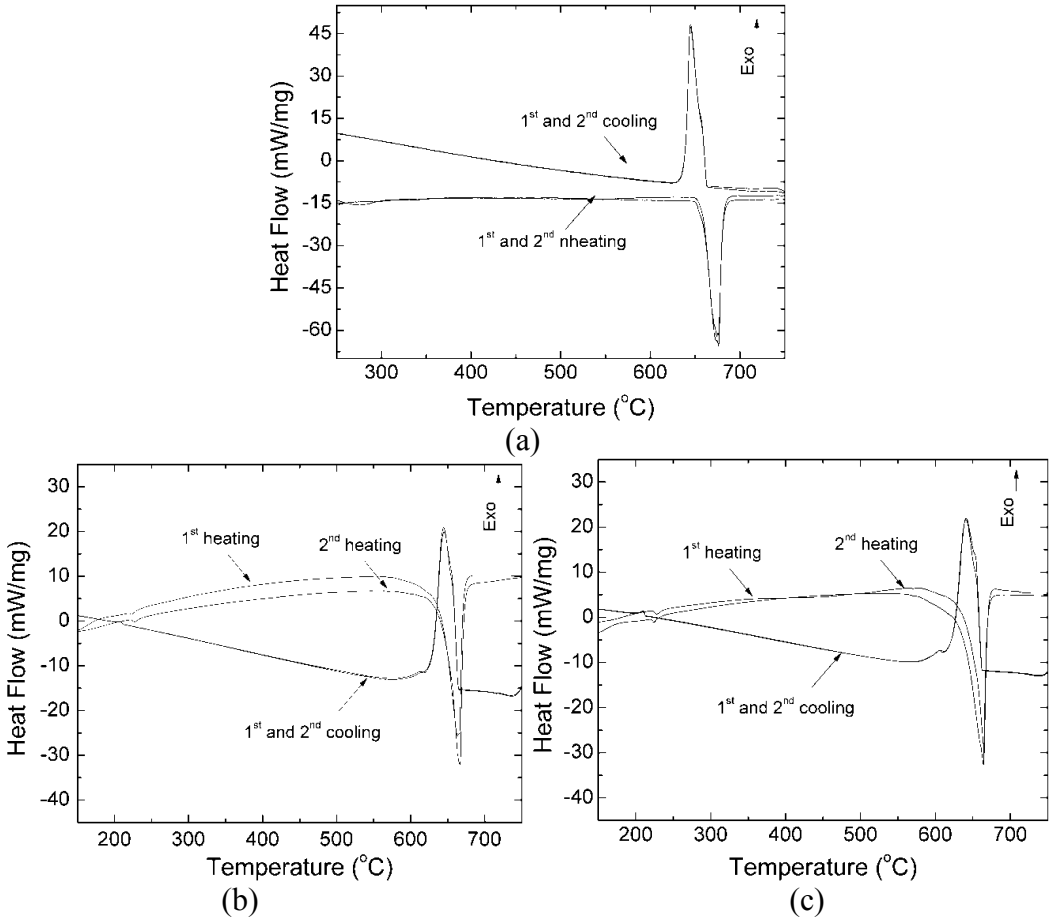

Figure 4.5: DSC results for Al–Sn–1wt.%Sn compacted powders at 300 ^{o}C: (a) pure Al, (b) Sn = 3 wt.%, and (c) Sn = 5 wt.%.

4.3.2. Processing parameters

There are numerous variables involved in the foaming process such as compaction method, powder size, foaming time, temperature. Of these, the influences of powder compaction temperature (200 and 300 ^{o}C) and foaming temperature (700, 725 and 750 ^{o}C) on the final Al foam structure were investigated. The foam structures are shown in Figure 4.6.

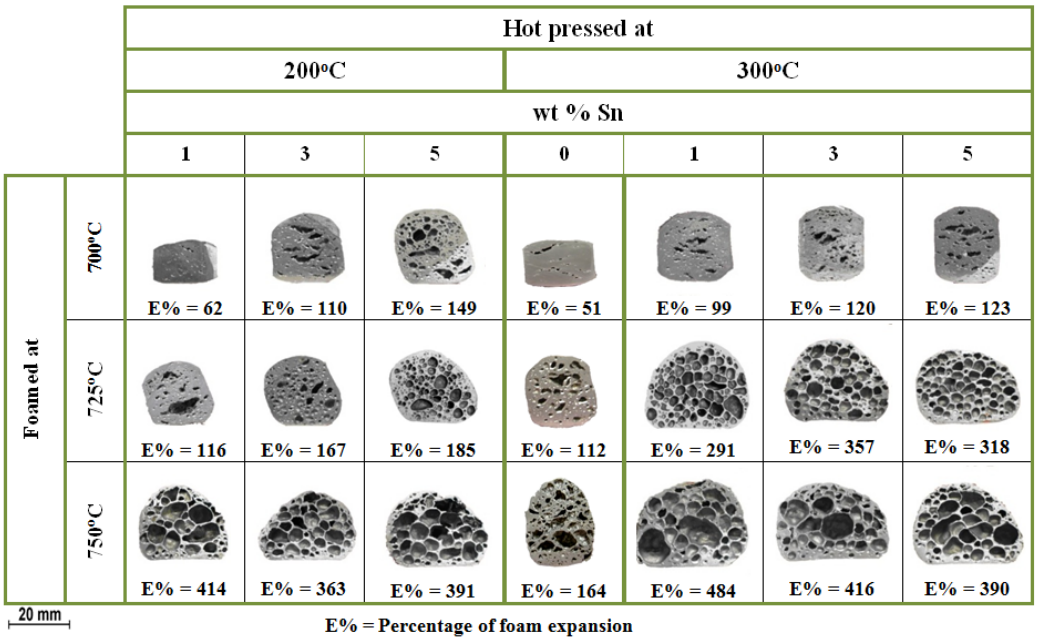

Figure 4.6: Foam structures obtained for Al and Al – Sn powders hot-pressed at 200 and 300 ^{o}C and foamed at different temperatures. Foaming time of all samples is 11 minutes.

4.3.2.1. Densification temperature

Kennedy [4] reported that powder densification over 94% of theoretical density is required to produce proper Al foaming. Good densification is required to retain a high level of hydrogen content, as the high compaction density seals the interconnected porosity [4, 18]. In order to evaluate the influence of densification in foamability, taking into consideration the melting temperature of Sn (232 ^{o}C),

hot pressings were performed at two temperatures, 200 and 300 ^{o}C. Greater densification was expected with the pressing at 300 ^{o}C. In fact, all Al–Sn compacts pressed at 300 ^{o}C attained higher densities (98–99%) than those pressed at 200 ^{o}C (95–96%). In case of pure Al, the densities of the precursors at 200 and 300 ^{o}C were in the same range (95–96%).

As seen in Figure 4.6, the expansions (E) of Al–Sn compacts pressed at 300 ^{o}C are greater than those of the same alloys pressed at 200 ^{o}C, this seems to be associated with the formation of molten Sn, which filled the voids between the Al particles during pressing and enhancing the retention of H_2 gas during the decomposition of TiH_2. A comparable effect was found for the extrusion of Pb–Sn foams preheated at the Sn melting point [12]. Thus, Al–Sn compacts pressed at 300 ^{o}C were investigated further. Although pure Al precursors pressed at 200 and 300 ^{o}C showed similar densities, the expansion of those pressed at 300 ^{o}C was higher than those at 200 ^{o}C. In the later case, the expansion was only about 50% regardless of foaming temperatures.

Precursors with higher content of Sn (up to 10wt.%) were also tested, but molten Sn leaked from the die through the insert during the compaction at 300 ^{o}C. According to Evans et al. [19], 5wt.%Sn is sufficient to form a complete molten layer covering Al grains. Therefore, the maximum amount of Sn was set to be 5wt.% in the present study.

4.3.2.2. Foaming temperature

Foaming should be carried out at temperatures above the melting temperature of Al or its alloys. For example, pure Al compacts are commonly foamed at 780 or 800 ^{o}C [6, 20, 21], while Al alloys with Si, Cu and Zn can be foamed at a lower temperature of 700 ^{o}C [10, 11]. Sn has similar alloying behavior to Si, Cu and Zn, and can decrease the foaming temperature to 700 ^{o}C even with only 1wt.%Sn addition. In the present study, 700, 725 and 750 ^{o}C were chosen as foaming temperatures.

According to the experimental results in Figure 4.6, all samples foamed at 700 ^{o}C showed crack-like pores regardless of the hot pressing temperature. Smaller rounded pores were observed for the samples pressed at 300 ^{o}C and foamed at 725 ^{o}C, while samples hot-pressed at 200 ^{o}C were still in the early stage of foaming. At a foaming temperature of 750 ^{o}C, all Al–Sn samples showed pore coarsening, but drainage of metal was barely observed. Although the foam expansion increased with the foaming temperature, the uniformity of the pores was reduced. For example, several large pores were observed for all samples compacted at 300 ^{o}C and foamed at 750 ^{o}C.

4.3.3. Foam Evolution

As better foams were obtained with precursors hot-pressed at 300 ºC in the pre-screen test shown in Figure 4.6, foam evolution experiments with foaming time were carried out only for the samples compacted at 300 ^{o}C. An iso-expansion contour map for the Al–Sn foams is presented in Figure 4.7. The contours for pure Al side were extrapolated based on the other literature data [3] and our own

experience [13]. The foam evolution of Al–Sn (0, 1, 3 and 5wt.%Sn) was investigated as a function of time with various foaming temperatures (700, 725 and 750 ^{o}C). Each experimental point in the graph is an average value of 3 to 4 samples. The standard deviations of each point were ± 4 to 6%. However, the standard deviation at maximum expansion (and the following 1 min) reached a maximum of ± 15%, which seems to result from bubble bursting as cell walls are very thin at this maximum state of expansion leading to partial foam collapse and variable foam macrostructure [22]. In addition, handling of the samples to interrupt the foaming process can introduce a large error at this maximum expansion state.

For all Al–Sn foams, foaming at 750 ^{o}C reached maximum expansion within 9 to 10 min. Decreasing the foaming temperature to 725 ^{o}C retarded the maximum expansion for another 2 min, while decreasing it to 700 ^{o}C delayed it by further 5 min. It is also worth noting that the expansion rate in the early stage of foaming varied significantly with foaming temperature. That is, the slope to reach maximum expansion is steeper at higher foaming temperature. These kinetics can result from a decrease in metal viscosity and an acceleration in the decomposition of the blowing agent with increasing temperature [23]. Therefore, greater expansions can be attained in shorter time with the increment in foaming temperature. It should also be noted that the Al–Sn foams keep their maximum expansion for a long time, while Al foam typically showed a very short expansion peak before collapsing.

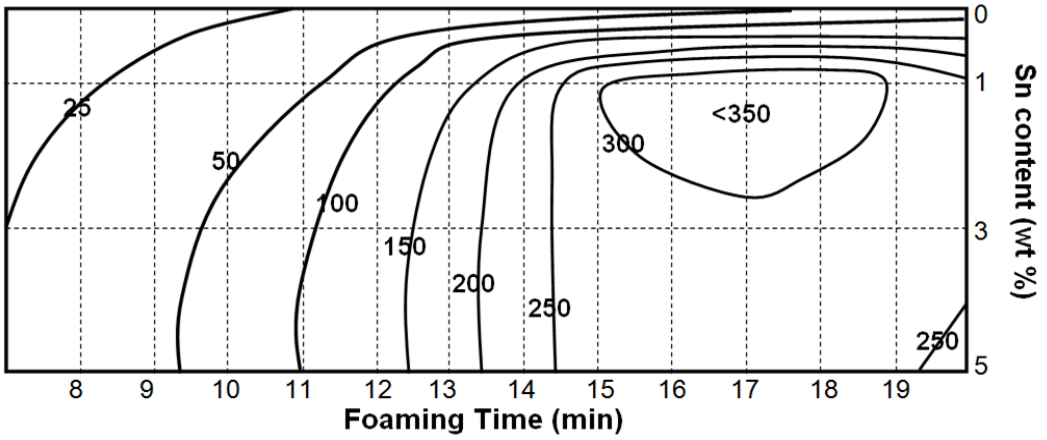

(a)

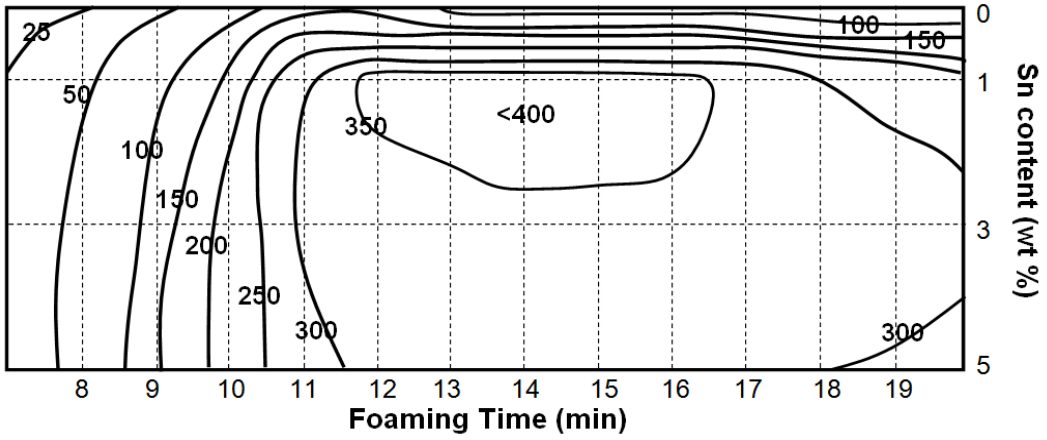

(b)

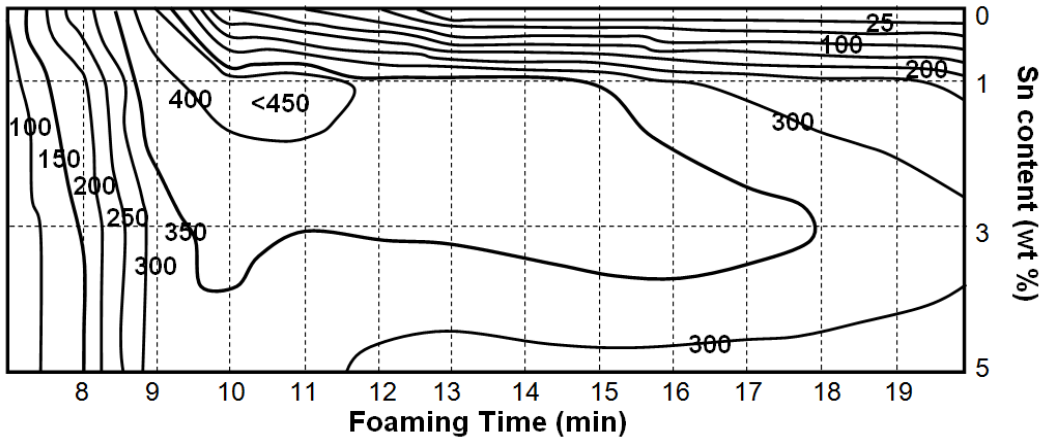

(c)

Figure 4.7: Expansion map for Al – Sn foam as function of foaming time and alloy composition at (a) 700, (b) 725, and (c) 750 ^{o}C.

The iso-expansion contour map in Figure 4.7 clearly shows the variation in Al–Sn foam stability with Sn content and temperature. As can be observed on the map, although the maximum expansion of Al–Sn foam can occur at about 1wt.%Sn, the duration of the maximum expansion is quite short at all temperatures. For the easy, safe and efficient control of the foaming process, the time span at the maximum foam expansion should be reasonably long, this can be achieved with 3wt.%Sn addition. For instance, Al–3wt.%Sn foam can maintain 350–400% expansion for over 10 min at 725 ^{o}C. In the case of Al–5wt.%Sn foam, the time span at maximum foam expansion becomes shortened and the maximum expansion is also smaller in comparison to the Al–3wt.%Sn foam. Therefore, from the foaming process viewpoint, Al with 2–3wt.%Sn precursor, which shows an expansion of 300–350% at 700 ^{o}C for over 6 min, 350–400% at 725 ^{o}C over 10 min and 400–450% at 750 ^{o}C for over 7 min, seems to be the most promising candidate for the Al–Sn system.

4.3.4. Foam Structure (Macro- and Microstructure)

To investigate the variation of pore population and sphericity of Al–Sn foams as a function of foaming time, the foam samples (interrupted at given times) were sectioned and photographed for image analysis with Clemex Vision PE/lite™ 3.5 software, which can distinguish pore from their surroundings and measure their characteristics. For all samples, three cross sections were examined and the results were averaged. The pore sphericity value was calculated as '4π(pore area)/(pore perimeter)' [24]. A perfect spherical pore would have a sphericity value equal to unity.

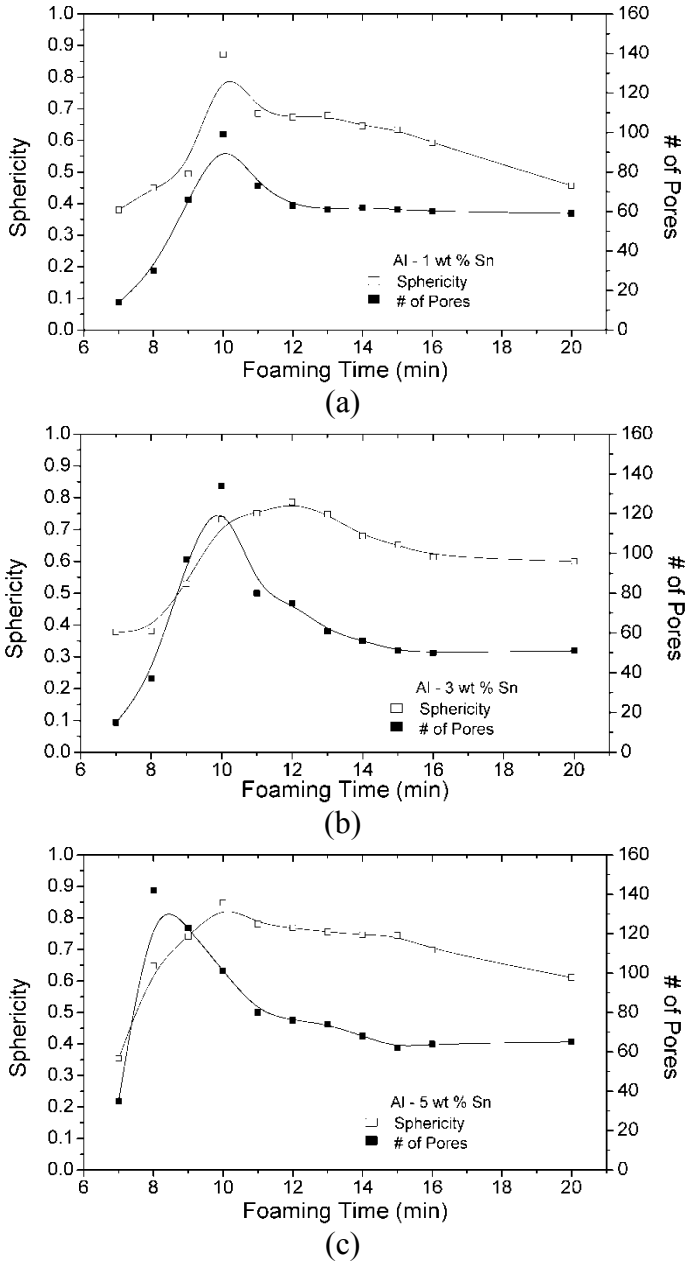

Figure 4.8: The variation of number of pores and sphericity of Al–Sn foam at 725 ^{o}C with foaming time. (a) Sn = 1wt.% (b) Sn = 3wt.% and (c) Sn = 5wt.%.

The variations of pore population and sphericity in the Al–Sn foams with foaming time at 725 ^{o}C are presented in Figure 4.8. As Sn content increased, the foaming time required to reach the maximum pore population was shortened and the maximum pore sphericity increased. Moreover, the maximum pore population

was increased from about 90 to 130 and 140 pores per cross section with an increase of Sn content from 1 to 3 and 5wt.%. Interestingly, the pore population became almost the same (60–70) for all Al–Sn samples after about 14 min of foaming. Although the time to reach the maximum pore sphericity of Al–Sn samples was about 10–12 min for all samples, a longer lapse time of foams with higher sphericity was obtained with increasing Sn content. The maximum sphericity for all Al–Sn foams in the present study was in the range of 0.8 to 0.85. The maximum pore sphericity was reached slightly after the maximum of pore population.

The pore size distribution of Al–Sn foam is plotted in Figure 4.9. Pore size was determined as the cross sectional area of each pore, and the number of pores for given pore size, d, was counted as the total number of pores of d ± 0.5mm size. Clearly, the fraction of smaller pores decreases with increasing foaming time for all Al–Sn samples due to pore coalescence [10, 17, 25]. Although it is difficult to determine the exact relationship between pore distribution and Sn content, in general, with increasing Sn content, in the foam there is a corresponding increase in the fraction of small pores.

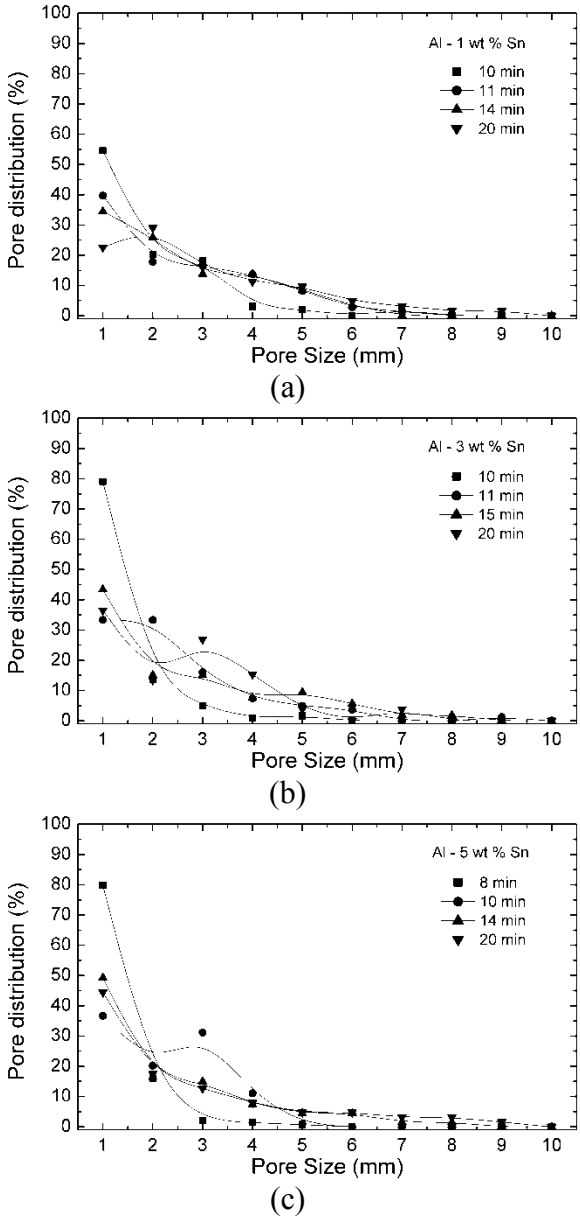

Figure 4.9: Distribution of pore size in Al - Sn foams with foaming time at 725 °C. (a) Sn = 1wt.% (b) Sn = 3wt.% and (c) Sn = 5wt.%.

In order to relate the foaming kinetics to the macrostructure of Al–Sn foams in more detail, the expansion rates (dE/dt) were calculated from the raw data in Figure 4.7 and are presented in Figure 4.10 along with the pore population and foam expansion. In addition, the dissociation rate (dD/dt) of TiH_2 in Al–Sn foam was calculated from our previous study [17] and is plotted on Figure 4.10. It is

very interesting to see that the maximum of dE/dt, dD/dt and number of pore all coincide. This means that the expansion of foam is mainly related to new gas bubble formation from dehydrogenation of TiH_2 rather than the increase of H_2 gas volume due to increasing temperature (ideal gas expansion). Furthermore, this shows that the bubble coalescence occurs predominantly at the end of the dehydrogenation process of TiH_2 and decreases the pore sphericity.

From a mechanical property viewpoint, the optimum cell macrostructure should contain a maximum number of pores with high sphericity. Of course, the foam should also have large expansion to obtain a low density. According to dE/dt curves in Figure 4.10, the optimum cell structure can be obtained at the foaming time when dE/dt has negative slope after reaching its maximum value: that is, 10 to 12 min of foaming time for Al–3wt.%Sn precursor. It should be also noted that the duration (about 2 min) of the optimum foaming time for Al–3wt.%Sn precursor is typically much longer than that for pure Al foam (less than 30 sec). Similar results were also obtained for Al–1 and 5wt.%Sn samples.

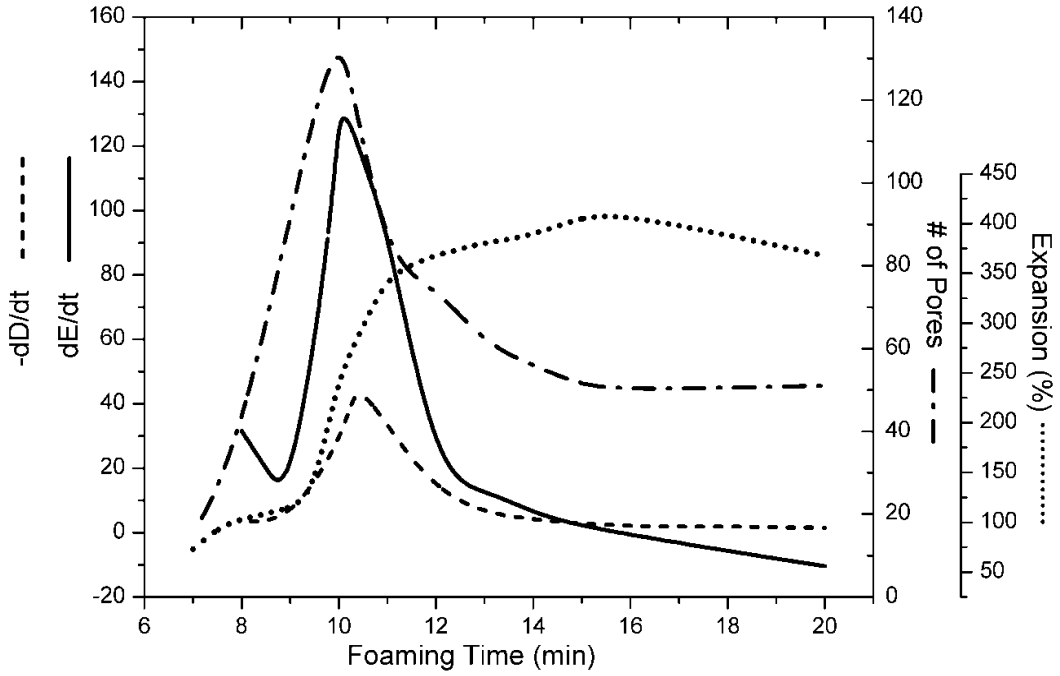

Figure 4.10: Relationship between the dissociation of TiH_2, foam evolution and macro-structural characteristics of Al–3wt.%Sn foam foamed at 725 ^{o}C.

Microstructures of the precursor and foam cell walls of composition Al–3wt.%Sn are presented in Figure 4.11. Figure 4.11a shows a large area where Sn (bright areas) distribution can be observed as well as Sn island formation. Furthermore, Figure 4.11b depicts Sn surrounding TiH_2 and Al powders after compaction.

Figure 4.11c and d corresponds to air cooled foams. Therefore, Sn is only observed along the grain boundaries and surface of pores. As Sn is insoluble in solid Al, Sn remained in liquid state during the foam solidification and finally solidified at 231 ^{o}C on the Al matrix grain boundaries (the pore surface is also considered as a boundary). The microstructure of the inner side of a pore, shown in Figure 4.11d, clearly illustrates evidence of Sn enrichment on pore surface due to solidification of the foam.

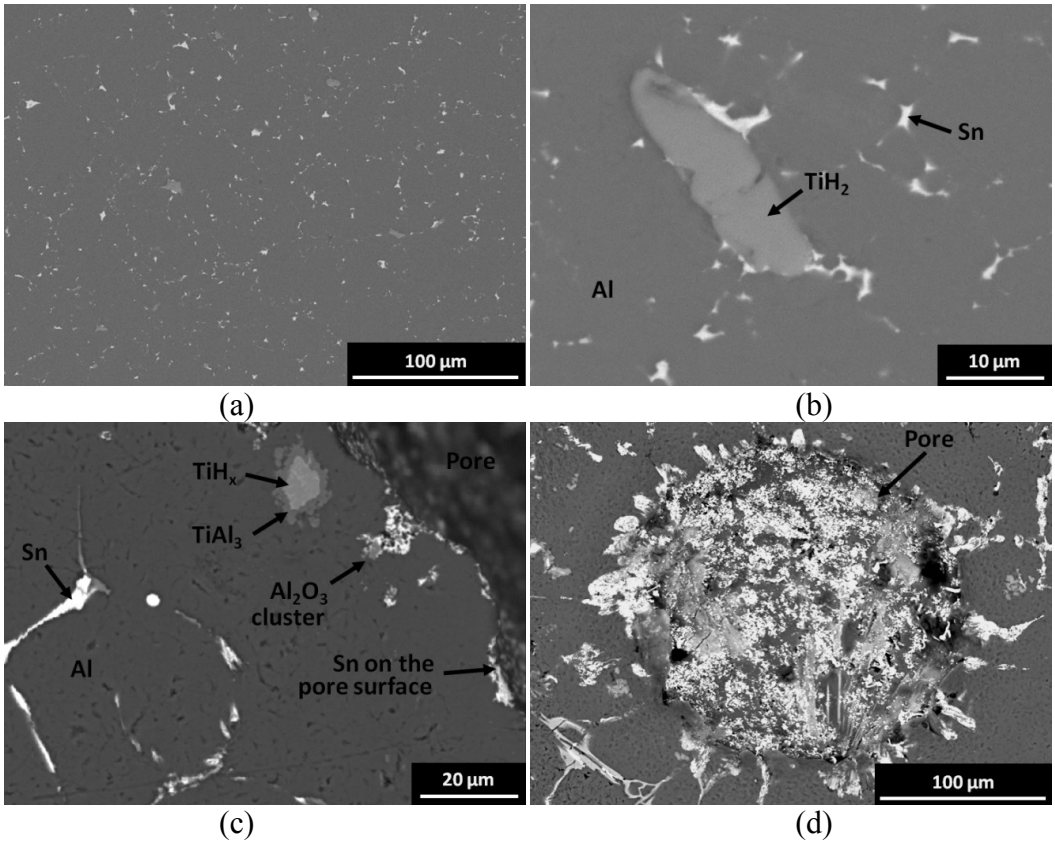

Figure 4.11: Backscattered images of Al–3wt.%Sn a) and b) precursor; c) foam cell wall and d) inside view of a pore.

Small amounts of Al_2O_3 oxide clusters (from Al powder oxidation) are also observed on the pore surface and along grain boundaries. These oxide clusters were studied as they are considered to be responsible for the stability of the Al foams because they do this by forming an oxide network, that when it breaks up and crumples, can behave as isolated particles [26].

TiH_x hydride particles (generated from the decomposition of TiH_2) surrounded by $TiAl_3$ are still embedded in the metal matrix. Since TiH_2 is decomposing to Ti and H_2 gas, Al and Sn melt completely and Al reacts with remaining Ti to form Al_3Ti.

4.3.5. Effect of Sn on Foam Formation

Good Al foaming can be achieved at 700–725 ^{o}C even with 1wt.%Sn addition, while pure Al foams are commonly obtained at 780–800 ^{o}C. It is hard to explain that the good foamability of Al−Sn precursors results simply from the decrease of liquidus temperature by Sn itself because that decrease for 5wt.%Sn is less than 10 ^{o}C. In fact, Sn plays an important role in the decomposition of TiH_2.

According to the DSC results in Figure 4.3 and Figure 4.5, both pure Al and Al−Sn loose powders have shown the decomposition of TiH_2 to occur at about 500–540 ^{o}C. However, neither of the powders compacted at 300 ^{o}C showed this DSC peak of TiH_2 decomposition. As mentioned previously [17], in the case of Al−Sn precursors, the liquid Sn formed at low temperature (231 ^{o}C) can enhance the decomposition of TiH_2 by the acceleration of $TiAl_3$ formation around TiH_2. The deformable liquid Sn can also relieve the pressure induced by the surrounding Al matrix to the TiH_2 and promote its decomposition.

As Sn can exist as a liquid from a low temperature, more H_2(g) can be retained in Al−Sn foam than pure Al foam. In particular, because Sn is insoluble to solid Al, liquid Sn exists between Al and TiH_2 particles. Thus, TiH_2 particles can naturally be encapsulated by liquid Sn. The increase of Sn content in Al−Sn foam can increase the possibility of the encapsulation of TiH_2, retaining more H_2(g) in the foam. As can be seen in Figure 4.8, the maximum number of pores is increased with increasing Sn content.

Two of the most striking effects of Sn are the drastic increase in foam stability (retention of maximum expansion) and the increase in pore sphericity, as shown

in Figure 4.8. As is well-known, the foaming behavior of pure Al shows a very sharp expansion peak and subsequent foam collapse, which makes the foaming process difficult. Thus, such a long foam stability exhibited by the Al−Sn foam is certainly an attractive feature. This long foam stability of Al−Sn foam is hardly explained by the early liquid Sn formation. Although the gradual decomposition of TiH_2 in Al−Sn foam can help keep the foam more stable than the abrupt decomposition of TiH_2 in pure Al foam, it still seems insufficient to explain such a high stability of Al−Sn foam.

Foam stability is directly related to its cell wall stability. If the cell walls become energetically unstable, the pore can coalesce and collapse to reduce the internal energy. Thus, the stability of Al−Sn foam seems to result from the stability of cell wall. Sn addition can modify the surface tension of Al cell walls. That is, the pore stability and sphericity can be changed with surface tension, which is similar to the influence of surfactants in liquid foams [27]. The surface tension of pure liquid Al is about 860 $erg \cdot cm^{-2}$ at 700 ^{o}C, and this can be reduced to 760 and 700 $erg \cdot cm^{-2}$ by the addition of 3 and 5wt.%Sn, respectively [28]. Energetically, the increase of the surface tension of the cell wall can accelerate the bubble coalescence to reduce the energy of foam, and on the other hand, the decrease of the surface tension by the addition of Sn will reduce bubble collapse and increase the foam stability.

The numerical simulation model for the foam formation in liquid metal with particle suspension was carried out by Körner [23]. In order to explain the experimental foaming results, the interplay of the different forces such as fluid

dynamics, capillarity forces and interfacial forces were considered in the model. Körner found that the capillarity velocity (υ_{Ca}), which is associated with the rising velocity of bubbles in liquid metal, is related to the surface tension (σ) and viscosity (η) of liquid metal: $\upsilon_{Ca} = \sigma/\eta$. A decrease in surface tension can therefore help the retention of more bubbles in liquid metal, which is consistent with the present results. In addition, due to the decrease of surface tension, the ratio of smaller pores increased with increasing Sn content, as can be seen in Figure 4.9.

As expected from Körner's model [23], the viscosity (η) of liquid metal is an important factor influencing the stability of a foam. As temperature decreases, the viscosity can increase steeply and the stability of the foam can increase. In the case of a previous study on Al-9wt.%Si-3wt.%Cu powders, the foaming was performed at 700 to 750 ^{o}C [11]. However, the foam stability of the system was much less than the present Al−Sn foam at the same temperature. Although there are no experimental data available to compare the viscosities of liquid Al-9wt.%Si-3wt.%Cu and Al−Sn alloys at this temperature, the viscosity of both liquids can be similar because both liquids are enriched with Al. Therefore, it can be concluded that the main influence of Sn on Al−Sn foam stability is the decrease in surface tension.

4.4. **Summary**

In order to investigate the influence of the addition of Sn on the foaming behavior of Al, pure Al and Al−Sn powders with 1, 3 and 5wt.%Sn contents were studied at various foaming temperatures of 700, 725 and 750 ^{o}C. 1wt.% of TiH_2 was

added as a blowing agent. Foam processing parameters such as densification and foaming temperature were investigated to establish the optimum Al−Sn processing route. In addition, DSC and thermodynamic analyses were carried out to understand the influence of Sn more comprehensively. The results of the present investigation can be summarized as follows:

(1) Al−Sn powder densification at 300 ^{o}C, which is above the melting temperature of Sn, shows better foaming behavior than with a compaction temperature of 200 ^{o}C. High densification of Al powders at 300 ^{o}C under 550 MPa induced the suppression of decomposition (dehydrogenation) of TiH_2 up to the melting temperature of the Al matrix. In the case of Al−Sn powders densified under the same conditions, the gradual decomposition of TiH_2 occurred prior to the melting of Al because the Sn-rich liquid accelerates the decomposition of TiH_2 [13].

(2) All Al−Sn powder precursors densified at 300 ^{o}C showed excellent foaming behavior at foaming temperatures of 700–750 ^{o}C. The best microstructure of Al–Sn foam was obtained at 725 ^{o}C with 3wt.%Sn addition; the optimum cell structure with about 300% volume expansion was obtained after 10–12 min foaming time, and a stable microstructure was maintained after this optimum foaming time for an additional 9 min without foam collapse.

(3) Sn addition to the Al foam reduced the foaming temperature and drastically increased foam stability. The reduction in foaming temperature is believed to be the result of the gradual and accelerated decomposition of TiH_2 and the effective retention of generated H_2(g). The increase in foam stability can be explained by

the decrease in surface tension of liquid Al with the addition of Sn, which produced energetically more stable cell walls.

Acknowledgements

The authors would like to thank NSERC, FQRNT, GM of Canada, and CONACyT for financial support. In particular, the authors wish to thank Dr. Carl Fuerst for his valuable ideas, comments and suggestions. The authors would like to acknowledge Shirley Mercier from IMI-NRC for performing the oxygen content analysis.

References

1. Banhart, J., *Manufacturing Routes for Metallic Foams.* Journal of Metals, 2000. 52(12): p. 22-27.

2. Ito, K. and H. Kobayashi, *Production and Fabrication Technology Development of Aluminum Useful for Automobile Lightweighting.* Advanced Engineering Materials, 2006. 8(9): p. 828-835.

3. Banhart, J., *Manufacture, Characterization and Application of Cellular Metals and Metal Foams.* Progress in Materials Science, 2001. 46: p. 559-632.

4. Kennedy, A.R., *The effect of compaction on expansion and gas release in Al-TiH_2 powder compacts.* Materials Science Forum, 2003. 416-418(1): p. 299-304.

5. Matijasevic-Lux, B., et al., *Modification of titanium hydride for improved aluminium foam manufacture.* Acta Materialia, 2006. 54(7): p. 1887-1900.

6. Kennedy, A.R., *The effect of TiH_2 heat treatment on gas release and foaming in Al-TiH_2 preforms.* Scripta Materialia, 2002. 47(11): p. 763-767.

7. Lehmhus, D. and G. Rausch, *Tailoring titanium hydride decomposition kinetics by annealing in various atmospheres.* Advanced Engineering Materials, 2004. 6(5): p. 313-330.

8. Matijasevic, B. and J. Banhart, *Improvement of aluminium foam technology by tailoring of blowing agent.* Scripta Materialia, 2006. 54(4 SPEC ISS): p. 503-508.

9. von Zeppelin, F., et al., *Desorption of hydrogen from blowing agents used for foaming metals.* Composites Science and Technology, 2003. 63(16): p. 2293-2300.

10. Baumgartner, F., I. Duarte, and J. Banhart, *Industrialization of Powder Compact Foaming Process.* Advanced Engineering Materials, 2000. 2(4): p. 168-174.

11. Lehmhus, D. and M. Busse, *Potential new matrix alloys for production of PM aluminium foams.* Advanced Engineering Materials, 2004. 6(6): p. 391-396.

12. Irretier, A. and J. Banhart, *Lead and lead alloy foams.* Acta Materialia, 2005. 53(18): p. 4903-4917.

13. Aguirre-Perales, L.Y., I.-H. Jung, and R.A.L. Drew, *Effect of Sn on the Dehydrogenation Process of TiH_2 in Al Foams.* Metallurgical and Materials Transactions A, 2011: p. 1-5.

14. Asavavisithchai, S. and A.R. Kennedy, *Effect of powder oxide content on the expansion and stability of PM-route Al foams.* Journal of Colloid and Interface Science, 2006. 297(2): p. 715-723.

15. Proa-Flores, P.M. and R.A.L. Drew, *Production of aluminum foams with Ni-coated TiH_2 powder.* Advanced Engineering Materials, 2008. 10(9): p. 830-834.

16. Bale, C.W., et al., *FactSage thermochemical software and databases.* Calphad, 2002. 26(2): p. 189-228.

17. Wang, L., et al., *Study on crack-like pores of Al foams made via the powder-metallurgy route.* Advanced Engineering Materials, 2010. 12(1-2): p. 50-53.

18. Kennedy, A.R. and S. Asavavisithchai, *Foaming of compacted Al-TiH_2 powder mixtures.* Materials Science Forum, 2002. 396-402: p. 251-258.

19. Evans, E.B., et al., *Effect of Inclusion Size on Grain Boundary Wetting in Al-Sn Alloys.* Applied Physics A: Solids and Surfaces, 1987. 42(4): p. 269-272.

20. Banhart, J., *Foam metal: the recipe.* Europhysics News, 1999. 30: p. 17-20

21. Kennedy, A.R. and S. Asavavisithchai, *Effect of ceramic particle additions on foam expansion and stability in compacted Al-TiH2 powder precursors.* Advanced Engineering Materials, 2004. 6(6): p. 400-2.

22. Babcsan, N. and J. Banhart, *Metal Foams: Towards High-Temperature Colloid Chemestry*, in *Colloidal particles at liquid interfaces*, B.P. Binks and T.S. Horozov, Editors. 2006, Cambridge University Press: New York.

23. Korner, C., *Foam formation mechanisms in particle suspensions applied to metal foams.* Materials Science and Engineering A, 2008. 495(1-2): p. 227-235.

24. *Clemex Vision PE/Lite^{TM} 3.5 User's Guide*, 2002, Clemex Technologies inc.: Longueuil.

25. Bhakta, A. and E. Ruckenstein, *Decay of standing foams: drainage, coalescence and collapse.* Advances in Colloid and Interface Science, 1997. 70: p. 1-124.

26. Korner, C., M. Arnold, and R.F. Singer, *Metal foam stabilization by oxide network particles.* Materials Science & Engineering A (Structural Materials: Properties, Microstructure and Processing), 2005. 396(1-2): p. 28-40.

27. Xu, Q., et al., *Effects of surfactant and electrolyte concentrations on bubble formation and stabilization.* Journal of Colloid and Interface Science, 2009. 332(1): p. 208-214.

28. Goumiri, L., et al., *Tensions superficielles d'alliages liquides binaires présentant un caractère dimmiscibilité: Al-Pb, Al-Bi, Al-Sn et Zn-Bi.* Surface Science, 1979. 83(2): p. 471-486.

Chapter 5

Effect of Sn on the Dehydrogenation Process of TiH_2 in Al Foams

Lydia Y. Aguirre-Perales[a], In-Ho Jung[a*], Robin A. L. Drew[a,b]

[a] Department of Mining and Materials Engineering, McGill University, 3610 University Street, Montreal, Qc, H3A 2B2, Canada

[b] Departament of Mechanical and Industrial Engineering, Concordia University, 1455 de Maisonneuve Blvd. W., Montreal, Qc, H3G 1M8, Canada

Corresponding author:
Prof. In-Ho JUNG
E-mail: in-ho.jung@mcgill.ca
Tel: 1-514- 398-2608 Fax: 1-514-398-4492

Published in:

Metallurgical and Materials Transactions A. 2012, vol. 43 (1), pp. 1-5.

As the first author of this manuscript, the Ph.D candidate performed the experiments, analysis, calculations and wrote the manuscript. Prof. Robin Drew and Prof. In-Ho Jung contributed to extensive discussions, critical analysis and supervision of this work.

This chapter presents a deeper explanation and understanding of the Al foam stabilization by Sn additions. The previous chapter explained the prevention of pore coalescence by the decrrease of Al surface tension. This chapter deals with the effect of Sn on the dehydrogenation of the blowing agent.

Abstract

The study of the dehydrogenation process of TiH_2 in aluminum foams produced by the powder metallurgy technique is essential to understand its foaming behavior. Tin was added to the Al foam to modify the dehydrogenation process and stabilize the foam. A gradual decomposition and more retention of hydrogen gas can be achieved with Sn addition resulting in a gradual and larger expansion of the foam.

5.1. **Introduction**

The production of metal foams by the powder metallurgy technique requires the proper mixture of a metal or alloy and blowing agent powders. Then, this mixture is compressed to high densities and finally the densified product (called precursor) goes through a heat treatment (above the metal's melting temperature) where the blowing agent releases gas that the molten metal matrix traps. As the heat treatment is interrupted, the metal solidifies and the foam is obtained [1]. In order to produce good metallic foams, with the powder metallurgy technique, the decomposition of the blowing agent has to be synchronized with the melting of the metal or alloy [2]. For the foaming process of Al, TiH_2 is the most commonly used blowing agent as it has the closest decomposition temperature range (about 450 ~ 650 ^oC) to the melting of Al (660 ^oC) [3].

According to the Ti – H phase diagram in Figure 5.1, solid TiH_2 (δ) can contain 2.06 to 4.05wt.%H. With increasing temperature, TiH_2 can be unstable and evolve to TiH_x (β) and Ti (α) with releasing H_2 gas [4]. Although TiH_2 can theoretically be dehydrogenated to pure Ti at high temperature and low pressure, it has been

reported that TiH_2 is degenerated to non-stoichiometric TiH_x (β) phase over a wide temperature range between 415 to 625 ^oC at ambient pressure [5] with weight loss of about 2.0 to 2.5wt.%. However, this decomposition temperature is still lower than Al melting temperature, and this mismatch of temperature should be still overcome. The ways to reduce the mismatch are: 1) increase of the decomposition temperature of TiH_2, and 2) decrease of the melting temperature of Al.

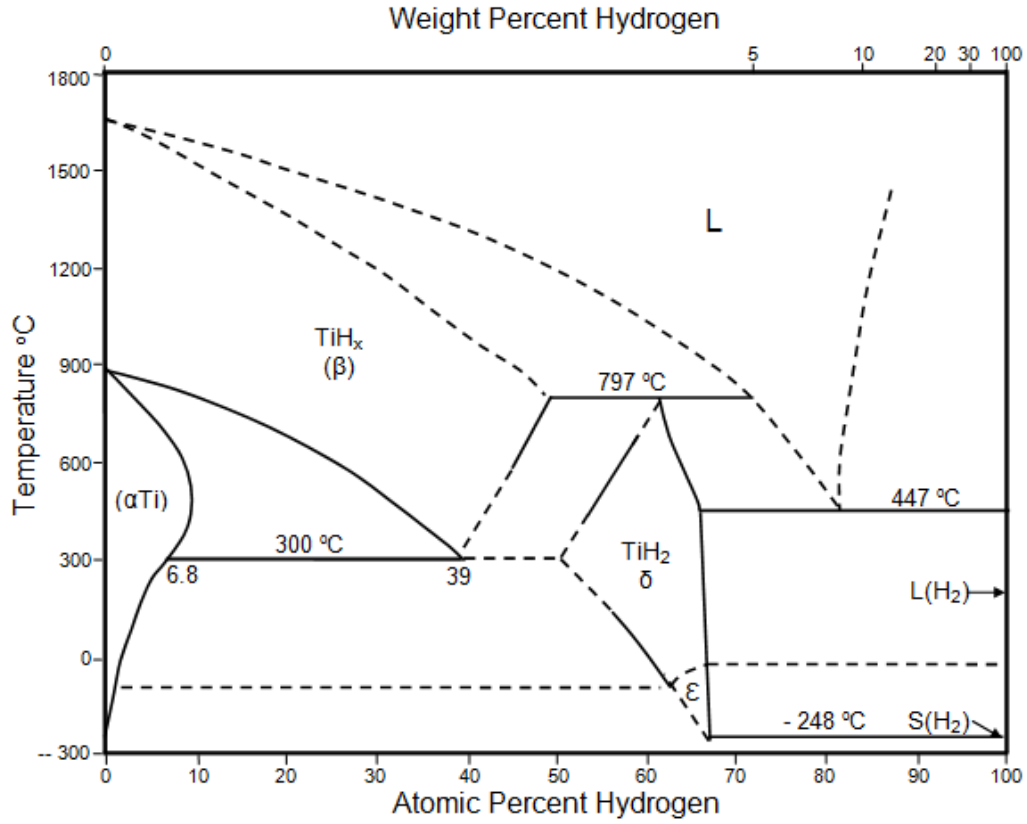

Figure 5.1: Ti – H phase diagram [4]

To increase the TiH_2 decomposition temperature, heat treatments (oxidation) of TiH_2 have been investigated under various atmospheres (air, argon and nitrogen) to create an oxide layer on the surface of the hydride that acts as a diffusion

barrier [2, 5-8]. The application of a Ni coating on the hydride has been studied to avoid hydrogen loss during the oxidation [9]. Furthermore, isothermal x-ray diffraction and thermal analysis on different particle sizes have been performed to better understand the dehydrogenation of TiH_2 [3, 10].

To decrease the melting temperature of the Al matrix, Al has been alloyed with melting point depressant elements. The wrought Al alloys commonly used for this purpose are the 2xxx and 6xxx series, which contain mainly Mg and Cu or Mg and Si, respectively. Casting alloys employed for metal foams are often combinations of Al-Si-Mg-Cu-Zn, which give a large solidification range. For example, Al–7wt.%Si–Mg (A356) or Al–9wt.%Si–3wt.%Cu, allows foaming at lower temperature in the semi-solid state [11, 12].

Regardless of the efforts for matching the degeneration temperature of TiH_2 and melting temperature of Al matrix, the foaming behavior of Al alloys should be further improved: although high maximum expansion can be reached, the metal foam stability is quite low (in most cases foam collapses within less than 30 seconds), due to pore coalescence and metal drainage [11-13]. In order to enhance foam stability and obtain higher expansions, a new alloying element (Sn) was investigated in the present study. Surprisingly, it was found that the addition of Sn can easily control the dehydrogenation process of TiH_2 in the Al foam, to achieve maximum foam expansion and enhance the foam stability.

5.2. **Experimental Procedure**

To study the effect of Sn on the dehydrogenation of TiH_2, Al powders containing 1wt.%TiH_2 were hot compacted with and without additional Sn (3wt.%) powder

into a cylindrical shape (0.71 cm in height and 2 cm in diameter) under an uniaxial load of 550 MPa at 300 ^{o}C. The particle sizes of Al, TiH_2 and Sn powders were all less than 44 μm and the purities of the powders were more than 99 %. The average size of TiH_2 powders was about 15~18 μm. The precursors were placed on an alumina plate in a Lindberg/Blue M furnace preheated at 725 ^{o}C. The foaming of the precursor was interrupted after a certain time by quenching the samples in air. Microstructural characterizations with scanning electron microscopy (SEM) and electron probe micro analysis (EPMA) were carried out on the sectioned foams.

5.3. **Results and Discussion**

To understand the difference in the decomposition behavior of TiH_2 in Al and Al–3wt.%Sn foam, the morphology of the remaining TiH_x was examined. Typical SEM morphologies of TiH_2 in Al and Al–3wt.%Sn foams with foaming time are presented in Figure 5.2. EPMA was used to confirm the Ti–Al phase on the surface of the TiH_x particle, identified as $TiAl_3$ intermetallic. In the case of pure Al foam, thin $TiAl_3$ layer formed on the surface of TiH_x until 12 min without any rupture. Then, abrupt rupture of the $TiAl_3$ layer was observed after 12 min and the amount of $TiAl_3$ was suddenly increased. In the case of Al–3wt.%Sn foam, continuous $TiAl_3$ layer was observed until 9 min. After 1 min, small fragments of ruptured $TiAl_3$ layer were observed around the TiH_x. The amount of $TiAl_3$ particles increased gradually with foaming time. It should be also noted that the size of $TiAl_3$ fragments in pure Al foam was larger than that in Al–3wt.%Sn foam.

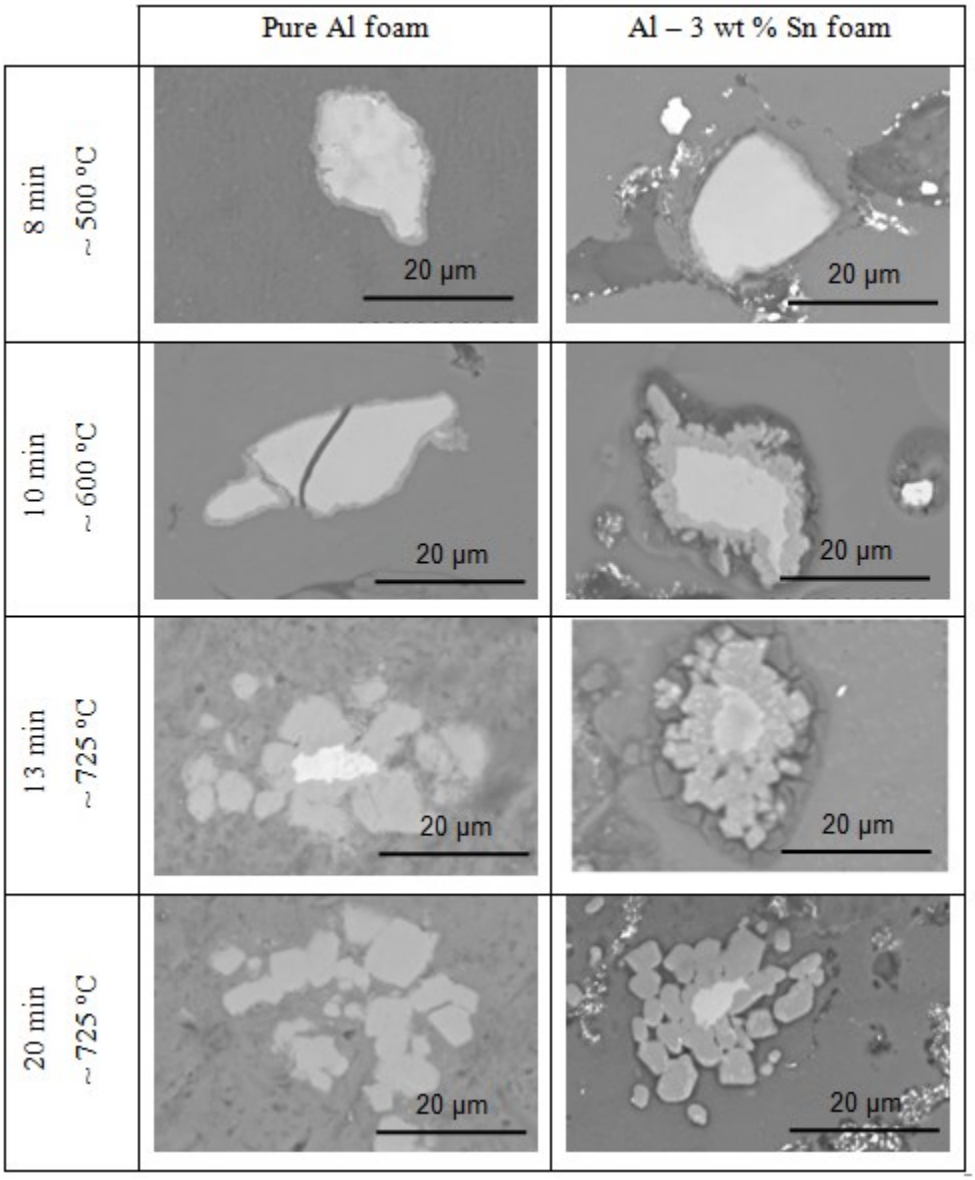

Figure 5.2. Evolution of typical morphologies of TiH_2 (SEM-BSE) in pure Al and Al–3wt.%Sn foams with foaming time.

As it is very difficult to ascertain the exact decomposition amount of TiH_2, this was determined from SEM images of the remaining Ti hydride particles in the foams. That is the extent of the decomposition was calculated as:

$$\text{Degree of decomposition (\%)} = \frac{\text{area of surrounding } TiAl_3}{\text{area of surrounding } TiAl_3 + \text{ area of } TiH_x} * 100$$

The amount of unreacted TiH_x (%) (100 – degree of decomposition) with foaming time is plotted in Figure 5.3. Each point in the figure is an average value of more than 10 Ti hydride particles of the mean size (15–18 μm). The estimated thermal history of the metallic foam was also plotted in Figure 5.3, as the decomposition behavior of TiH_2 is highly dependent on temperature, it is important to know the thermal histories of the Al and Al–Sn foams. The decomposition of pure Al foams increased slowly up to 12 min, and showed an abrupt increase at 12 min. On the other hand, the decomposition of Al–3wt.%Sn foams increased slowly until about 8 min, and then a large but gradual decomposition occurred between 9 and 12 min. After 15 min, the remaining Ti hydride (TiH_x (β) phase) was less than 20 % of an original TiH_2. Thus, the presence of Sn certainly led to a gradual and earlier decomposition of TiH_2.

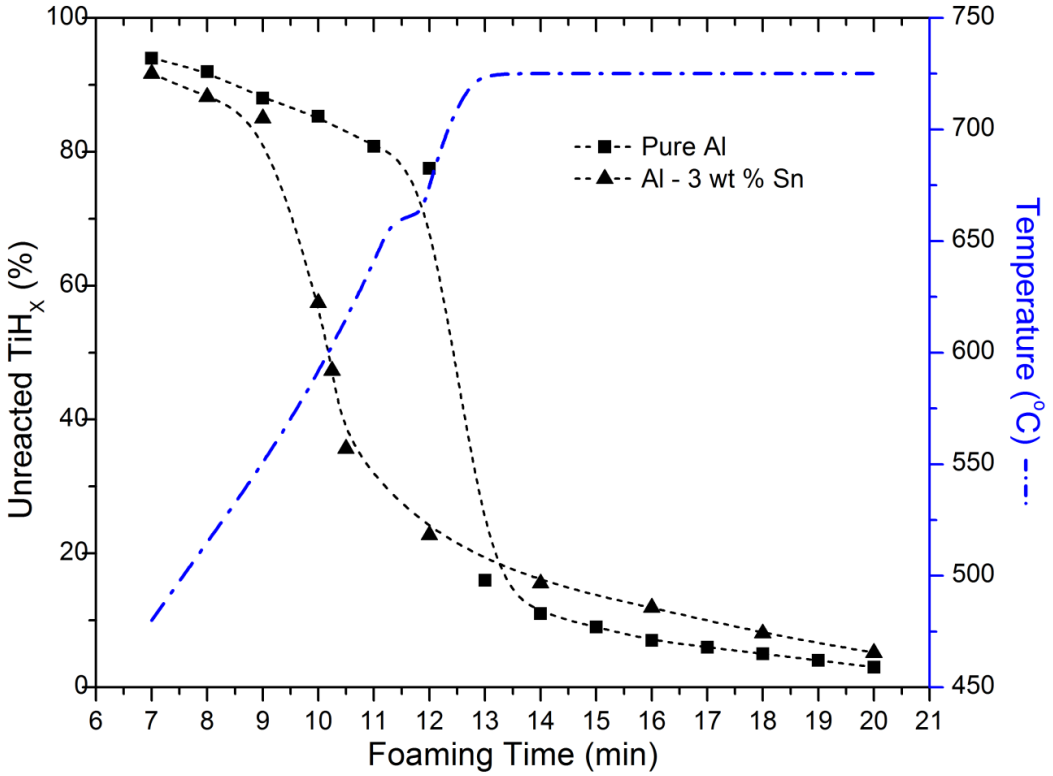

Figure 5.3: Relationship between TiH_2 decomposition (100% - unreacted TiH_2%) for pure Al and Al–Sn foams along with the estimated thermal history.

The expansion behavior of Al and Al–3wt.%Sn foams at 725 ^oC is presented in Figure 5.4 along with their decomposition behavior of TiH_2. The foam expansions were determined using the Archimedes principle. As can be seen, in Figure 5.4 the foam expansion of Al–3wt.%Sn foam is directly related to the decomposition behavior of TiH_2. That is, the gradual and large expansion of the foam occurred between 9 min and 11 min when a large decomposition of TiH_2 took place. Pure Al foam showed a maximum expansion at 11 min, which is coincident with the melting temperature of Al. The maximum expansion of the Al foam (250%) is lower than that of Al–3wt.%Sn foam (400%). In addition, while the Al foam collapsed after maximum expansion at 11 min, Al–3wt.%Sn foam was stable for long time.

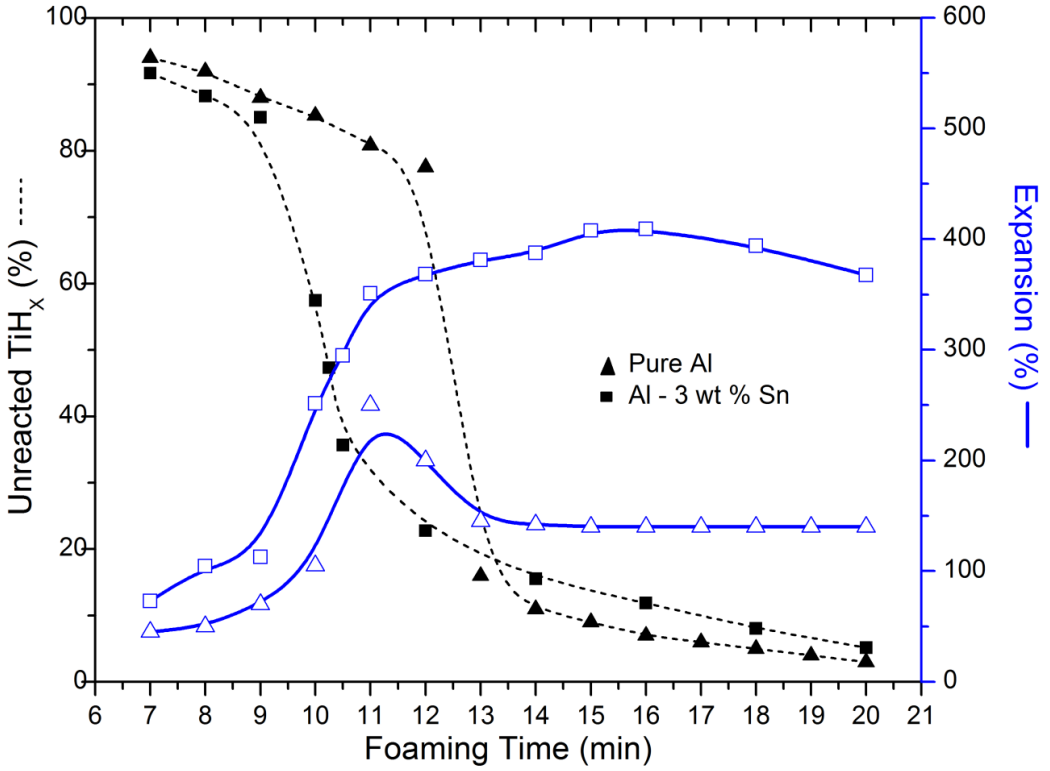

Figure 5.4: Relationship between TiH_2 decomposition (100% - unreacted TiH_2%) and foam expansion during the foaming process for pure Al and Al–Sn foams.

Based on the present experimental results and the thermodynamic behavior of Al–Sn system, the effect of Sn on the decomposition behavior of TiH_2 can be explained. The schematic diagram of the microstructural evolution of TiH_2 in Al and Al–Sn foams during the foaming process is depicted in Figure 5.5. In the case of pure Al foam, TiH_2 can react with solid Al to produce a thin solid layer of $TiAl_3$ around TiH_2 (reaction-1). Although the self-decomposition reaction of TiH_2 to TiH_x (reaction-2) can occur between 450 and 650 ^oC under ambient pressure, the decomposition is not observed for Al foam at this temperature range. This seems to be induced by the high pressure exerted on the TiH_2 (covered by $TiAl_3$) by the surrounding solid Al matrix (pressed to 550 MPa), which can effectively increase the decomposition temperature of TiH_2. Therefore, it is expected that

H_2(g) pressure can build up inside the $TiAl_3$ layer at the temperature range of 450 ^oC and 650 ^oC, as depicted in Figure 5.5. Immediately after melting of the Al matrix, when the hydrogen pressure generated by the self-decomposition reaction (reaction-2) can overcome the suppressed pressure of the Al matrix, H_2(g) can be released with the abrupt rupture of $TiAl_3$ layer. According to the present experimental results in Figure 5.2, Figure 5.3 and Figure 5.4, the rupture of $TiAl_3$ layer was not observed until the melting of Al (660 ^oC) at 12 min. At 12 min, the abrupt rupture of $TiAl_3$ and drastic decomposition of Ti hydride were observed. Unfortunately, H_2(g) released during this abrupt decomposition of Ti hydride cannot be effectively retained in liquid Al matrix. The Al foam collapsed due to the drainage of liquid Al and bubble bursting with increasing temperature.

$$TiH_2(s) + 3Al(s) = TiAl_3(s) + H_2(g) \qquad (1)$$

$$TiH_2(s) = TiH_x + (2\text{-}x)/2H_2(g) \qquad (2)$$

In the case of Al–3wt.%Sn foam, Sn-rich liquid can already form above 231 ^oC. As TiH_2 is in contact with Sn-rich liquid saturated with solid Al, the formation of the solid $TiAl_3$ layer can be promoted due to a faster diffusion of Al via liquid Sn (reaction-3) up to about 550 ^oC. Similarly to the pure Al foam scenario, a certain pressure of H_2(g) can build up inside the $TiAl_3$ layer by reaction-2. Once the temperature reaches about 550 ^oC, the amount of liquid Sn–Al can increase steeply and subsequently relieve the surrounding pressure on TiH_2 ($TiAl_3$) because the liquid medium can be deformable. Therefore, the solid $TiAl_3$ layer can be ruptured releasing H_2(g). Of course, after the rupture of the $TiAl_3$ layer, its

recovery (formation of $TiAl_3$) can easily occur by the presence of liquid Al (in Sn). This rupture/recovery process can be continued with a gradual release of $H_2(g)$. In the present study, this process can be observed between 9 min and 12 min. Moreover, this explanation can explain the smaller size of $TiAl_3$ fragment in Al–Sn foam than pure Al foam.

$$TiH_2(s) + \underline{Al} \text{ (in liquid Sn)} = TiAl_3(s) + H_2(g) \qquad (3)$$

As $H_2(g)$ can be gradually released from low temperature to 660 ^oC and liquid Al–Sn can be formed even below 660 ^oC (i.e. about 5 and 15wt.% of the Al–Sn foam is liquid at 600 ^oC, and 630 ^oC, respectively), a relatively high amount of $H_2(g)$ can be retained in the Al – Sn foam, which in turn increases its expansion. The Al–Sn foam showed about 360 % expansion at 12 min and further expanded to 410 % at 16 min. Furthermore, the addition of Sn can significantly increase the foam stability (durability) of Al foam. This can be explained as a result of surface energy modification of the cell wall by Sn, which is discussed in detail elsewhere [14].

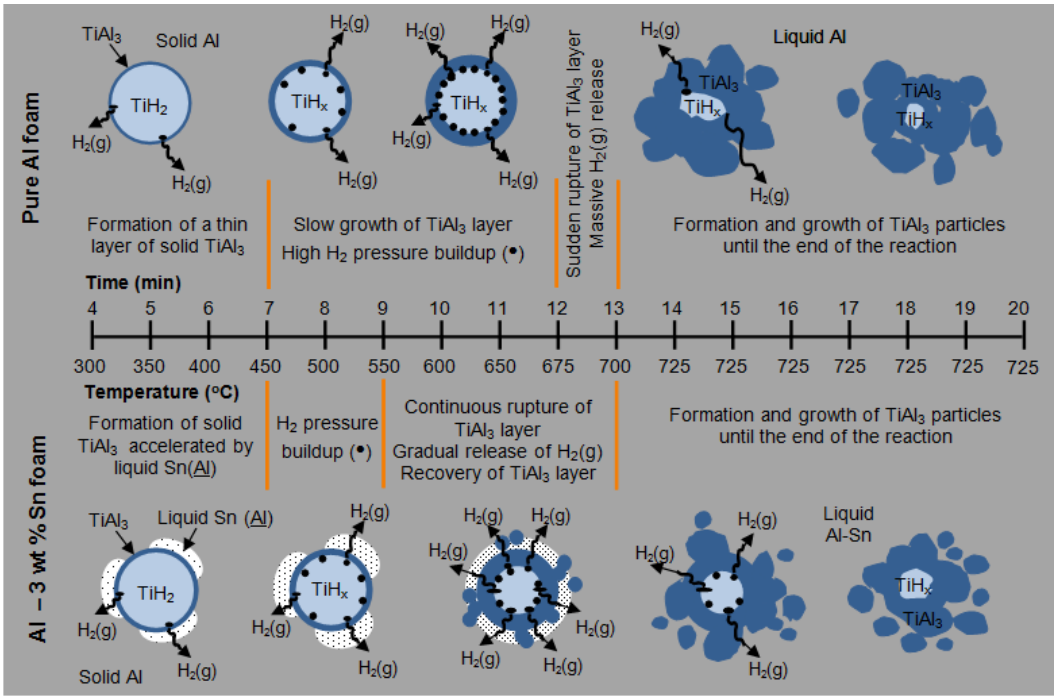

Figure 5.5: Schematic diagram of the decomposition process of TiH_2 in pure Al and Al–Sn foams.

In summary, the gradual and larger expansion of Al foam can be achieved with Sn addition. This results from the formation of Sn-rich liquid below the melting temperature of Al, which can promote a gradual and earlier decomposition of TiH_2 and help to retain more $H_2(g)$ in the Al foam.

References

1. Banhart, J., *Manufacture, characterisation and application of cellular metals and metal foams.* Progress in Materials Science, 2001. 46(6): p. 559-632.

2. Matijasevic, B. and J. Banhart, *Improvement of aluminium foam technology by tailoring of blowing agent*. Scripta Materialia, 2006. 54(4 SPEC ISS): p. 503-508.

3. Malachevsky, M.T. and C.A. D'Ovidio, *Thermal evolution of titanium hydride optimized for aluminium foam fabrication*. Scripta Materialia, 2009. 61(1): p. 1-4.

4. Okamoto, H., *H-Ti (hydrogen-titanium).* Journal of Phase Equilibria, 1992. 13(4): p. 443-443.

5. Matijasevic-Lux, B., et al., *Modification of titanium hydride for improved aluminium foam manufacture.* Acta Materialia, 2006. 54(7): p. 1887-1900.

6. Kennedy, A.R., *The effect of TiH_2 heat treatment on gas release and foaming in Al-TiH_2 preforms*. Scripta Materialia, 2002. 47(11): p. 763-767.

7. Lehmhus, D. and G. Rausch, *Tailoring titanium hydride decomposition kinetics by annealing in various atmospheres*. Advanced Engineering Materials, 2004. 6(5): p. 313-330.

8. von Zeppelin, F., et al., *Desorption of hydrogen from blowing agents used for foaming metals.* Composites Science and Technology, 2003. 63(16): p. 2293-2300.

9. Proa-Flores, P.M. and R.A.L. Drew, *Production of aluminum foams with Ni-coated TiH_2 powder.* Advanced Engineering Materials, 2008. 10(9): p. 830-834.

10. Bhosle, V., et al., *Dehydrogenation of TiH_2.* Materials and Engineering, 2003. A(356): p. 190-199.

11. Lehmhus, D. and M. Busse, *Potential new matrix alloys for production of PM aluminium foams*. Advanced Engineering Materials, 2004. 6(6): p. 391-396.

12. Baumgartner, F., I. Duarte, and J. Banhart, *Industrialization of Powder Compact Foaming Process.* Advanced Engineering Materials, 2000. 2(4): p. 168-174.

13. Duarte, I. and J. Banhart, *Study of aluminium foam formation - kinetics and microstructure.* Acta Materialia, 2000. 48(9): p. 2349-2362.

14. Aguirre-Perales, L.Y., I.-H. Jung, and R.A.L. Drew, *Foaming Behaviour of Powder Metallurgical Al - Sn Foams.* Acta Materialia, 2011.

Chapter 6

The Effect of In-Situ Intermetallic Formation on Al-Sn Foaming Behavior

Lydia Y. Aguirre-Perales[a], Robin A. L. Drew[a,b], In-Ho Jung[a*]

[a] Department of Mining and Materials Engineering, McGill University, 3610 University Street, Montreal, Qc, H3A 2B2, Canada

[b] Departament of Mechanical and Industrial Engineering, Concordia University, 1455 de Maisonneuve Blvd. W., Montreal, Qc, H3G 1M8, Canada

Corresponding author:
Prof. In-Ho JUNG
E-mail: in-ho.jung@mcgill.ca
Tel: 1-514- 398-2608 Fax: 1-514-398-4492

Published in:

Metallurgical and Materials Transactions A. 2014, vol. 45 (9), pp. 3714-27.

As the first author of this manuscript, the Ph.D. candidate performed all the experimental characterization, analysis, calculations and wrote the manuscript. Prof. Robin Drew contributed with discussions and corrections. Prof. In-Ho Jung who is the principal investigator of the present work contributed to critical analysis particularly on the thermodynamic calculations and supervision of this work.

This chapter presents the foaming behavior of Al-Sn in the presence of different alloying elements which form in-situ intermetallic phases.

Abstract

The effect of in-situ intermetallic formation on the foaming behavior of Al–3wt.%Sn alloy has been investigated by introducing five different alloying elements, Co, Mg, Mn, Ni and Ti. The alloying elements were designed, using thermodynamic calculations, to form various intermetallic phases i) stable until final foaming temperature and ii) dissolved during the foaming process. Thermal analysis using DSC was carried out to characterize the formation and dissolution of intermetallic phases during the foaming process. The foaming tests of the Al–3wt.%Sn–X alloy were carried out using a mechanical expandometer and the macrostructure of the foam were scanned with an x-ray tomographer. It is found that the foaming behavior and foam stability of Al–3wt.%Sn alloy can be actively controlled by the alloying elements.

Keywords: Al-Sn foam, intermetallic, thermodynamic alloy design, foam characterization.

6.1. **Introduction**

The metallic foams often exhibit excellent stiffness to weight ratios, high mechanical energy absorption and good acoustic and thermal insulating properties [1]. Metallic foams with closed cell porosity can be obtained by the powder metallurgy technique where a large variety of metals are employed. Nevertheless, foam reproducibility is one of the processing issues because foaming happens at elevated temperatures involving a sudden foam expansion and rapid collapse with problems of drainage and pore coalescence. Foam reproducibility can be directly related to foam stability [1].

Foam stabilization using powder metallurgical route has been addressed mainly by the existence of solid oxides networks [2, 3]. Experiments performed under micro-gravity demonstrated that small amount of solid components (Al_2O_3 from oxidized powder surface) can prevent films (cell walls) from coalescing but with very little influence on viscosity [4]. Other experiments [5] using Reduced Pressure Tests (RPT) technique indicate that surface tension and viscosity of the melt (without adding stabilizing particles) play an important role in pore nucleation and stabilization at different stages of the foaming process. Surface tension would influence pore nucleation while viscosity determines if there is pore coalescence during solidification. Although extensive research [6] has been carried out to understand the mechanisms governing the stabilization of metallic foams, the mechanism is not well known yet.

Recently we proposed a Al-Sn foam with stability which was significantly improved compared with that of other Al foams [7, 8]. The foam stabilization in the Al-Sn alloy results mainly from the gradual decomposition of TiH_2 and the decrease in surface tension of the cell wall by the addition of small amounts of Sn, which can prevent the coalescence of pores. By optimizing the process parameters, the Al–3wt.%Sn alloy was found to have the best expansion and foam stability.

The purpose of the present study is to further investigate the foam stabilization and expansion of Al–3wt.%Sn alloy with addition of alloying elements which can generate solid intermetallic compounds during the foaming process. These alloying elements can modify the Al-Sn foaming behavior by 1) enhancing foam

expansion (reaching higher maximum expansion) and/or 2) stabilizing the foam (regularizing pore size and distribution) by means of intermetallic formation. As a consequence, such alloying elements can homogenize the mechanical properties of Al foam. In order to design the alloying elements, thermodynamic calculations were extensively used and thermal analysis employing DSC was carried out. Five different alloying elements were selected to change the foaming behavior, type of intermetallics and foam macrostructure.

6.2. **Alloy design concept**

6.2.1. Foaming behavior of Al-Sn alloy

In the powder metallurgical route, titanium hydride (TiH_2) is the most commonly used blowing agent for Al foaming process. Previously, the interaction of the Al–3wt.%Sn base alloy with the foaming agent (1wt.%TiH_2) was evaluated by thermodynamic calculation and corroborated with DSC [7]. From the foaming experiments, it was found that Sn can play a key role in TiH_2 dissociation and modification of the surface tension of liquid Al [8]. In comparison to pure Al foam, Al-Sn ($1 \leq$ wt.%Sn ≤ 5) foam can expand earlier due to the formation of liquid Sn (melting temperature of Sn is 232 ^{o}C) between solid Al powder particles, which can accelerate the dissociation of TiH_2 by the dissolved Al in liquid Sn at a temperature much lower than pure Al melting: Al (in liquid Sn) + $TiH_2(s) = TiAl_3(s) + H_2(g)$. This early liquid formation can also help to retain $H_2(g)$ bubbles and enhance foam expansion. Moreover, due to the decrease of surface tension of liquid Al by the addition of Sn, the foam becomes thermally

stable, compared to pure Al foam (Al–3wt.%Sn foam can be expanded up to 350 % at 725 ^{o}C and retain an average expansion of 325 % for more than 12 min), without foam collapse.

The foaming process of Al-Sn alloy is depicted in Figure 6.1, along with the schematic representation of TiH_2 decomposition in the presence of Sn [8]. In the first stage (I) up to about 400 ^{o}C, the Al (dissolved in liquid Sn) promotes the formation of $TiAl_3$ layer around the original TiH_2 particles leading to a small decomposition of TiH_2. When the temperature reaches about 400 ~ 450 ^{o}C, the decomposition of TiH_2 can occur and release about 5% of TiH_2 (stage II) [8]. The decomposition of TiH_2 can expand the foam to about 140%. After this first expansion, the first plateau happens (stage III). In stage III, although the temperature of foam keeps increasing, little expansion is occurring, which can be explained only by the small decomposition of TiH_2. In fact, as presented in our earlier work [8], it was found that TiH_2 in this stage is completely surrounded by $TiAl_3$ and the decomposition rate of TiH_2 was low. It is believe that the H_2(g) pressure can be built up inside the rigid $TiAl_3$ shell, which can suppress the decomposition. Once the temperature of foam increases to about 600 ^{o}C, the decomposition can be accelerated to make the second expansion (stage IV). In this stage, according to microstructure examination [8], there is rupturing and healing of the $TiAl_3$ layer leaving small fragments of $TiAl_3$ in the surroundings and releasing H_2(g). Finally, in the stage V of the second plateau with maximum expansion, a small amount of remaining TiH_2 (less than 10% of original amount) continues to be decomposed with releasing H_2(g) until the completion of the

reaction. Foaming of pure Al under the same condition has a similar behavior during the initial stages (stages I to III). Then, there is a sudden rupture of the $TiAl_3$ layer with a massive $H_2(g)$ release during stage IV, but it shows less expansion and rapid foam collapse (stage V). As mentioned earlier, Sn addition can improve the expansion by retaining more $H_2(g)$ resultant from earlier liquid formation, and the stability of foam by reduction of surface tension of cell wall.

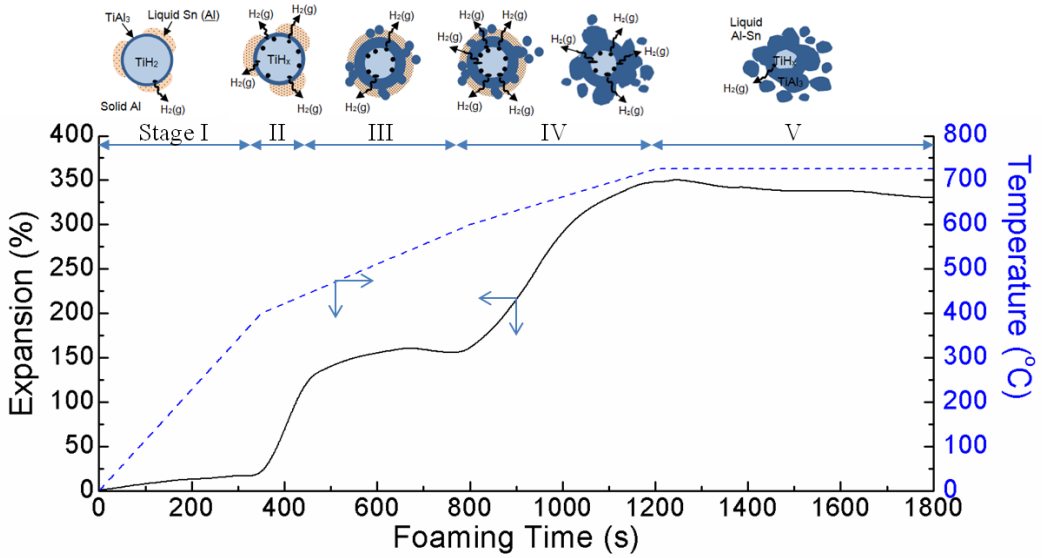

Figure 6.1: Foam expansion behavior of Al–3wt.%Sn foamed at 725 ^{o}C along with schematic diagram of TiH_2 decomposition process.

6.2.2. Key factors in alloy design

As shown in the foaming behavior of Al-Sn alloy in Figure 6.1, the key factors to produce thermally stable and highly expanded foam are:

(a) the acceleration of TiH_2 dissociation at low temperature,

(b) the formation of a liquid phase at the normal TiH_2 decomposition temperatures, (~ 450 ^{o}C to 650 ^{o}C) which can capture $H_2(g)$, and

(c) the decrease of surface tension of Al melt to maintain the foam for a long time at high temperature.

In the Al-Sn alloy studied previously [7, 8], no intermetallic phases except Ti_3Al originated from TiH_2 were formed during the foaming process. However, it is commonly known that the presence or addition of solid particles help to stabilize the foam but the exact mechanism is still not fully understood [3, 9-11]. For example, in the Alporas® process, the creation of Al_4Ca intermetallics in liquid Al prior to foaming process can stabilize its foam structure during expansion and cooling [12]. Similarly, Al 6061 alloy was modified by additional 4wt.%Cu, creating Al_4Cu intermetallics that improved foam stabilization [13]. Furthermore, it was reported that $Al_{13}Fe_4$ platelets were created during stirring using a stainless steel stirrer, which improved the stability of the cell structure [14].

After consideration of the above-mentioned factors producing a thermally stable Al-Sn alloy and the role of intermetallic phases in foam stabilization, the following criteria were used for the alloy design in the present study:

(i) Foam expansion

   a. Acceleration of TiH_2 dissociation by formation of liquid at low temperature like Sn.

   b. Increasing the amount of liquid below 650 ^oC (the melting temperature of Al) to capture the hydrogen decomposed from TiH_2.

(ii) Foam stabilization

   a. Stable intermetallics at foaming temperature

b. Reduction of surface tension of liquid Al like Sn

(iii) Mechanical property enhancement

a. Formation of finely distributed intermetallics existing at room temperature

The alloying elements for Al-Sn based alloy which can meet the above criteria except surface tension can be selected based on the phase diagram information. However, as it requires the phase diagram information for the Al-Sn-X-TiH_2 system (where X is an alloying element), which is not readily available in literature, the CALPHAD type thermodynamic calculations have been performed to predict the phase distributions of the alloys with temperature.

6.3. **Experimental Procedure**

6.3.1. Thermodynamic calculations

In order to select alloying elements for Al-Sn based alloy, thermodynamic calculations were performed using the FactSage™ 6.2 software with FTlite and FACT53 database [15]. All thermodynamic calculations were done in the "Equilib" module. For example, the amounts of various equilibrium phases including solid fcc Al, liquid and various intermetallic phases were calculated with temperature in order to simulate the heating process. In this way, the type and amount of intermetallic phases forming during the foaming process could be predicted, and the change of liquidus and liquid amount with temperature could also be calculated. For the simulation of the cooling process, Scheil cooling calculation for non-equilibrium cooling were performed which could qualitatively

predict what kind of intermetallic phases would be precipitated during the cooling of the metallic foam. Many common metallic elements, which could possibly form intermetallics with Al or Sn during the foaming process, were evaluated.

6.3.2. Foaming test

The powders used for the foam tests were purchased from Alfa Aesar. All powders have a – 325 mesh size and at least 99 % purity. The metal powders were mixed in the appropriate ratio (3wt.%Sn + various wt.% additional element + Al balance) along with 1wt.% of TiH_2 in a tumbler mixer for 30 minutes. To obtain precursors (compacted powders) with densities above 99 % of its theoretical density and a volume of 10.6 cc, the correct amount of powder mixture was loaded into a steel die of 3 cm in diameter and kept in the hot press for 30 min at 350 ^{o}C to ensure temperature homogenization followed by the uni-axial pressing at 360 MPa for 10 min.

Foaming experiments were performed using a mechanical expandometer. The precursor was placed in a preheated stainless steel crucible (coated with boron nitride to facilitate sample removal) that is suspended inside a vertical tube furnace at 725 ^{o}C. A counterweighted piston lays on top of the precursor as a laser records its displacement registering foam expansion versus foaming time. Interruption of the foaming process was done by the removal of the crucible containing the foam and placed in a stainless steel block at room temperature to accelerate the cooling of the foam.

6.3.3. Foam characterization

50 mg of the powder mixture of each alloy was taken after 30 minute mixing in a tumble mixer and was loaded to a differential scanning calorimeter (DSC; Netzsch STA 449 Jupiter® thermo-gravimetric analyzer) with Al_2O_3 crucible to characterize the thermal behavior of the powder. Two cycles were run from room temperature to 750 ^oC with a heating/cooling rate of 10 ^oC per min under high purity argon atmosphere.

The foam structure was examined by employing an X-ray microtomograph (SkyScan 1172). To obtain cross sectional images, the samples were scanned using a Cu-Al filter with an accelerating voltage of 103 kV and medium resolution. For the chemical analysis of the foam cell walls, the foams were cut in their transverse direction using an Isomet diamond saw followed by polishing and cleaning in an ultrasonic bath, and then they were examined on a Hitachi S-3000N variable pressure SEM with Oxford INCA EDS system.

6.4. **Results and Discussion**

6.4.1. Selection of alloying elements

In the present study, the alloying elements for Al-Sn based foam were chosen among the metallic element relatively abundant and inexpensive. Obviously, it is hard to find the alloying element which can meet the criterion of (i)-a the acceleration of TiH_2 dissociation in section 2.2. Zinc (Zn) would be the most feasible candidate for this criterion. According to the phase diagrams of binary Al-Zn and Zn-Sn system and ternary Al-Sn-Zn system, the liquidus temperature

of Al–3wt.%Sn system can be decreased noticeably only with a large amount of Zn addition. But the surface tension of liquid Al cannot be changed with the addition of Zn [16] while Sn can significantly decrease the surface tension of liquid Al [17] which is helpful for the foam stabilization. Therefore, Zn was not considered as a candidate alloying element in the present study.

The following candidates of alloying element were chosen mainly based on their possibility to form different precipitates with Al or Sn in the Al-Sn based foam, which can meet the criteria for foam stabilization and enhancement of mechanical properties: Co, Mg, Mn, Ni, and Ti. These candidate elements can also influence to the melting behavior of Al-Sn based foam, which can change the foam expansion. Although it was not considered in the alloy design, it was found that the in-situ formation of intermetallics could produce a strong exothermic heat accelerating of the decomposition of TiH_2 and local melting, which will be discussed later. Different amounts of the alloying element were added to Al-Sn based alloy: 1, 3 and 5wt.% for Mn, Ni, Co and Ti, while only 0.5, 1 and 2wt.% for Mg. Main reason for this reduction of Mg content is due to the strong reaction of Mg with liquid Sn to form Mg_2Sn at low temperature to consume all liquid Sn, which can result in no beneficial effect of Sn in Al foam.

The calculated liquid fractions of the Al–3wt.%Sn–1wt.%TiH_2–X alloys are shown in Figure 6.2. The calculated phase evolutions for the same alloys during heating (fully equilibrium calculation) and cooling (Scheil solidification calculation) are presented in Figure 6.3. The measured DSC scans are plotted in Figure 6.4 for the heating and cooling cycles. Detailed explanations on the thermal

behavior of each alloy are explained below. For the sake of simplicity, the results for the Al-Sn alloy with maximum amount of alloying element are shown in Figure 6.2-Figure 6.4, but the calculation and DSC tests were done for all the alloy combinations.

6.4.1.1. Thermodynamic calculations for melting behavior

As reported in the previous study [7], Sn can melt already at 232 ^{o}C and the fraction of liquid slowly increases with temperature. After passing 600 ^{o}C, the liquid fraction steeply increases with increasing temperature. The addition of alloying elements can change the melting behavior of Al–3wt.%Sn alloy. As can be seen in Figure 6.2, Mg and Ni accelerate the melting of matrix. In particular, the alloy containing 2wt.%Mg drastically increases the liquid fraction from 3 % to over 10 % at 604 ^{o}C by melting of existing Mg_2Sn. However, Ti and Co have no influence on the melting behavior except the decrease on the total amount of liquid above 660 ^{o}C. It is hard to correlate the onset point of melting in DSC experiments to the thermodynamic calculations, but it can be said that the temperature of significant increase of liquid fraction (for example, temperature corresponding to 10% of liquid fraction) could be identified as the onset point of melting in the DSC experiment. For instance, the alloy containing Mg would reach 10 % at 604 ^{o}C, the one with Ni at 612 ^{o}C, and the other alloys at about 620 ^{o}C.

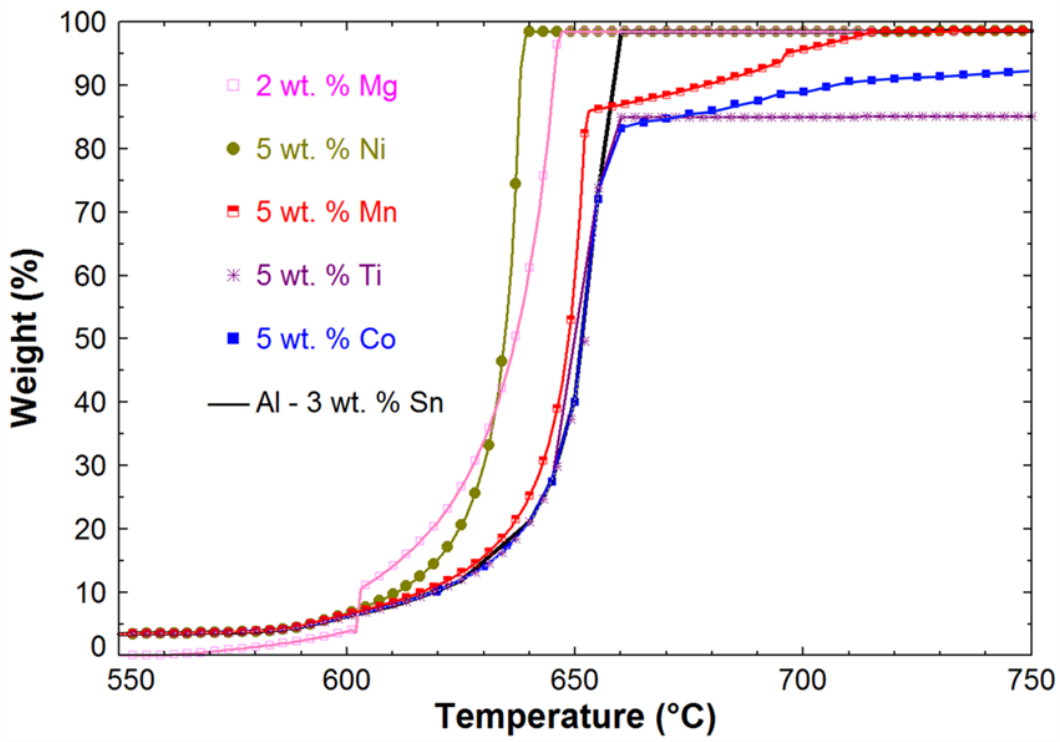

Figure 6.2: Thermodynamic calculation for liquid fraction in various Al–3wt.%Sn–X alloys during heating process.

6.4.1.2. Thermodynamic calculations for intermetallics formation

Figure 6.3 shows the results of thermodynamic calculations for equilibrium heating and Scheil cooling of the Al-Sn alloy containing various alloying elements.

a. Al intermetallic stable during entire foaming process: Ti and Co

The addition of Ti to the Al-Sn alloy can form a stable intermetallic $TiAl_3$ (melting temperature 1350 ^oC) with Al from room temperature to above the melting temperature of Al, and the amount of $TiAl_3$ is not changing with temperature. Even with an amount as small as 1wt.%Ti, $TiAl_3$ phase can be calculated to be stable up to 805 ^oC. Of course, this intermetallic phase is not formed at room temperature due to slow kinetics, but it is expected to form before

the complete melting of Al. Once there is enough liquid in the system, as in the case of Al–3wt.%Sn alloy, the kinetics to form this intermetallic can be faster [8]. The Scheil solidification calculation for cooling of the alloy shows that there is nearly no additional precipitation forming during solidification.

The addition of Co can generate a high melting point intermetallic phase Co_2Al_9 (melting temperature 970 ^oC). According to the Al-Co phase diagram [18], with the addition of 1 to 5wt.%Co the melting point of this binary alloy can increase from 660 to 820 ^oC. As can be seen in Figure 6.3, the intermetallic Co_2Al_9 phase formed at 5wt.%Co alloy can be dissolved partially into Al melt during the foaming process. The same can happen for the alloy with 3wt.%Co addition. In the case of 1wt.%Co addition, Co_2Al_9 can be dissolved completely before 660 ^oC during the foaming process.

b. Al intermetallics dissolved during foaming process: Mn and Ni

In the case of Mn addition, Al_6Mn intermetallics can be thermally stable close to or just above the complete melting of Al. The maximum stable temperature of Al_6Mn phase can be varied depending on the amount of Mn: 625, 675 and 700 ^oC with additions of 1, 3 and 5wt.% of Mn, respectively. Thus, this intermetallic compound can be formed in early stage of foam formation but eventually dissolve into the liquid melt when Al-Sn foam reaches the maximum process temperature of 725 ^oC. The Scheil solidification calculations show that the Al_6Mn can be back-precipitated during the solidification process.

Thermodynamic calculation for Ni additions to the base alloy shows the similar precipitation behavior as that of Mn addition. $NiAl_3$ produced before the complete melting of Al can be dissolved in liquid Al-Sn alloy in the temperature range between 600 and 625 ^oC and no thermally stable Ni_3Al intermetallic phase is expected to exist during the final foaming stage of 725 ^oC. With 5wt.%Ni additions, Ni_3Al can be precipitated during the cooling of the foam at about 620 ^oC.

c. Sn intermetallics dissolved during foaming process: Mg

Mg can form Mg_2Sn by reacting with Sn. According to the thermodynamic calculations, Mg_2Sn is stable up to only about 600 ^oC and be completely dissolved into liquid Al. Mg_2Sn can be precipitated again during the foam cooling below 600 ^oC. It is hard to find metallic elements to form intermetallics stable above 700 ^oC with Sn in the Al–3wt.%Sn alloy. It should be noted that the formation of intermetallics with Sn can reduce the beneficial effect of Sn in Al–3wt.%Sn foam by consumption of liquid Sn.

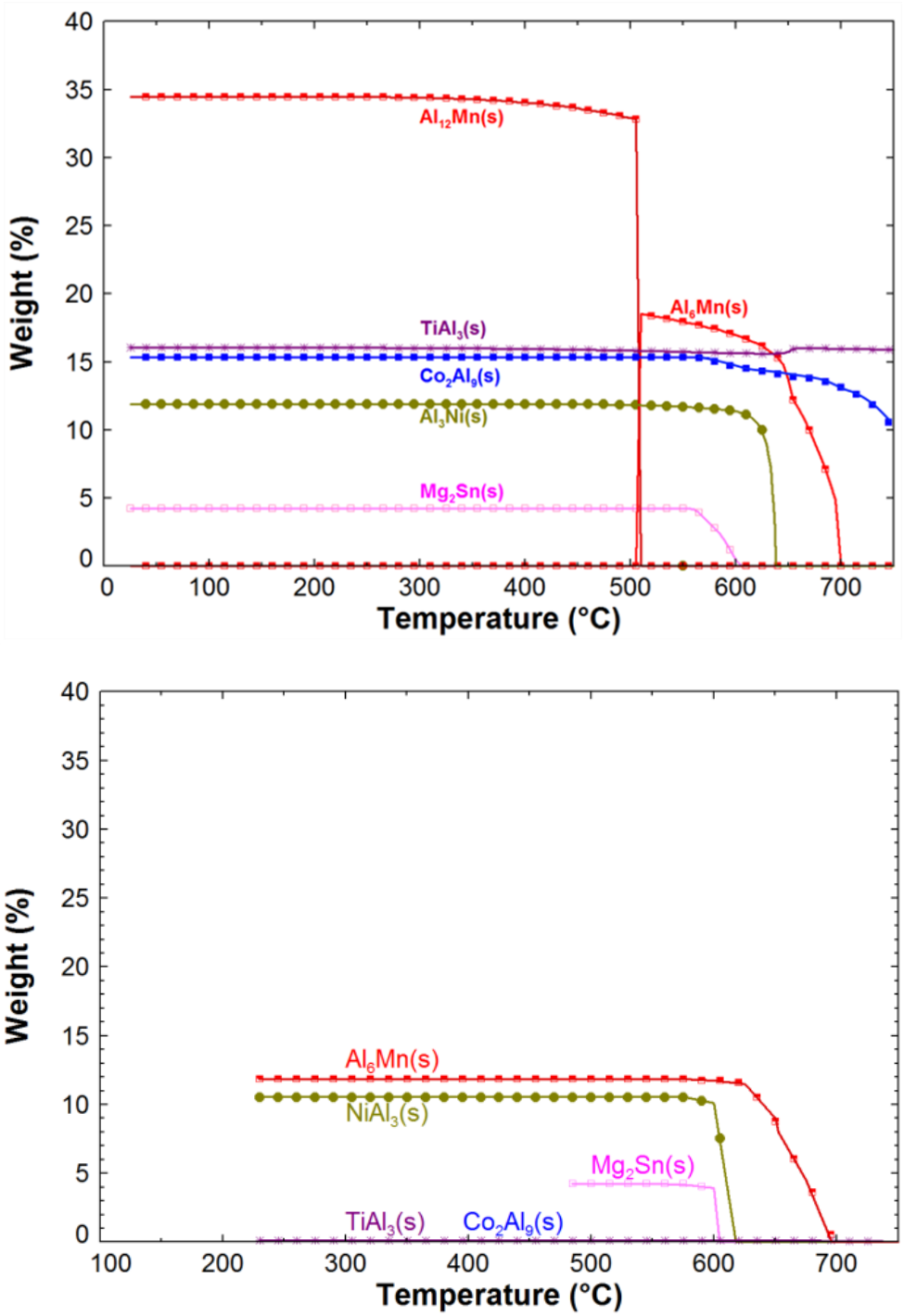

Figure 6.3: Thermodynamic calculations for solid compound formation in various Al

–3wt.%Sn–X alloys during (a) heating and (b) cooling process. Heating process is calculated using equilibrium calculation and cooling process is calculated using the Scheil cooling calculation.

6.4.2. Thermal analysis: DSC results

The heat flow curves of the first heating/cooling cycles of Al–3wt.%Sn base alloy and alloys with the additions of maximum amount of each alloying element are compared in Figure 6.4, and the results are summarized in Table 6.1. The DSC curve of Al–3wt.%Sn base alloy exhibits an endothermic peak near 520 ^{o}C (more precisely between 490 and 550 ^{o}C), corresponding to the TiH_2 decomposition. After the decomposition of TiH_2, there is a large endothermic heat flow which corresponds to the melting of Al matrix. However, it was hard to point out an exact onset temperature of the melting from the thermal curve. Therefore, the peak temperature of melting was recorded instead of the onset temperature. During the cooling cycle, the initial solidification was detected at 661 ^{o}C. The melting and solidification of Sn were observed at 231 ^{o}C reversibly.

The addition of alloying elements changed the thermal behavior of Al–3wt.% Sn base alloy. Two important features were observed. As all alloying elements were designed to form precipitates with Al or Sn, the thermal peaks related to the formation of the precipitates were recorded at the heating cycle of DSC curve. If the precipitates were dissolved in liquid during the foaming process, back-precipitations were recorded during the cooling cycle. The other feature is the change of the melting temperature of Al matrix during the heating cycle or solidification temperature of Al matrix during the cooling cycle by the alloying elements.

In the cases of Co, Ti and Ni additions, very noticeable exothermic heat flows were observed around 600 ^{o}C before the melting of Al matrix. These are believed

to be the formation of Co_2Al_9, $TiAl_3$ and $NiAl_3$ intermetallics. Although these intermetallics could form thermodynamically at room temperature, they seem to form at high temperature prior to the melting of Al matrix due to the slow kinetics at low temperature. In the case of Mn addition, a small exothermic peak corresponding to $Al_{12}Mn$ or Al_6Mn was recorded at about 593 ^oC. The addition of Mg shows an exothermic peak at about 517 ^oC for the formation of Mg_2Sn and an endothermic peak at about 605 ^oC for the melting of Mg_2Sn.

During the cooling cycles of the DSC runs, the alloys containing Mg and Ni clearly show the precipitations of intermetallics at 601 ^oC and 630 ^oC, respectively. In the case of Mn addition, the peak was recorded at 690 ^oC prior to the solidification of Al matrix. In the case of the alloys containing Ti and Co, no exothermic peaks associated with precipitation of intermetallics were observed during their cooling cycles.

The solidification temperatures recorded during cooling cycles of alloys containing Ni and Mg containing alloys were 643 ^oC and 651 ^oC, respectively, which are noticeably lower than that of the Al–3wt.%Sn base alloy (661 ^oC). The solidification temperatures of the other alloys containing Mn, Ti and Co were within 5 ^oC lower than that of the base alloy. As mentioned earlier, it is hard to point out the onset temperature of melting of Al matrix, the onset temperature of Mg and Ni containing alloys are certainly lower than the other alloys as can be seen in the heating cycle curves of Figure 6.4.

It should be noted that all the results of DSC analyses are consistent with the thermodynamic calculation results in Figure 6.2 and Figure 6.3

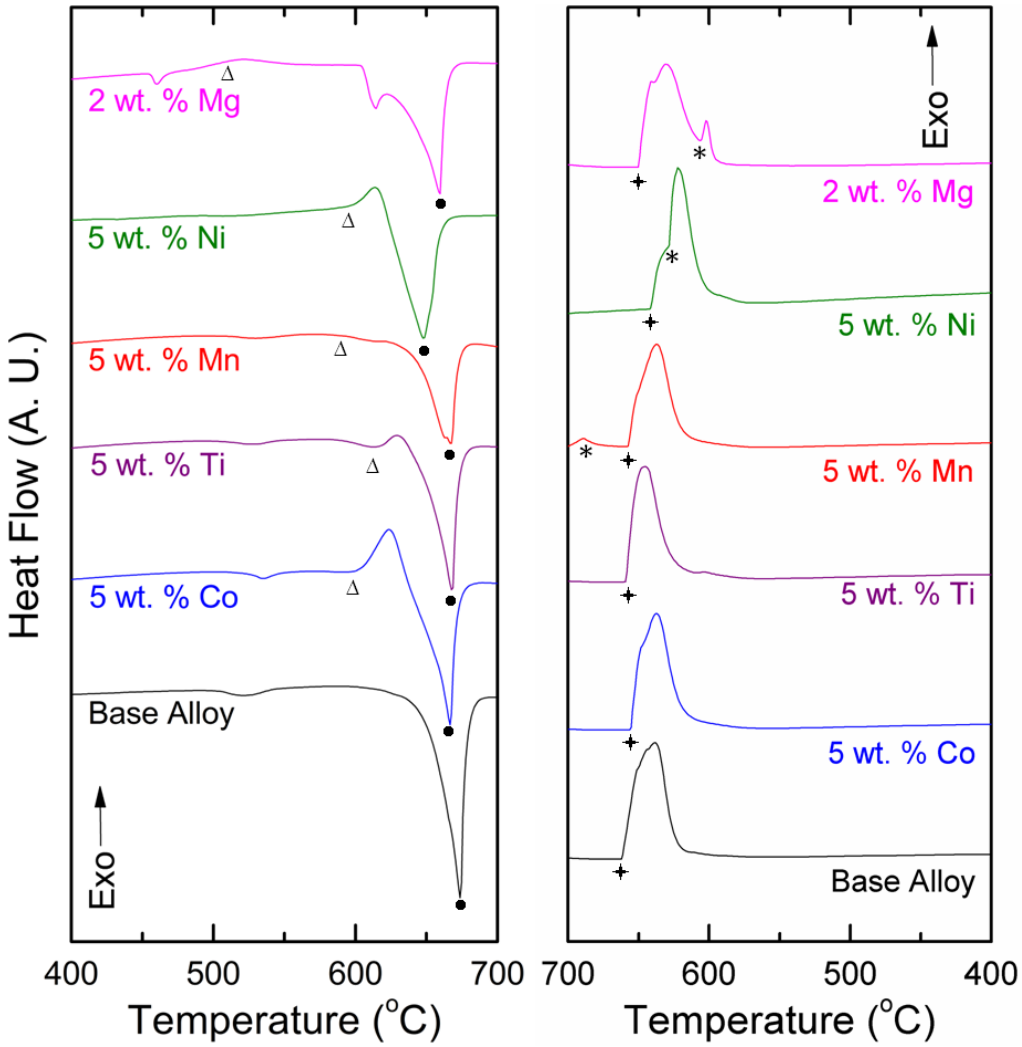

Figure 6.4: DSC curves of various Al–3wt.%Sn–X alloys during (a) heating and (b) cooling cycle. Δ Formation of precipitate during heating, ● minima of melting peak, ✦ solidification point, and * formation of a precipitate during cooling.

Table 6.1. Summary of DSC results for the Al–3wt.%Sn–1wt.%TiH_2 with addition of alloying elements.

	Reaction	Al + 3wt.% Sn	Al - 3 wt. % Sn + 5wt.% Mn	5wt.% Ni	5wt.% Co	5wt.% Ti	2wt.% Mg
Δ	Formation of precipitate (heating)	--	593	590	596	614	517
●	Melting (minima)	678.9	667	647	666.9	667	659.5
	Hydride decomposition	497 - 534	508 - 540	490 - 550	519 - 546	500 - 549	454 - 471
✦	Solidification	661	659	643	655.5	659.3	651.2
*	Formation of precipitate (cooling)	--	690	630	--	--	601

6.4.3. Foaming behavior and Structural characterization

Precursors, the powders compacted at 350 ^{o}C under 360 MPa, were foamed in a mechanical expandometer at a temperature of 725 ^{o}C. During expansion, experiments were interrupted at specific times (before, at and after maximum foam expansion for each alloy) in order to characterize pore distribution, drainage and precipitates at cell wall. More than 3 samples were examined for each condition and the average values were used in the interpretation. The standard deviations of the results were small for the samples taken before and after the peak expansion (1st and 2nd plateaus). The deviations were a bit larger for the samples taken during the expansion in-between the plateaus because a small change in sampling time can end up a quite different expansion, but still reproducible. In the present study, the foam expansion (%) was calculated as: (foam height – precursor height)/(precursor height) x 100%.

Although many macro- and micro-structures of the samples were examined for each alloy, the microstructure just before the maximum expansion for each alloy is shown in this study due to the lack of space. The foam expansion behavior and sphericity values at the optimum condition of each alloy are summarized at Table 6.2 and Table 6.3, respectively.

Table 6.2. The effect of alloying element on the foaming behavior of Al–3wt.%Sn alloy.

Alloying element (wt.%) / intermetallics		T_m (^oC) of Intermetallics*	DSC (exothermic heat, J/g)	Duration (sec)			Expansion max. (%)
				1st plateau	Slope	2nd plateau	
Al–3wt.%Sn		-	No heat	300	350	Stable	350
Mn/ Al_6Mn	1	625	Small (overlapped)	400	300	Stable	320
	3	675		300	200	Stable	320
	5	700		200	125	Stable	320
Ni/ $NiAl_3$	1	625	64.17	200	300	Stable	320
	3	612		100	150	250	450
	5	615		50	175	Collapsed	500
Co/ Co_2Al_9	1	660	69.06	200	200	Stable	375
	3	740		175	200	Stable	380
	5	820		150	150	Stable	330
Ti/ $TiAl_3$	1	1350	20.68	400	500	Stable	380
	3	1350		150	150	Collapsed	450
	5	1350		150	150	Collapsed	440
Mg/ Mg_2Sn	0.5	525	13.81	400	100	Stable	190
	1	600		450	100	Stable	200
	2	610		350	100	Stable	175

* Calculated from thermodynamic database.

Table 6.3. Sphericity index (SI) values of Al and Al–3wt.%Sn alloys at their optimum foam structure.

		Al +		Al – 3wt.%Sn +									
wt. % Al	SI	wt. % Sn	SI	wt. % Mn	SI	wt. % Ni	SI	wt. % Co	SI	wt. % Ti	SI	wt. % Mg	SI
100	0.67	1	0.85	1	0.72	1	0.75	1	0.74	1	0.70	0.5	0.80
		3	0.80	3	0.77	3	0.77	3	0.75	3	0.66	1	0.81
		5	0.82	5	0.77	5	0.76	5	0.76	5	0.68	2	0.87

Pure Al and Al–3wt.%Sn

The foaming behaviors of pure Al with 1wt.%TiH_2 at various temperatures between 700 ^oC and 800 ^oC and that of Al–3wt.%Sn at 725 ^oC are compared in Figure 6.5. As expected, the foaming process of pure Al was accelerated with increasing foaming temperature because the decomposition of TiH_2 and melting of Al were accelerated. In addition, the higher maximum peak expansion was obtained with the higher foaming temperature but the duration at maximum expansion was greatly shortened. The Al–3wt.%Sn alloy showed two plateaus. This first plateau can be mainly related to the partial decomposition of TiH_2. Also water vapor coming from the ambient humidity attached to the powders and small amount of gas entrapped in the precursor during compaction can contribute to this expansion [19]. It is interesting to see that the expansions at 800 s for both Al-Sn and pure Al precursors are the same. As mentioned earlier, the Al-Sn foams exhibited a remarkable expansion (350 %) for long duration time at 725 ^oC, while

Al foam expanded only to a maximum of 220 % for several seconds at 725 ^{o}C and collapsed.

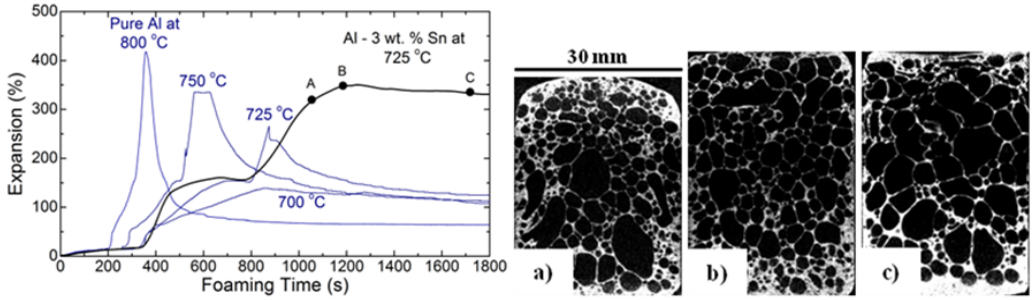

Figure 6.5: Expandometer curves for pure Al recorded at different foaming temperatures (800, 750, 725 and 700 ^{o}C) and Al–3wt.%Sn alloy foamed at 725 ^{o}C. a) to c) are the macrostructures of Al–3wt.%Sn alloys from x-ray tomographer.

The cross sectional views of the cell structures of the Al-Sn foam at points A, B and C during the expansion were analyzed using X-ray tomography, and they are presented in Figure 6.5. At point A prior to the maximum expansion, the foam was not completely expanded yet as witnessed from the rounded edges at the top of the foam. At point B of the maximum foam expansion, the cell structure is homogeneous and no drainage was observed. At point C, after the maximum expansion, a little drainage can be observed on the bottom of the sample which is a typical feature of over-aged foam. In addition, the size of pores in the middle part of the sample is larger than that of the side, which resulted from the foam coalescence. Typically, the optimum foam structure can be obtained just before reaching the maximum expansion of foam [3]. In the case of the Al-Sn based alloy, the point B cell structure can be considered as the optimum cell structure.

Al–3wt.%Sn with Co

The foam expansion curves for Al–3wt.%Sn + Co alloys and their cell structures are presented in Figure 6.6. With the addition of Co, the length of the first plateau became shortened and therefore the second expansion happened earlier than Al–3wt.%Sn base alloy. However, the maximum expansions of Co containing alloys are similar to that of Al-Sn base alloy except for the alloys containing 5wt.%Co of which maximum expansion reached only 300 %. The microstructures of cell wall were examined by SEM-EDS and the typical features are presented in Figure 6.6. Homogeneous distribution of Co_2Al_9 intermetallic was observed in 1, 3 and 5wt.% addition of Co. However, the shape of Co_2Al_9 changed from needle to agglomerate with increasing Co amount. According to the thermodynamic calculations, the Co_2Al_9 intermetallic phase in the alloys containing 1 and 3wt.% of Co can be dissolved during the foaming process and precipitated back during cooling of the foam. However, the intermetallic phase in the alloy with 5wt.%Co can be stable up to 725 ^{o}C and only a small amount of the intermetallic phase will be precipitated during cooling. This could be possible reason for the shape difference of the intermetallic phase. With increasing Co content, the average size of cell increased and the shape of cell became more polygonal. In addition, the pore coalescence became more noticeable. The sphericity of the cell is about 0.75 which is lower than the base alloy of 0.82.

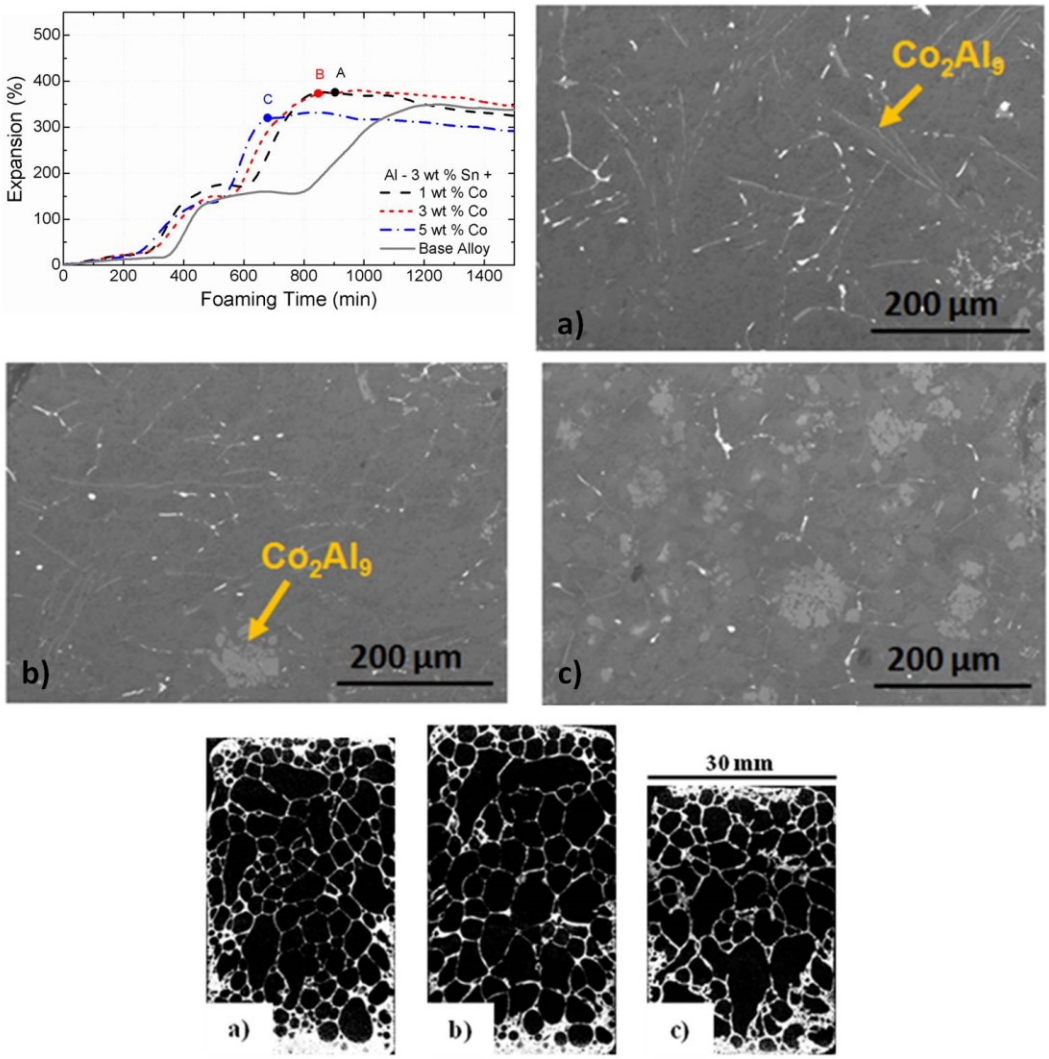

Figure 6.6: Expansion behaviour, macrostructure and microstructure of Al–3wt.%Sn–Co (wt. % Co = 1, 3 and 5) foam produced at 725 ^{o}C. The microstructures are from 1, 3 and 5wt.%Co from left to right.

Al–3wt.%Sn with Ti

According to the thermodynamic calculation in Figure 6.3, precipitation behavior of Ti containing alloy is similar to that of the Co containing alloy. That is, both alloys form stable precipitates up to 725 ^{o}C. However, the foaming behavior of Ti containing alloy is completely different from that of Co containing alloy. As can be seen in Figure 6.7, with 1wt.%Ti addition, the expansion curve follows the same trajectory as that of the base alloy. For the cases of 3 and 5 % Ti additions, interestingly, the first plateau almost disappeared and foam expansion reached more than 450 % and collapsed in short time to the same expansion level as Al–3wt.%Sn base alloy or even lower. The pores are typically in polyhedral shape. $TiAl_3$ intermetallic particles originating from metallic Ti addition and TiH_2 hydride powders were observed in the microstructure. The intermetallic particles originated from TiH_2 hydride typically formed agglomerates [8] .On the other hand, the intermetallic particles from metallic Ti formed very fine precipitates uniformly distributed in cell wall. The sphericity of the cell is about 0.68 which is the lowest value among all alloys.

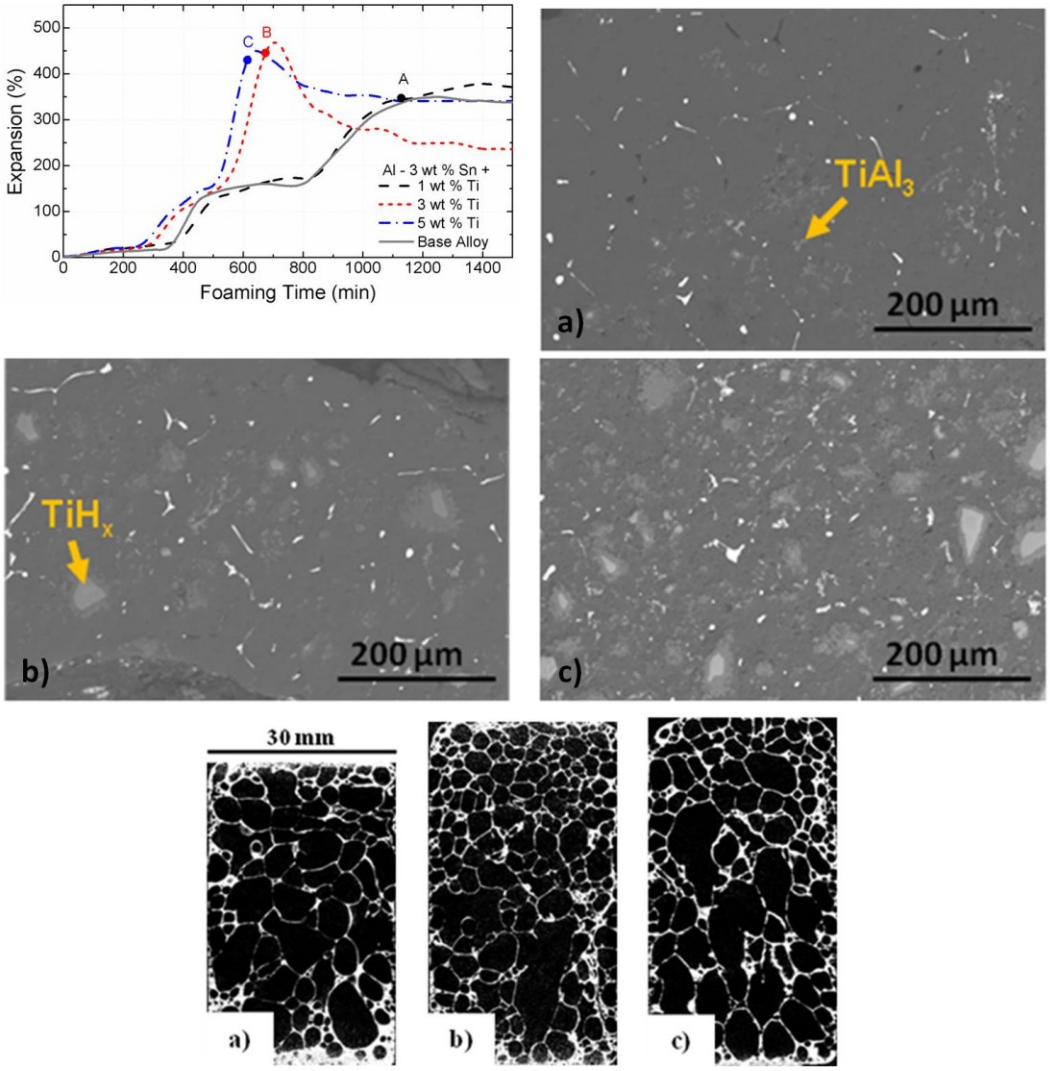

Figure 6.7: Expansion behaviour, macrostructure and microstructure of Al–3wt.%Sn–Ti (wt.%Ti = 1, 3 and 5) foam produced at 725 ^{o}C. The microstructures are from 1, 3 and 5wt.%Ti from left to right.

Al–3wt.%Sn with Mn

Figure 6.8 shows the foaming behavior of the alloy containing Mn. The foaming behavior of this alloy is very similar to that of Co containing alloy. The more Mn was added, the faster the maximum expansion was reached. A large amount of Al_6Mn intermetallic particles were found in the cell wall. Like the Co containing alloy, the shape of Al_6Mn intermetallic phase was also changed with Mn content. It seems that the intermetallic particles with needle shape are formed during the solidification and the nodular particles are formed during the heating process and stable thereafter. According to the thermodynamic calculation, the dissolution temperature of Al_6Mn intermetallic phase in the alloy containing 5wt.%Mn is about 700 ^{o}C. However, as the dissolution temperature of the Al_6Mn is close to the final processing temperature of 725 ^{o}C, the dissolution of Al_6Mn could not be completed during foaming. The sphericity of the cell is about 0.76 which is very similar to that of Co containing alloy.

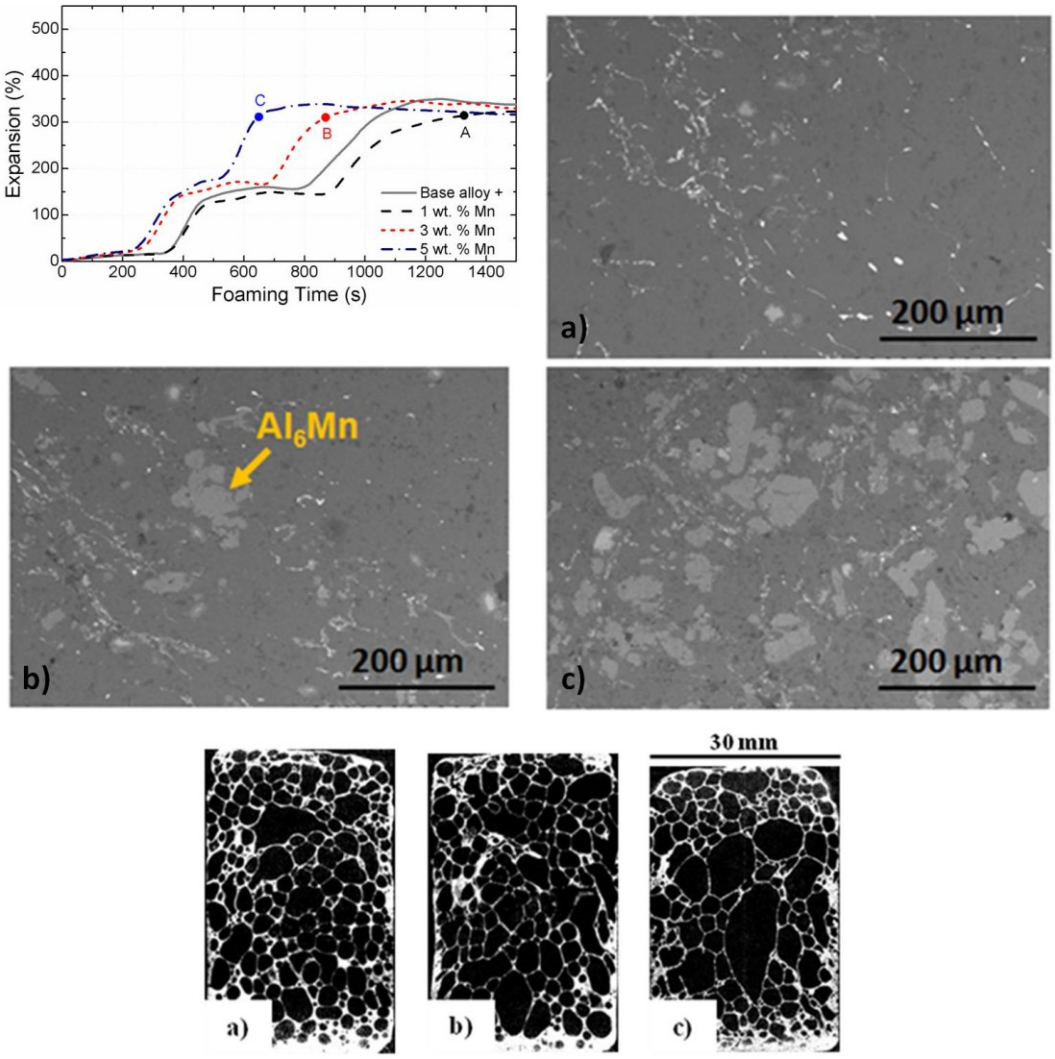

Figure 6.8: Expansion behaviour, macrostructure and microstructure of Al–3wt.%Sn–Mn (wt.%Mn = 1, 3 and 5) foam produced at 725 ^{o}C. The microstructures are from 1, 3 and 5wt.%Mn from left to right.

Al–3wt.%Sn with Ni

Figure 6.9 shows the foaming curves of the base alloy with 1, 3 and 5wt.%Ni additions and the macrostructures at specific foaming times. The addition of 1wt.%Ni showed the same foaming behavior as the base alloy. Interestingly, the 3 and 5wt.% addition of Ni showed the abrupt change in the foaming behavior. The foaming behavior of these alloys is similar to that of Ti containing alloy. However, the onset of expansion is even earlier than Ti containing alloy, and the maximum expansion reaches more than 470 %. The stability at the maximum expansion for the alloy containing 3wt.%Ni was about 4 min, which was the much longer than that of Ti containing alloy. After collapse of the foam, the expansion became similar or lower than that of the base alloy. The microstructure in the cell wall shows that $NiAl_3$ intermetallics were mainly formed in the dendrite boundary for 1 and 3wt.%Ni containing alloys, and also eutectic type precipitation for 3 and 5wt.%Ni alloys. This microstructure tells that the $NiAl_3$ phase was completely dissolved during the heating process and precipitated back during cooling, as predicted from thermodynamic calculations in Figure 6.3 and characterized in DSC cooling curve at 630 ^{o}C. The macrostructure of the foam with 3wt.%Ni is still excellent and the sphericity of the cell is about 0.76.

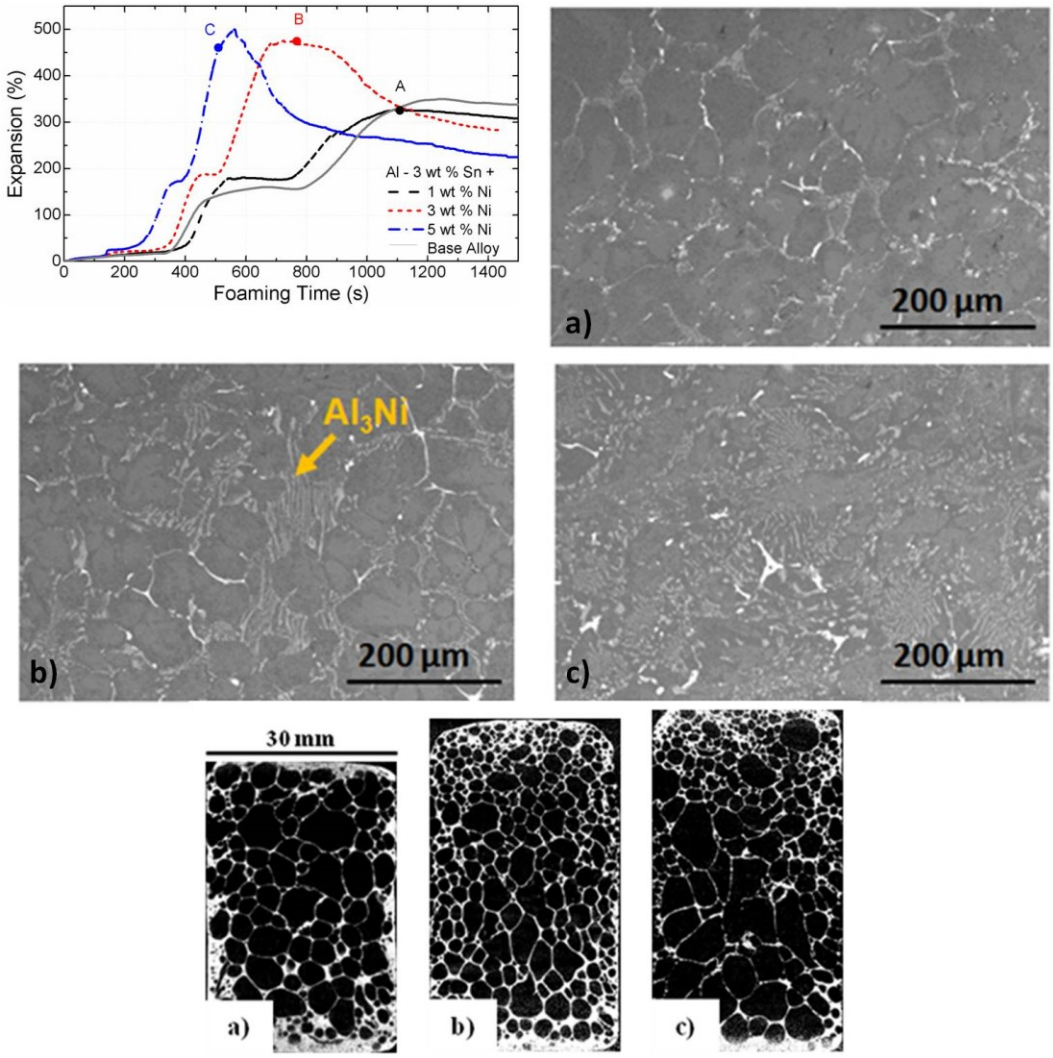

Figure 6.9: Expansion behaviour, macrostructure and microstructure of Al–3wt.%Sn–Ni (wt.%Ni = 1, 3 and 5) foam produced at 725 ^{o}C. The microstructures are from 1, 3 and 5wt.%Ni from left to right.

Al–3wt.%Sn with Mg

The foaming behavior and foam macro- and micro-structure of alloy containing Mg are presented in Figure 6.10. Both first and second plateaus for all alloys containing up to 2wt.%Mg occurred earlier than those of the Al–3wt.%Sn base alloy. However, the expansion levels for both plateaus were much lower, even less than 200 %, than the base alloy. The lower expansion can be easily explained by the formation of thick skin (presumably due to the formation of MgO or $MgAl_2O_4$). This oxide skin impeded the foam growth, but neither pore coalescence nor drainage happened for long foaming times. Very small pores with sphericity of 0.83 were found from macrostructure. Mg_2Sn was observed along dendrite boundary in cell wall, which means the precipitation occurred during solidification as predicted in the thermodynamic calculation.

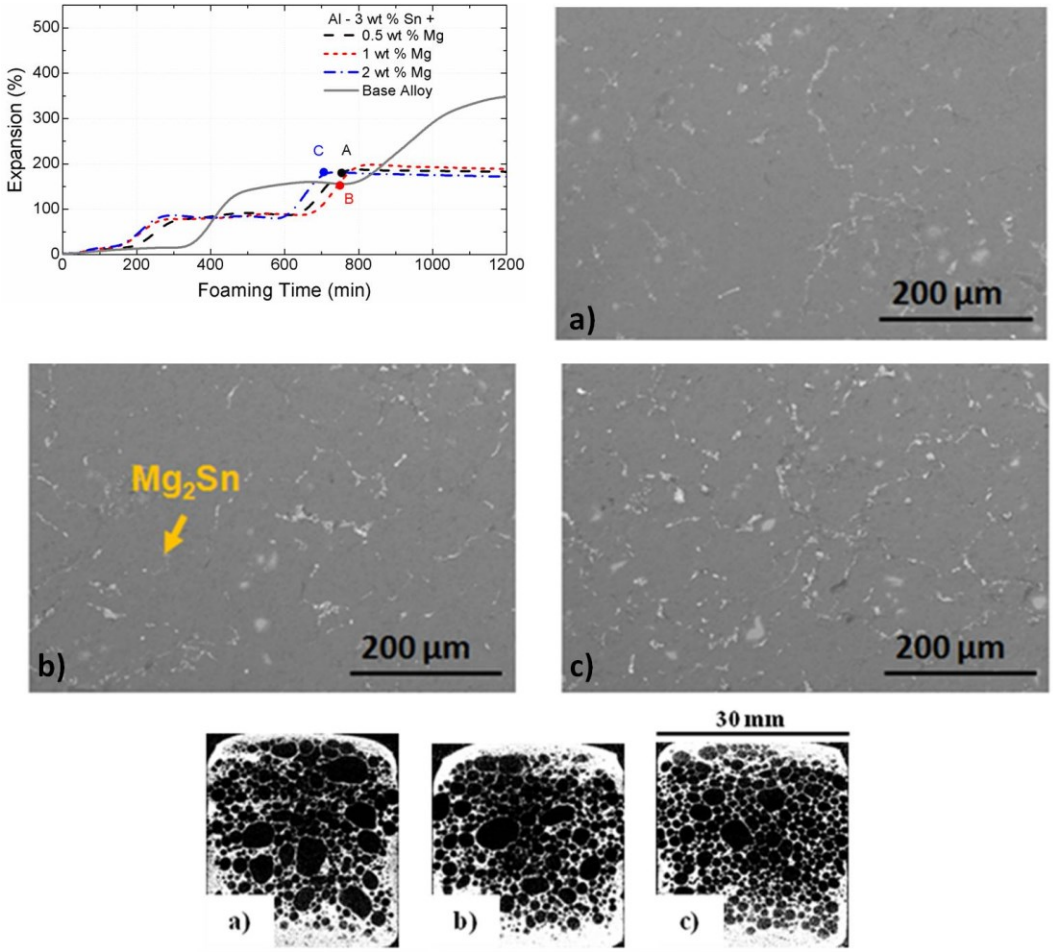

Figure 6.10: Expansion behaviour, macrostructure and microstructure of Al–3wt.%SnMg (wt.%Mg = 0.5, 1 and 2) foam produced at 725 ^{o}C The microstructures are from 0.5, 1 and 2wt.%Mg from left to right.

6.4.4. Effect of alloying elements on the foaming behavior

The effect of alloying elements to the foaming behavior can be summarized as:

(a) Production of the exothermic heat during the formation of intermetallic phases in the temperature range of the decomposition of TiH_2, which can release H_2(g)

(b) Formation of a stable intermetallic phase during the foaming process, which can increase the viscosity and increase the rigidity of cell wall

(c) Change in the melting behavior (solidus and liquidus temperatures) of Al matrix.

(d) Change in surface tension of alloy, which can influence the stability of cell wall.

The alloying elements used in the present study can contribute to one or more than one of the above effects to change the foaming behavior of Al–3wt.%Sn alloy. In order to compare the roles of the alloying elements, the foaming curves of all alloys are summarized in Figure 6.11. The roles of each alloying elements can be understood based on the thermodynamic calculations, DSC results and foaming behavior presented in Figure 6.2, Figure 6.3, Figure 6.4 and Figure 6.11.

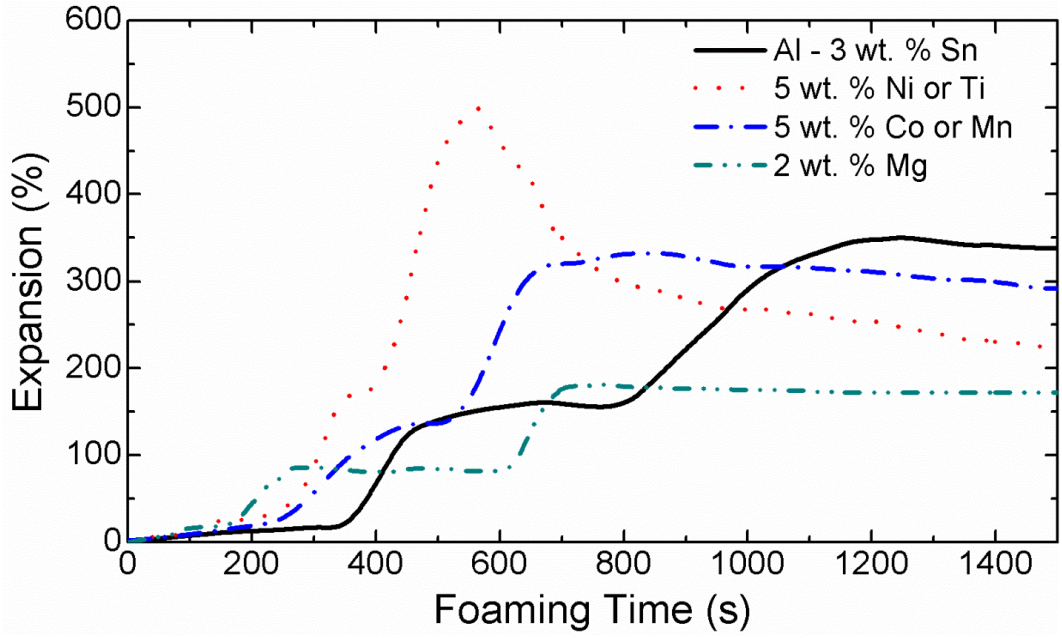

Figure 6.11: Comparison of the effects of different alloying elements on the foaming behaviour of the Al–3wt.%Sn base alloy.

The alloying elements Co, Mn, Ti and Ni can shorten the first plateau of the foaming curve. As explained in Figure 6.1, the first plateau occurs due to the suppression of TiH_2 decomposition in the temperature range 450 to 600 ^oC. The addition of all these alloying elements can produce a significant amount of exothermic heat during the formation of intermetallics with Al at about 600 ^oC (for example, the addition of Co produced about 64 J/g, which is about 1/5 of the heat required for the melting of the entire Al matrix), as analyzed in DSC results for loose powder samples in Figure 6.4. It is believed that compacted powders, like the precursors, can produce the intermetallics earlier than loose powders because Al and alloying elements are already well contacted to form intermetallic phases. The release of the exothermic heat can locally increase the temperature of the sample which can accelerate the decomposition of TiH_2 and even make a partial melting of the surrounding Al matrix. This is believed to be the reason for the shortening of the first plateau leading the earlier second expansion.

The alloys containing Ti and Ni showed the increase of maximum expansion than the Al-Sn base alloy, but no such increase was observed for Co and Mn containing alloys. Typically the maximum foam expansion can be determined by various factors including the amount of $H_2(g)$ captured during the foaming process, viscosity of melt, and surface tension of the molten cell wall.

In case of Ni containing alloy, the melting of Al matrix occurred about 20 to 40 ^oC earlier than the other alloys, as can be analyzed in DSC results in Figure 6.4, and the predicted melting behavior from thermodynamic calculations in Figure 6.2 also shows earlier liquid formation than other alloys. This premature liquid

formation can help to capture more H_2(g) during the decomposition of TiH_2. Moreover, the $NiAl_3$ intermetallics formed before the melting of the matrix can be back-dissolved into liquid (according to the thermodynamic calculation is about 625 ^oC) during the foaming process between 600 and 725 ^oC. This means there are no obstacles in the cell walls during foam expansion, which can allow higher expansions. However, the foam of maximum expansion is not retained but collapsed due to the surface tension [20] of the cell wall is not low enough to maintain the cell structure. The final expansion level is similar to that of Al-Sn base alloy.

In the case of Co and Mn containing alloys, the intermetallics of Co_2Al_9 and Al_6Mn are stable in the course of foam expansion between 600 and 725 ^oC. Strictly speaking, thermodynamic calculations shows that Co_2Al_9 can be partially dissolved into liquid Al during the process and Al_6Mn can be dissolved at about 700 ^oC. Therefore, the intermetallic particles can increase the viscosity of the melt during foaming and can act as obstacles to the stretching of the cell walls, which can limit the expansion of those foams to the same level as Al-Sn base alloy.

The foaming behavior of Ti containing alloy is difficult to explain completely up to our knowledge. The addition of Ti can form $TiAl_3$ intermetallic particles which are stable over the entire course of foaming. Therefore, it would be expected that the foaming curve is similar to the case of the Co and Mn containing alloys. However, the real foaming curve shows that the maximum expansion of the Ti containing alloy reached much higher than Al-Sn base alloy. The only microstructural difference of Ti containing alloy from Co and Mn containing

alloys are the morphology of intermetallics. As presented in Figure 6.7 to Figure 6.9, the morphology of Ti intermetallic is very fine and uniformly distributed in the cell wall while the Co and Mn intermetallics are agglomerated together.

The addition of Mg can largely change the foaming behavior of Al-Sn alloy. Both the first and second plateaus occurred earlier than the base alloy, but the first and second expansions were lower by almost 50% of the base alloy. The earlier occurrences of the first and second plateaus can be due to the formation of Mg_2Sn intermetallic phase with exothermic heat and lower melting temperature of the Al matrix by Mg addition, respectively, as can be witnessed from DSC results and thermodynamic calculations in Figure 6.2 and Figure 6.4. As mentioned earlier in the section 4.3, the main reason for lower expansion can be the oxidation of precursor during hot pressing and foam during the foaming process. The resultant oxide shell can constrain the foam expansion. Interestingly, the macrostructure of the foam consist in the fine and uniform pores. As can be seen in Figure 6.10, the pore size of higher Mg containing alloys is smaller and more uniform. This can happen because Mg can reduce surface tension of Al-Sn alloy further. For example, 1wt.%Mg can reduce the surface tension of Al from 860 dynes/cm to 660 dynes/cm at 700 ^{o}C [21].

It is well known that mechanical properties of metallic foams are closely related to the foam density and the properties of the cell wall material [22-24]. Also retaining a homogeneous pore structure and density (which is achieved at plateau of maximum expansion for Al-Sn and/or Al-Sn-X foams) will render the foam a better energy absorber. Precipitations of intermetallic phases in the cell wall can

enhance the mechanical property of Al foam. The presence of intermetallics promotes the incoherence between the intermetallic and the matrix, modifying the failure mechanism from ductile to brittle and in turn improving the foam compression strength [25].

Among all the candidate alloying element additions, Co and Mn are the optimum alloying elements because the foam is very stable for a long time with the benefit of intermetallic phase formation. Furthermore the presence of intermetallic phases in the microstructure can enhance the energy absorption capacity and efficiency, which is important for the crashworthiness of automotive application. i.e. Al-3wt.Sn - 5wt.%Mn foam containing Al_6Mn intermetallics can strain up to 70%, absorbing up to 5 MJ/m^3 at only 7.5 MPa of stress, while Al-3wt.%Sn foam would require about 17 MPa to absorb the same energy at the same strain. The complete test method and results are presented elsewhere [25].

Although it is possible to quench a small foam sample in laboratory at any time of foaming process, it is hard to stop the foaming process of a large industrial component all instantly. Therefore, it is desirable to have Al alloys which can keep the optimum foam structure for longer times. For instance, pure Al foam can only retain maximum expansion for a few seconds while Al-3wt.%Sn can retain about 300% expansion for 10 minutes. Longer plateau at maximum expansion is kept when adding Co or Mn to the base alloy, therefore the entire part or component can have a reasonably homogeneous and optimum macro- and micro-structure. In the present study, the Al-Sn alloys with Co and Mn can satisfy this industrial production requirement.

6.4.5. Summary

The effect of in-situ intermetallic formation on the foaming behavior of Al–3wt.%Sn alloy has been investigated by introducing five different alloying elements, Co, Mg, Mn, Ni and Ti. The alloying elements forming intermetallic phases with Al and Sn were chosen among many abundant and inexpensive metallic elements based on comprehensive thermodynamic calculations. The thermal analyses of the designed alloy powders were performed using DSC and the real foaming tests were carried out using a mechanical expandometer. The macrostructure and microstructure of the foam were analyzed with an x-ray tomograph and SEM, respectively.

It is found that the foaming behavior and foam stability of Al–3wt.%Sn alloy can be actively controlled by the alloying elements. The base alloy Al–3wt.%Sn alloy with 1wt.%TiH_2 showed two plateaus in the foam expansion curve. The addition of alloying elements to produce intermetallic phases has shortened the first plateau in the foaming curve due to the exothermic heat generated during the formation of the intermetallic phase. The increase of the maximum expansion was observed for the Ni and Ti containing alloys, but the foams collapsed back to the level of the Al–3wt.%Sn base alloy. Only the foam containing 3wt.%Ni presented a plateau for few minutes before collapsing. The alloys with Co and Mn showed the same maximum expansion as the base alloy with very stable foam.

It is found that the increase of foam expansion of Al alloys with TiH_2 can be achieved by the decreasing of melting temperature of Al allowing the capture of more hydrogen gas. The formation of in-situ intermetallic phases can produce an exothermic heat and result in the acceleration of TiH_2 decomposition and local melting of the Al matrix, which helps foam expansion. The foam stabilization can be achieved by the formation of intermetallic particles and introduction of the alloying elements decreasing the surface tension of the cell wall. This alloy design concept can be applied to any metallic foam using powder metallurgical route to optimize the foaming behavior.

Acknowledgements

The authors would like to thank NSERC, FQRNT, GM of Canada, and CONACyT for financial support. The author (L.Y. Aguirre-Perales) also thanks to Korean Institute of Metals for the financial support.

References

[1] J. Banhart:, Prog. Mater. Sci., 2001, vol. 46, pp. 559-632.

[2] S. Asavavisithchai, and A.R. Kennedy: J. Colloid Interface Sci., 2006, vol 297, pp. 715- 723.

[3] J. Banhart: Adv. Eng. Mater., 2006, vol. 8, pp. 781-794.

[4] T. Wubben, H. Stanzick, J. Banhart, and S. Odenbach:, J. Ph: Conden. Matter, 2003, vol. 15, pp. S427-S433.

[5] G.S. Vinodkumar, and S. Sundarraj: Metall. Mater. Trans. B, 2010, vol. 41B, pp. 495- 499.

[6] C. Korner: Mater. Sci. Eng. A, 2008, vol. 495, no. 1-2, pp. 227-235.

[7] L.Y. Aguirre-Perales, I.-H. Jung, and R.A.L. Drew: Acta Mater., 2012, vol. 60, pp. 759-769.

[8] L. Aguirre-Perales, I.-H. Jung, R.A.L. Drew: Metall. Mater. Trans. A, 2012, vol 43, pp. 1-5.

[9] A. Haibel, A. Rack, and J. Banhart: Appl. Phys. Lett., 2006, vol. 89, pp. 1-3.

[10] Korner, M. Arnold, and R.F. Singer: Mater. Sci. Eng. A, 2005, vol. 396, pp. 28-40.

[11] S. Asavavisithchai,and A.R. Kennedy: Scr. Mater.,2006, vol. 54, pp. 1331-1334.

[12] M. Nosko, F. Simancík, K. Izdinský, P. Svec, and R. Florek: Mater. Lett., 2011, vol 65, no. 9, pp. 1378-1380.

[13] R.E. Raj, and B.S.S. Daniel: Int. J. Adv. Manuf. Technol., 2008, vol. 38, pp. 505-512.

[14] R.E. Raj, and B.S.S. Daniel: J. Allo. Compd, 2009, vol. 467, pp. 550-556.

[15] C.W. Bale, P. Chartrand, S.A. Degterov, G. Eriksson, K. Hack, R. Ben Mahfoud, J. Melançon, A.D. Pelton, and S. Petersen: Calphad, 2002, vol. 26, no. 2, pp. 189-228.

[16] L.C. Prasad, and A. Mikula: Ph B: Cond. Matter, 2006, vol. 373, no. 1 pp. 142-149.

[17] L. Goumiri, J.C. Joud, P. Desre, and J.M. Hicter: Surf. Sci., 1979, vol. 83, pp. 471-486.

[18] A.J. McAlister: ASM Handbook: Alloy Phase Diagrams, vol. 3, p. 288, ASM Inter., 1989.

[19] C. Jimenez, F. Garcia-Moreno, J. Banhart, and G. Zehl: International conference on porous metals and metallic foams, DEStech Publications Inc, Montreal, Quebec, 2007.

[20] I. Egry, and J. Brillo: J.Chem. Eng. Data, 2009, vol. 54, pp. 2347-2352.

[21] C. Garcia-Cordovilla, E. Louis, and A. Pamies: J. Mater. Sci., 1986, vol. 21, no. 8, pp. 2787-2792.

[22] A.R. Kennedy: J. Mater. Sci., 2004, vol. 39, no. 9, pp. 3085-3088.

[23] H.-P. Degishcher, and B. Kriszt: Handbook of Cellular Metals: Production, Processing and Applications, WILEY-VCH Verlag Gmbh, 2002.

[24] J. Baumeister, J. Banhart, and M. Weber: Mater.Design, 1997, vol. 18, no. 4/6, pp. 217- 220.

[25] Aguirre-Perales, L.Y., R.A.L. Drew, and I.-H. Jung: McGill University. 3610 University Street, Montreal, QC, H3A 2B2, Canada, Unpublished research, 2014.

Chapter 7

Effect of Intermetallics on the Mechanical Behavior of Al-Sn Foams

Lydia Y. Aguirre-Perales[a], Robin A. L. Drew[a,b], In-Ho Jung[a*]

[a] Department of Mining and Materials Engineering, McGill University, 3610 University Street, Montreal, Qc, H3A 2B2, Canada

[b] Department of Mechanical and Industrial Engineering, Concordia University, 1455 de Maisonneuve Blvd. W., Montreal, Qc, H3G 1M8, Canada

Corresponding author:
Prof. In-Ho JUNG
E-mail: in-ho.jung@mcgill.ca
Tel: 1-514- 398-2608 Fax: 1-514-398-4492

Materials & Design
Special Issue on
"Lightweight Materials and Structural Solutions for Transport Applications"

Under consideration, August 2014.

As the primary author of this manuscript, the Ph.D candidate performed all experiments, analyses, and calculations. The manuscript was also written by the Ph.D. candidate. Prof. Robin Drew conceptualized the tests to be performed. Prof. In-Ho Jung, who is this manuscript's principal investigator contributed to the critical analysis and supervision of this work.

The role of intermetallics in the mechanical properties of Al-Sn foams is presented in this chapter, particularly with regards to the capacity and efficiency of its energy absorption.

Abstract

The energy absorption behaviors of metallic foams of Al-3wt.%Sn alloys with alloying elements like Co, Mg, Mn, Ni and Ti were investigated using compression testing. The intermetallic phase's precipitation behavior was calculated using the thermodynamic database. In general, the energy absorption capacity and efficiency of Al-Sn based foams increased as the amount of intermetallics formed by the reaction of the alloying elements and Al increased. In particular, Al-Sn foams containing Ti (3, 5wt.%), Mn (5wt.%) or Ni (5wt.%) show promising energy absorption capacities even at very low loading pressure. The change in the alloys' stress-strain curves was correlated with the cell wall's fracture mode.

Keywords*: Metal foam; energy absorption; microstructure; intermetallics*

7.1. **Introduction**

Metallic foams, especially Al foams, are of great interest to the automotive industry due to their particular properties. Fuel consumption can be reduced by substituting heavy parts with light metallic foam while maintaining a high stiffness to weight ratio. Aluminum foam structures or foam sandwich panels can be potentially used in car frames, hoods and sliding roofs [1]. Components that require energy absorption and impact energy dissipation like bumpers, crash boxes and A- and B- pillars are good potential applications. Furthermore, most car parts require sound and vibration damping, along with high heat resistance; metallic foams can easily achieve this combination [2].

There are various methods to produce metal foams, but direct foaming of melts and powder metallurgy (PM) are the most common. Regardless of the method, foam reproducibility, which is related to foam stability, has always been the main difficulty of foam processing [3].

In order to improve foam stability, many researchers have studied stabilizing methods, such as adding ceramic particles [4-9], conditioning and melt foaming while creating intermetallics (ALPORAS process) [10-16] , and alloy design with the PM foaming method, targeting a certain liquid fraction, viscosity, and/or surface tension [17-19]. Furthermore, the cell wall microstructure can be controlled through alloy design and heat treatment, which has a direct impact on the mechanical properties of aluminum foams, as reported in [20-22].

Previous studies reported that Al foam's stability can be significantly improved by adding small amounts of Sn, leading to the gradual decomposition of TiH_2 and a decrease in the cell walls' surface tension [23, 24]. Relying on information from these studies, Al-3wt.%Sn alloy foamed at 725 °C was selected as the best foam candidate, as it combined a good compromise between high expansion and foam stability.

In order to tailor Al-Sn based foams' foaming behaviors, experimental and thermodynamic calculation studies were done to optimize the Al-3wt.%Sn alloy with the addition of a third element [25]. The main idea behind this optimization was to induce the formation of in-situ intermetallics during the foaming process of Al-Sn alloy to further improve the expansion, stability, and mechanical properties

of Al-Sn foam. The key factors to be considered for the alloy design include: (a) the acceleration of TiH_2 dissociation at low temperature, (b) the formation of a liquid phase at the normal TiH_2 decomposition temperatures, (~ 450 ^oC to 650 ^oC), which can capture $H_2(g)$, and (c) the decrease of surface tension of Al melt to maintain the foam for a long time at high temperature [25].

Alloying elements like Co, Mg, Mn, Ni and Ti were selected based on thermodynamic calculations done using the FactSage™ 6.2 software with FTlite and FACT53 databases [26]. Ni and Ti additions were found to increase the Al-Sn foams' maximum expansion but collapsed back to the maximum expansion level of the Al-Sn base alloy [25]. However, Al-Sn foams containing Co and Mn can further stabilize the maximum expansion level of Al-Sn base alloy. When Mg was added, Sn's beneficial effect was eliminated due to the consumption of Sn in the formation of Mg_2Sn, which rendered the foaming behavior inferior to the base alloy. In all cases, adding alloying element can shorten the time to reach the maximum foam expansion [25].

This paper presents the mechanical properties of Al-3wt.%Sn alloy combined with various alloying elements (Co, Mg, Mn, Ni and Ti) under compression. In particular, the energy absorption properties of Al-Sn foams incorporating intermetallics were investigated.

7.2. **Experimental Procedure**

7.2.1. Preparation of Al-Sn foams: Powder Metallurgy Technique

Al-Sn based foams were produced using metallic powders purchased from Alfa Aesar. Each powder's characteristics as given by the supplier are listed in Table 7.1.

Table 7.1. Characteristics of powders used for the production of Al-based foams.

Powder	Al	Sn	Ni	Co	Ti	Mg	TiH_2
Metal basis, %	99.5	99.8	99.5	99.5	99.5	99.5	99
Particle size	----------Less than 45 microns----------						

The selected metal powders were mixed in the appropriate ratios (3wt.%Sn + 1, 3 or 5wt.% additional element) along with 1wt.% of TiH_2 in a tumbler mixer for 30 minutes. Due to Mg's strong affinity with Sn, leading to the formation of Mg_2Sn, Mg was added in smaller amounts (0.5, 1 and 2 wt.%). The powder mixtures were loaded into a steel die, 3 cm in diameter, and kept in the hot press at 350 °C for 30 min under no load (to ensure temperature homogenization before hot pressing); next, a pressure of 360 MPa was applied for 10 min at the same temperature to prepare precursors. The resulting precursors had densities above 99% of their theoretical densities and a height of 1.5 cm was set as a standard for all alloys.

Foaming occurred in a mechanical expandometer preheated to a set temperature of 725 °C. The mechanical expandometer's body is composed of a vertical tube furnace in which a stainless steel crucible is suspended. The crucible's inner

diameter is 34 mm and it is coated with boron nitride to facilitate sample removal after foaming. The precursor inside the crucible is in contact with a counterweight piston. A laser records the piston displacement and registers foam expansion against foaming time. The precursor's heating rate was 0.6 ^{o}C/s—the foam's cooling was not registered as the foaming process was interrupted by the removal of the crucible containing the foam, which was placed in a stainless steel block at room temperature to accelerate cooling.

The foaming process was interrupted at optimum foaming conditions, where a maximum number of pores with high sphericity can be obtained. To determine this condition, a foaming experiment was first done and the derivative of expansion as a function of time was calculated, as determined per [23]. Sphericity values at the optimum foaming conditions of the alloys studied are given in [25].

7.2.2. Compression Testing

A uniaxial compression test was carried out on an MTS compression machine equipped with a 100kN load cell, using a constant strain rate of 10^{-3}/s. The compression test was concluded when the engineering strain reached 0.7. Resulting load-displacement curves were converted to stress-strain curves. From an application perspective, the stress-strain curves allow important mechanical properties like energy absorption efficiency and capacity to be determined. Foam samples used for compression tests should have at least 6-7 pores in each direction to obtain a representative measurement [20]. Therefore, samples were scanned using X-ray microtomography (SkyScan 1172) to ensure the homogeneity of pore size and to determine the number of pores. To minimize

density gradients, cylindrical foams with a diameter of 3.4 cm were machined. The top and bottom parts of the original foam were removed based on tomography results: the higher density foam skin was always observed at the bottom and top of foams, which can lead to variations in the mechanical properties [27]. The peripheral foam skin was kept to avoid damaging or smearing the pores due to lathe machining. The sample was weighed and its dimensions measured to determine its density. Finally, the machined sample was placed between the 7.5 cm diameter MTS anvils and a layer of mica coated with boron nitride (to prevent friction or sample sticking). Three foam samples were tested for each alloy and the average results were used to generate the stress-strain curve for each alloy.

7.3. **Results and Discussion**

7.3.1. Thermodynamic calculations

Thermodynamic calculations can predict phase evolution, melting, and solidification behavior of alloys. For the scope of this research the calculations were carried out with FactSage™ 6.2 software using FTlite and FACT53 databases. Thermodynamic calculations were done in the "Equilib" module during heating and Scheil cooling was calculated in non-equilibrium during the cooling simulation. For example, Figure 7.1 shows the thermodynamic calculation results of the intermetallic phase fractions of Al-3wt.%Sn-5wt.%X alloys with temperature. X represents different alloying elements individually added for the purposes of this study: Ni, Co, Ti, Mn and Mg. In the case of Mg, the amount was

set at 2wt.% instead of 5wt.% [25]. The first calculation in Figure 7.1 is a full equilibrium calculation and the second calculation is for the Scheil cooling calculation.

It has been found that intermetallic phases mostly begin to form during the melting of precursors and remain during the foaming and the cooling of the foam. A certain fraction of intermetallics can also be formed during the cooling process due to solubility differences in liquid Al-Sn with temperature. Some alloying elements can be completely dissolved into the Al-Sn alloy during melting and then precipitated back during the cooling process. The thermodynamic calculations accurately predicted intermetallic phases during melting and solidification of each Al-Sn alloy, and the amount of intermetallics calculated at the end of solidification (Scheil cooling calculation) also in agreement with the amount observed for each alloy. According to the thermodynamic calculations, Mn, Ni and Mg can be completely dissolved in liquid Al-3wt.%Sn alloy during the heating/melting process (foaming process) and be precipitated as intermetallic phases of Al_6Mn, Al_3Ni, and Mg_2Sn, respectively, during the solidification process. The solubility of alloying elements like Ti and Co in an Al-3wt.%Sn alloy is limited, so most of such alloying elements react with Al to form Al_3Ti and Al_9Co_2 respectively during the heating/melting process, and they remain as intermetallics. Considering this process, the type and amount of intermetallics possibly formed in Al-3wt.%Sn alloys are calculated in Table 7.2. It should be noted that the amount of intermetallics increases as the amount of alloying elements increases, but it is not linearly proportional to the alloying amount.

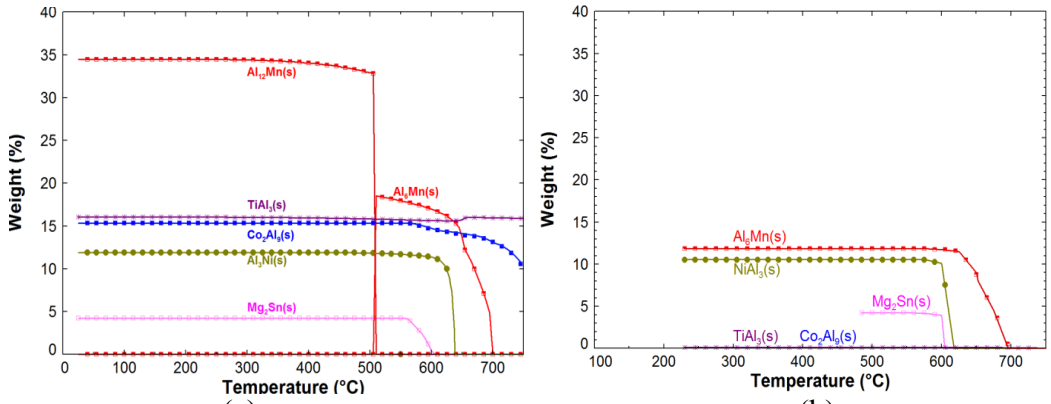

(a) (b)

Figure 7.1. Thermodynamic calculations for intermetallic formation in various Al–3wt.%Sn–X alloys during (a) heating and (b) cooling process. Heating process is calculated using equilibrium calculation and cooling process is calculated using the Scheil cooling calculation. X = 5wt.% of Mn, Ti, Co and Ni, and 2wt.% of Mg.

7.3.2. Cell Wall Microstructure

SEM images of the cell wall microstructures of various alloys are shown in Figure 7.2. EDS mapping of alloying elements was also done to determine the location of the intermetallic phases.

Adding Ni clearly formed the eutectic Al_3Ni phase (see Figure 7.2 (a)). As shown in the thermodynamic calculations in Figure 7.1, Ni up to 5wt.% can be completely dissolved in liquid Al-Sn alloy during the alloy's melting (foaming process) and can then be precipitated at the end of solidification as a eutectic phase. Mn up to 5wt.% can be completely dissolved in liquid Al-Sn alloy at above 700 ^{o}C, but the precipitation behavior of Al-Mn intermetallic (Al_6Mn) is somewhat different than that of Ni. According to the thermodynamic calculations, for an Al-Sn alloy with a small amount of Mn added (1wt.%), Mn is mostly precipitated out near the end of solidification, while still above eutectic temperature. With the increase of Mn content, the Al_6Mn phase is precipitated out from the liquid phase even before the

Al alloy solidifies. This means the Al_6Mn phase can form as a primary crystalline phase, after which the Al matrix phase can be formed. As a result, the microstructure of Mn containing Al-Sn alloys does not have a eutectic structure like alloys which contain Ni. Instead, large irregularly shaped Al_6Mn particles are distributed in the Al matrix phase, as can be seen in Figure 7.2 (b).

According to the thermodynamic calculations, Co and Ti are mostly undissolved in liquid Al-Sn alloy and can remain solid in liquid Al-Sn. By reaction with liquid Al, the Al_9Co_2 and Al_3Ti phase can be formed. In contrast to Ti, a small amount of Co can be dissolved in liquid Al-Sn alloy when Co is added in 5wt.%, as can be seen in Figure 7.1. But for lower additions of 1 and 3wt.%Co, dissolution can take place, and needle-like precipitation occurs, as seen in Figure 7.2 (c). The Al_9Co_2's morphology of in Al-3wt.%Sn-5wt.%Co changed for the most part from needle-like precipitates to agglomerated particles, as these particles are not dissolved during heating; however, small amounts of needle-like Al_9Co_2 particles were still observed [25]. Agglomerated particles of Al_3Ti were observed in all Ti-containing Al-Sn alloys, such as the one depicted in Figure 7.2 (d).

In the case of Mg, small amounts of Mg_2Sn are observed through the cell wall in the grain boundary, but most Mg is either oxidized and present in the foam skin, or homogeneously distributed inside the pores as shown in Figure 7.2 (e).

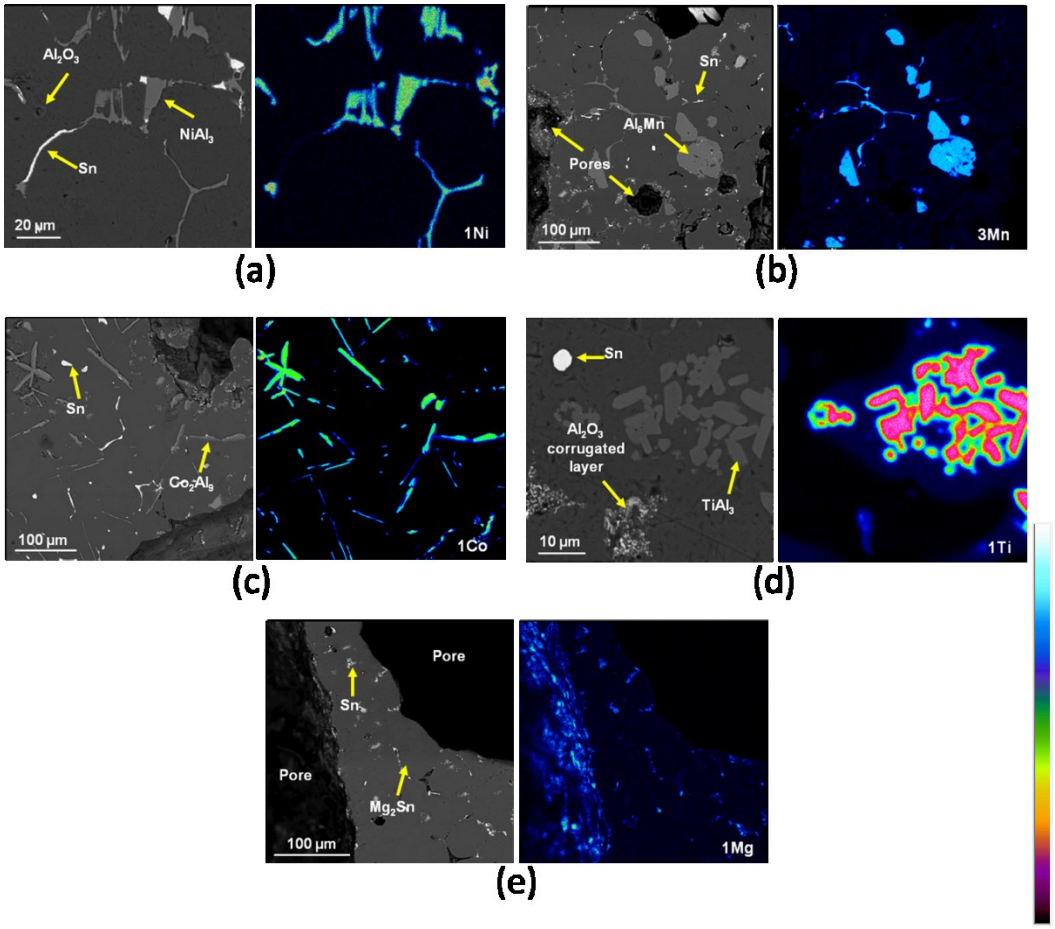

Figure 7.2. Close up image (SEM) and compositional scans for the cell wall of various Al-3wt.%Sn-X alloy foams (X = Ni, Mn, Co, Ti and Mg). (a) 1wt.%Ni, (b) 3wt.%Mn, (c) 1wt.%Co, (d) 1wt.%Ti and (e) 1wt.%Mg.

7.3.3. Mechanical properties

In the stress (σ) - strain (ε) curve of Al foam, three typical regions are presented: a linear elastic region, a plateau region where the stress is kept almost constant during increasing strains, and a densification region, which is characterized by a steep rise in stress. The energy absorption capacity per unit volume (E_v) can be determined by the area under a strain-stress curve in a certain strain interval, and can be calculated by [20]:

$$E_v = \int_{\varepsilon_1}^{\varepsilon_2} \sigma(\varepsilon) d\varepsilon \qquad (1)$$

The energy absorption efficiency (η) is a ratio between the energy absorbed by the real material vs. that absorbed by an ideal plastic material, and can be calculated by [20]:

$$\eta = \frac{\int_{\varepsilon_1}^{\varepsilon_2} \sigma(\varepsilon) d\varepsilon}{\sigma_0(\varepsilon_2 - \varepsilon_1)} \qquad (2)$$

The mechanical properties of metallic foams are known to be closely related to the foam density and the properties of the cell wall material [20, 28, 29]. For instance, a denser foam has higher compressive strength. It is also well-known that the best energy-absorbing foam, from a practical viewpoint, is one that can withstand impact energy at relatively low constant stress levels [29]. In the discussion below, E_v and η for all alloys were calculated from their strain-stress curves using a compression test. To simplify the analysis, the energy absorbed at all stresses is plotted.

In the following subsections, the mechanical properties and macrostructure of pure Al foam and Al alloy foams are discussed.

7.3.3.1. Pure Al and Al-Sn base alloy foams

In order to verify whether the present experimental mechanical property results are compatible with the data found in the literature, pure Al foams (foamed at

their optimum condition at 800 °C) were tested in the current setup. Al-3wt.%Sn foams were also tested for comparison. Since Al and Al-3wt.%Sn foams have different densities at their optimum expansions (0.60 g/cm^3 for pure Al and 0.53 g/cm^3 for Al-Sn alloy), an additional Al-3wt.%Sn foam with a density of 0.61 g/cm^3 was also prepared for mechanical testing.

The comparative strain-stress curves of pure Al and Al-3wt.%Sn foams and their cell macrostructures are presented in Figure 7.3. According to the standard ISO 13314:2011(E) [30], the plateau stress was measured as the mean stress between 0.2 and 0.4 strain. Next, each foam's energy absorption was measured up to the plateau end strain. Pure Al foam and Al-3wt.%Sn foams with a density of 0.6 g/cm^3 had an absorbed energy of 1.63 and 2.32 MJ/m^3, for their plateau end stresses at 6.84 and 8.37 MPa, respectively. This suggests the benefit of the addition of Sn addition in energy absorption.

The energy absorbed at a specific strain of 0.3 was calculated for these foams, and compared to pure Al foams found in the literature. Energy absorption of pure Al foams at 0.3 strain gave 1.1 MJ/m^3, which is slightly higher but still compatible with the experimental data, 0.72 MJ/m^3 in the literature [29, 31, 32]. Again, there is an improvement in energy absorption when 3wt.% Sn is added to Al foam. For example, energy absorption of 4 MJ/m^3 can be obtained at a compression stress of 13 MPa for optimum Al-3wt.%Sn alloy foam, compared to 16 MPa for pure Al foam. Even for Al-3wt.%Sn foam with the same density (0.61 g/cm^3) as Al foam (0.60 g/cm^3), energy absorption is improved slightly. This improvement can be understood by examining the foam macrostructure in Figure 7.3. Comparing the

macrostructure of pure Al to Al-3wt.%Sn foam with a similar density clearly shows the difference in pore size. Al-3wt.%Sn foam has larger pore size than pure Al foam, as well as a higher sphericity index. In fact, the sphericity index of Al-3wt.%Sn foam is 0.80 compared to 0.67 in pure Al foam [25]. In addition, pure Al foam has a cell wall thickness of 0.2 to 0.5 mm, while Al-3wt.%Sn foam has a cell wall thickness of 0.1 to 0.25 mm. Raj and Daniel [13] reported that for samples with the same relative density, increasing pore size (that is, decreasing cell wall thickness) can increase the plateau stress (σ_{pl}), a finding which has also been observed in this study, as shown in Figure 7.3.

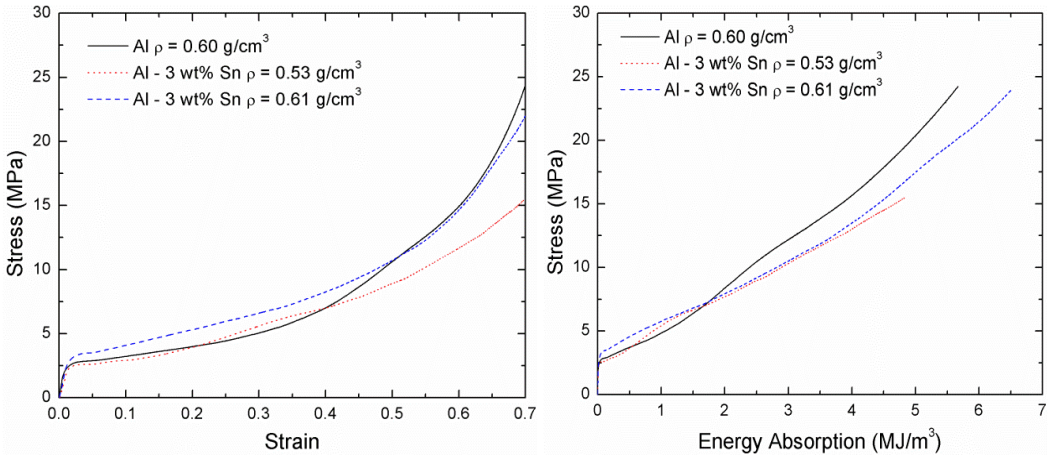

(a) (b)

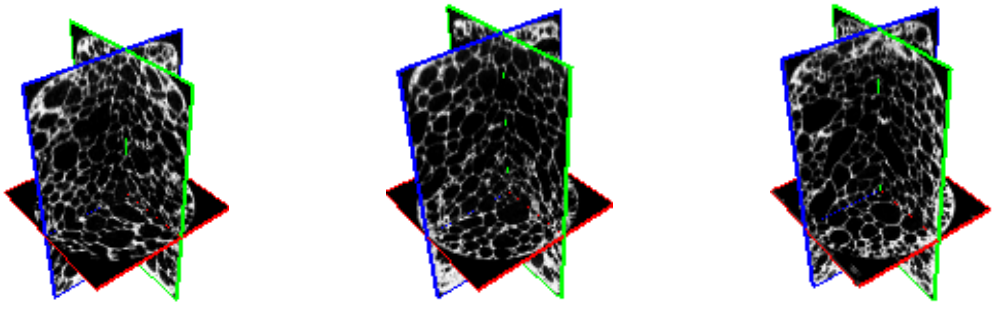

(c) (d) (e)

Figure 7.3. Compression test results for Al and Al-3wt.%Sn base alloy foams. (a) Stress-strain curves from compression tests, (b) stress-energy absorption relationships, foam macrostructures of (c) pure Al foam with a density of 0.60 g/cm^3, Al-3wt.%Sn with densities of (d) 0.53 g/cm^3 and (e) 0.61 g/cm^3.

7.3.3.2. Al-3wt.%Sn-X alloys foams: X = Ni, Mn, Co, Ti and Mg

Figure 7.4 to Figure 7.8 plot the mechanical properties of Al-3wt.%Sn foams alloyed with an in situ intermetallic former element. The stress-strain curves, the energy absorption efficiency calculated (η), the energy absorption capacity (E_v) and the representative foam macrostructure of each alloy are presented. The macrostructure is illustrated as a 3-plane view; the size of the horizontal plane is a 3 cm square. If η is high, it can be considered as a better material for energy absorption applications. When the same amount of energy absorption (E_v) is obtained at lower stress (σ) the slope of σ-E_v curve is less steep, and the materials are preferable for impact energy absorption applications. In all foams, with the exception of Mg-added Al-3wt.%Sn alloys foams, the higher amount of alloying elements can improve η, and the slope of σ-E_v curve becomes somewhat lower than that of Al-3wt.%Sn base alloy foams, depending on the amount of the alloying element. In the case of Mg-added alloys, both efficiency and energy absorption capacity worsened as more Mg was added, compared to pure Al-3wt.%Sn alloy foam, as shown in Figure 7.4. The foam macrostructures show that all Mg-containing foams have thicker surrounding skin and many pores homogeneously distributed with thicker cell walls. These characteristics are common in a metal foam that will densify faster during compression testing. In fact, the plateau end strain for these foams is as high as 15 MPa.

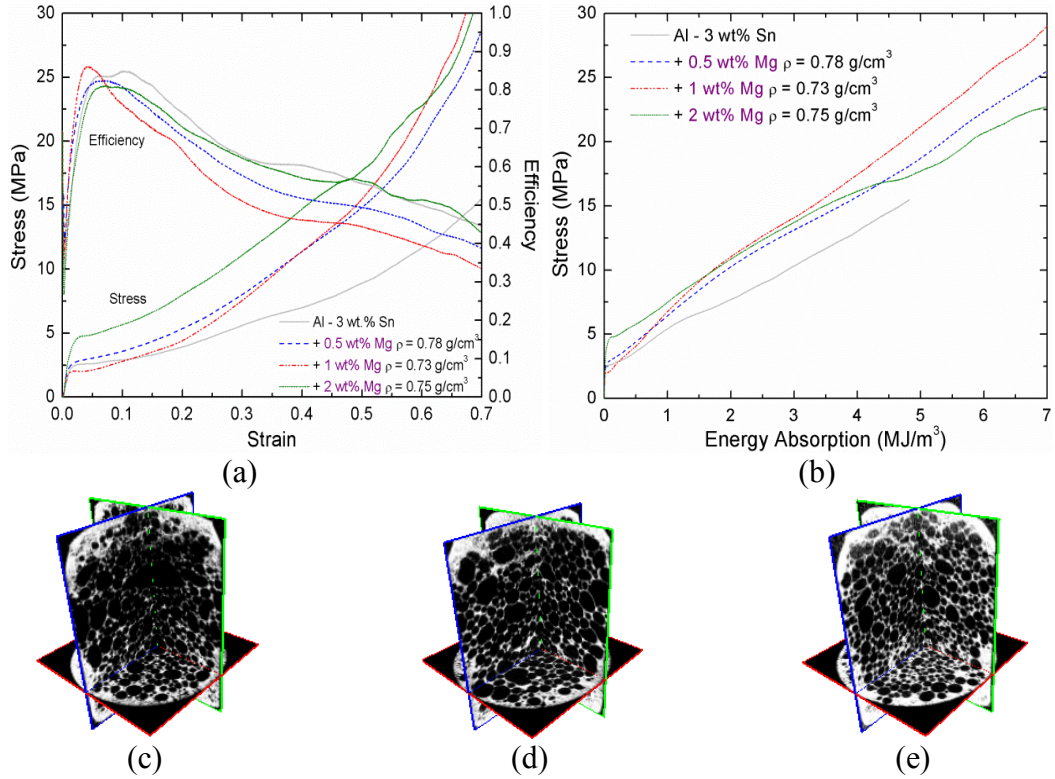

Figure 7.4. Compression test results for Al-3wt.%Sn-(0.5, 1 and 2)wt.%Mg base alloy foams. (a) Stress-strain curves from compression test and efficiency, (b) stress-energy absorption relationships, foam macrostructures of Al-3wt.%Sn- (c) 0.5wt.%Mg (0.78 g/cm^3), (d) 1wt.%Mg (0.73 g/cm^3), and (e) 2wt.%Mg (0.75 g/cm^3).

The stress-strain curves of Ni- and Co-containing Al-Sn alloy foams are similar. As a result, the energy absorption efficiency (η) and the σ-E_v curves are also similar (Figures 7.5 and 7.6). The only exception is the fact that the initial maximum compressive strength for Ni-containing foams is higher than the Co-containing foams in all cases; however, this maximum decreases as the intermetallic phase in the foam increases, suggesting a more brittle foam, which agrees with the amount of intermetallics reported in Table 7.2.

A noticeable difference can be found in foams with 5wt.%Mn, while the stress-strain curves for Al-3wt.%Sn foams with 1 and 3wt.%Mn addition were similar to

the Al-3wt.%Sn base-alloy foam. The stress in the stress-strain curve for the 5wt.%Mn alloy was almost constant with increasing strain, which improved η significantly. Higher E_v was obtained at low stress, as seen in Figure 7.7. The first maximum compressive strength is obtained at 7 MPa and is almost constant through the whole compressive test. This is probably due to the bigger pores, which are easily crushed when their cell walls contain large amounts of intermetallics that were back-precipitated during the cooling process.

Similar improvements in mechanical properties were also found for all foams containing Ti, as shown in Figure 7.8. The addition of Ti to the base alloy also kept a constant stress level over a wide range of strain, and the energy absorption efficiency was calculated to be higher than 80% until strain reached about 0.5. The densification of these foams started at a strain of 0.6, which is the highest of all tested foams.

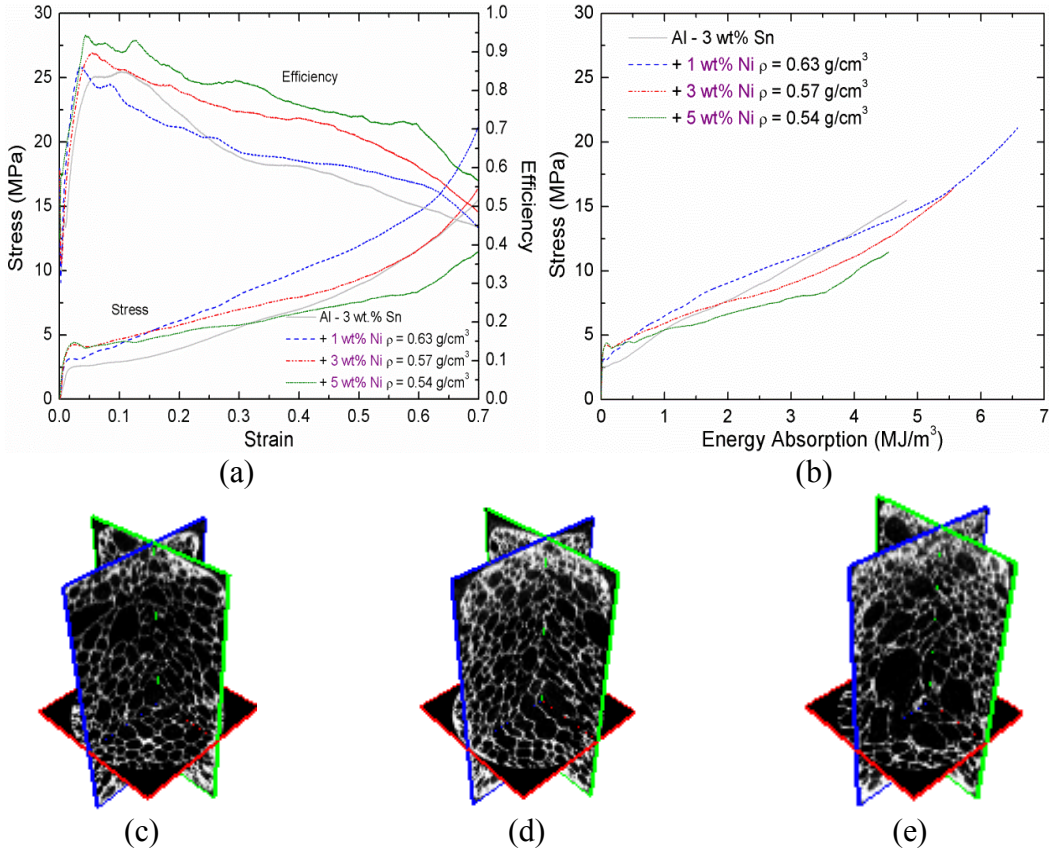

Figure 7.5. Compression test results for Al-3wt.%Sn-(1, 3 and 5)wt.%Ni base alloy foams. (a) Stress-strain curves from compression test and efficiency, (b) stress-energy absorption relationships, foam macrostructures of Al-3wt.%Sn- (c) 1wt.%Ni (0.63 g/cm^3), (d) 3wt.%Ni (0.57 g/cm^3), and (e) 5wt.%Ni (0.54 g/cm^3).

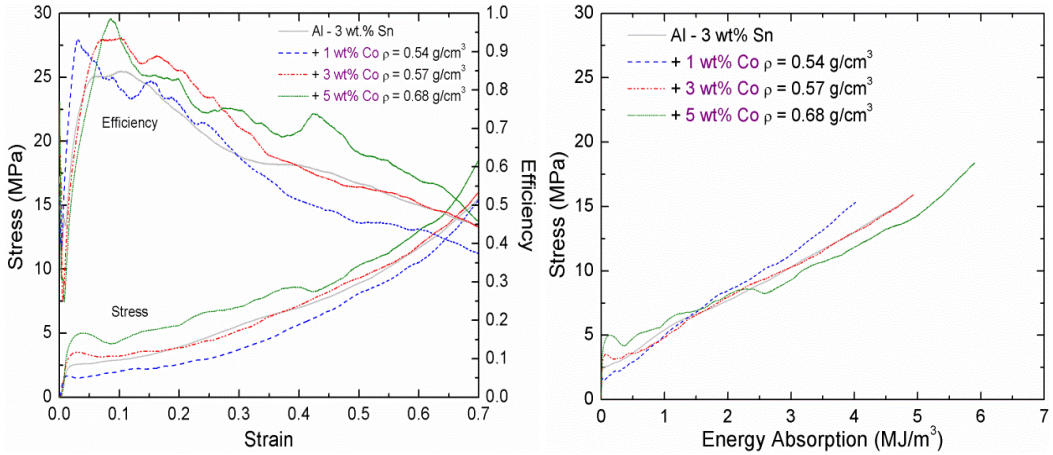

(a) (b)

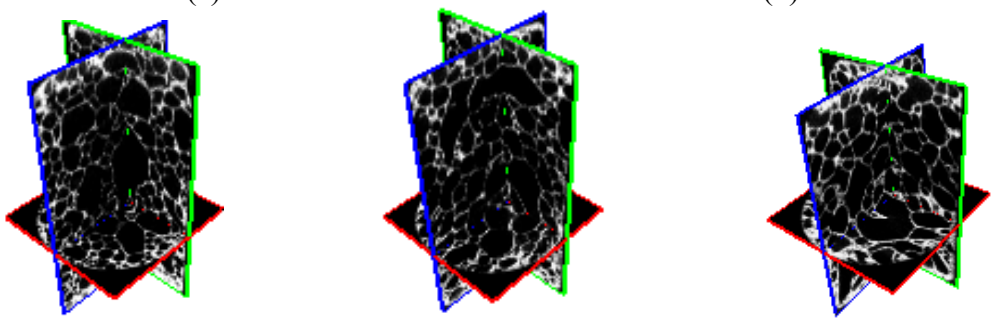

(c) (d) (e)

Figure 7.6. Compression test results for Al-3wt.%Sn-(1, 3 and 5)wt.%Co base alloy foams. (a) Stress-strain curves from compression test and efficiency, (b) stress-energy absorption relationships, foam macrostructures of Al-3wt.%Sn- (c) 1wt.%Co (0.54 g/cm^3), (d) 3wt.%Co (0.57 g/cm^3), and (e) 5wt.%Co (0.68 g/cm^3).

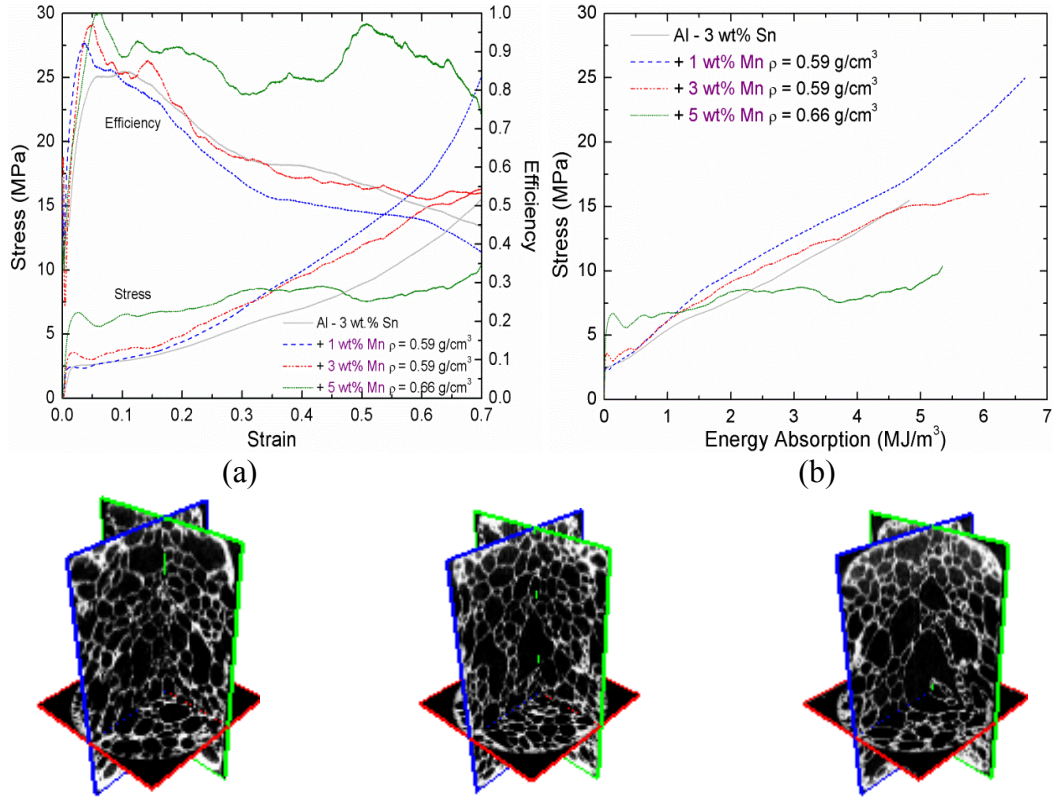

Figure 7.7. Compression test results for Al-3wt.%Sn-(1, 3 and 5)wt.%Mn base alloy foams. (a) Stress-strain curves from compression test and efficiency, (b) stress-energy absorption relationships, foam macrostructures of Al-3wt.%Sn- (c) 1wt.%Mn (0.59 g/cm^3), (d) 3wt.%Mn (0.59 g/cm^3), and (e) 5wt.%Mn (0.66 g/cm^3).

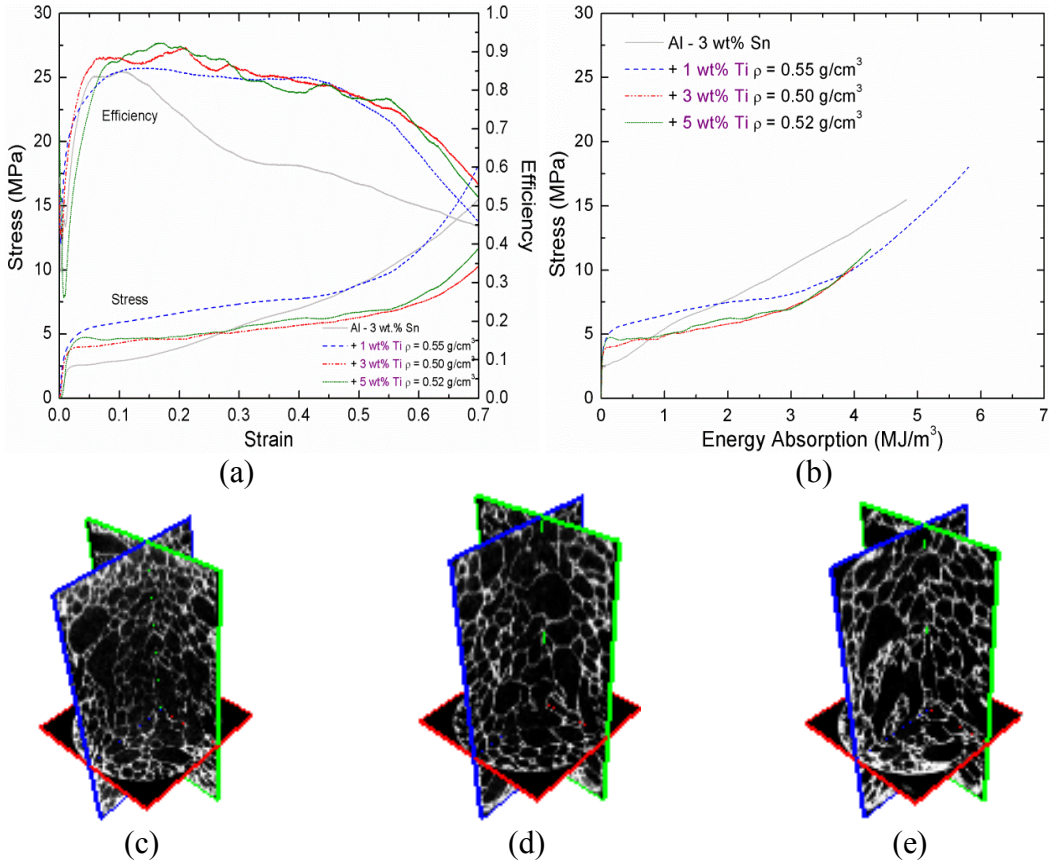

Figure 7.8. Compression test results for Al-3wt.%Sn-(1, 3 and 5)wt.%Ti base alloy foams. (a) Stress-strain curves from compression test and efficiency, (b) stress-energy absorption relationships, foam macrostructures of Al-3wt.%Sn- (c) 1wt.%Ti (0.55 g/cm^3), (d) 3wt.%Ti (0.50 g/cm^3), and (e) 5wt.%Ti (0.52 g/cm^3).

Table 7.2. Amounts of intermetallics based on thermodynamic calculations [7].

X	Ni	Mn	Ti	Co		Mg
Intermetallic formed (wt.%)	$NiAl_3$	Al_6Mn	$TiAl_3$	Co_2Al_9		Mg_2Sn
1 wt.% X	2	0.5	5.3	3	0.5 wt.% X	1.3
3 wt.% X	6	8	10.6	9.3	1 wt.% X	4.2
5 wt.% X	10.6	11.9	16	15.2	2 wt.% X	4.3

7.3.3.3. Effect of intermetallics on mechanical properties of metallic foams

The main focus in designing crushable components in cars is the absorption of the kinetic energy into plastic deformation, in order to minimize the danger to humans and equipment. Metallic foams are excellent energy absorbers, since they can sustain large strains at relatively low constant stress levels.

When searching for foams with an optimum energy absorption capability, one can compare the total energy absorbed up to a certain amount of deformation (until the given strain) or prior to densification. To compare the foams of the current study under similar conditions (as some of them densify at much lower strains than others) a strain of 0.3 was set for comparison.

Figure 7.9 shows the total energy absorbed versus stress at a strain of 0.3. The energy absorbed by 3wt.%Ti and 5wt.%Ti containing foams is much greater than that absorbed by Al-3wt.%Sn foam with a density of 0.53 g/cm^3, or by pure Al foams. Obviously this type of graph would give a different result depending on the strain measured, but the Ti containing foams are superior to Al-3wt.%Sn base alloy or pure Al foams for most strains. For most foams, increasing the alloying element increases the energy absorption capability, which would be logical as more intermetallics are formed. Nevertheless, this behaviour is not seen with the Ti containing foams, as increasing the Ti content resulted in decreased energy absorption.

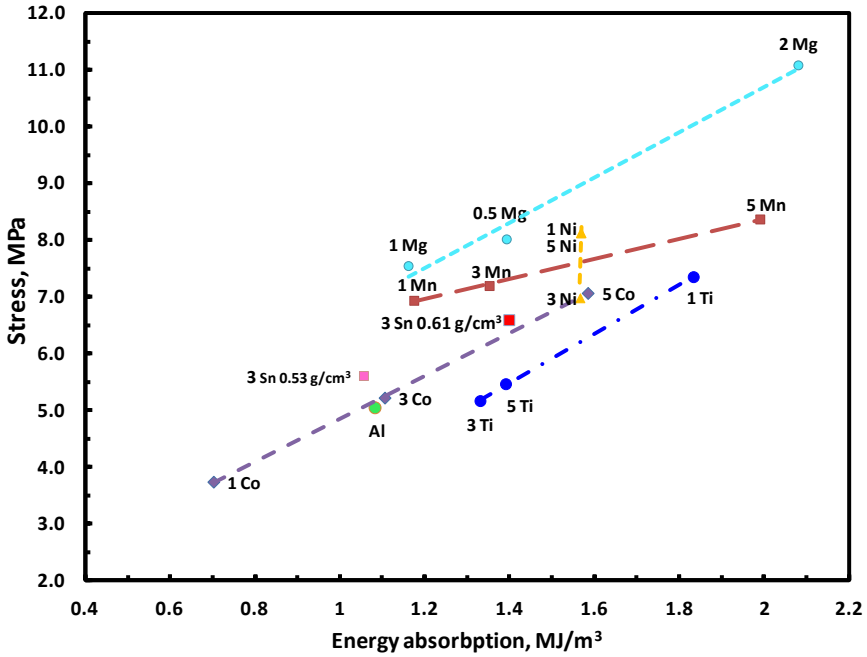

Figure 7.9. The relationship between stress and total energy absorption at 0.3 strain from compression test.

The corresponding load when the total amount of absorbed energy is 3 MJ/m^3 is plotted for each foam in Figure 7.10. The load also correlates to the amount of intermetallics. If the same amount of energy can be absorbed at lower load conditions, the materials can be considered superior in terms of energy absorption capability. For most foams, increasing the intermetallic content decreased the stress needed to attain 3 MJ/m^3 of energy absorption, except for those foams containing Mg. The noticeable difference in Mg containing foams can be attributed to the thicker foam skin and smaller pore size. The thickening of the foam skin occurred during the oxidation of Mg, forming MgO; afterwards, foam expansion was limited, generating small homogeneous porosity. Compared to Al-3wt.%Sn foams, all Ti containing foams have much lower corresponding stress levels. Foams made with alloys containing 5wt.%Ni, 5wt.%Co, 5wt.%Mn and

3wt.%Ni also absorb 3 MJ/m^3 with lower stress. It is important to note that even when the stress decreased as intermetallic content increased, the registered values—particularly of Ti- and Co-containing foams—are comprised in the standard deviation of ±1MPa. Therefore, when selecting the foam material, the benefit and the cost of adding an additional element to the foam should be taken into account.

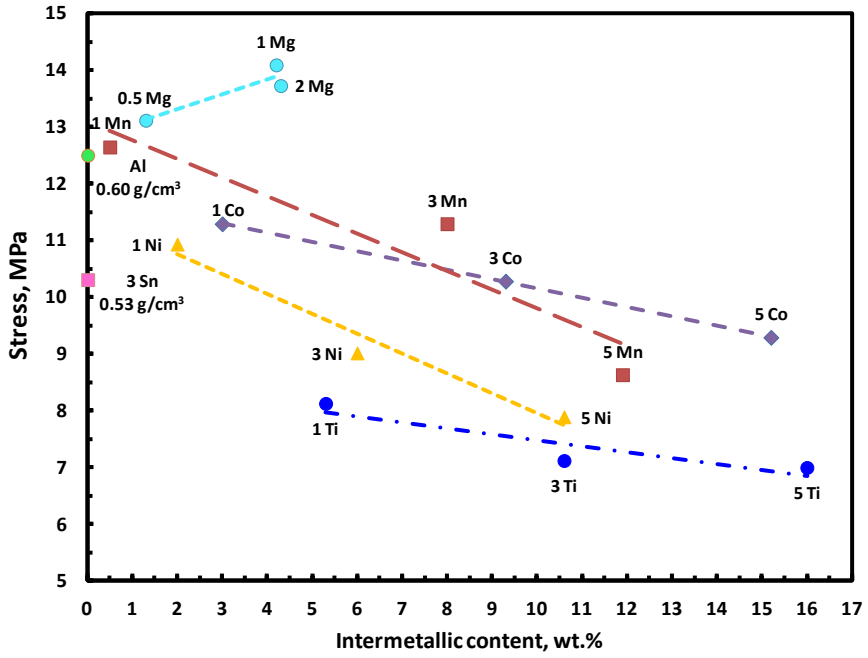

Figure 7.10. The relationship between stress and intermetallic content when the foam absorbs the energy of 3 MJ/m^3 for various Al-3wt.%Sn-X alloy foams.

A close analysis of the stress-strain curves in Figure 7.4 to Figure 7.8 shows that the slope of the stress-strain curve at the plateau region can be lower for foams with certain alloying elements (as 5wt.%Ni, 5wt.%Mn and 1, 3 and 5wt.%Ti) than with the Al-3wt.%Sn foam. As the foaming conditions were the same and the foam macrostructure resemble each other (larger pores with low sphericity) for these compositions, the difference can be attributed to the cell wall

microstructure. The curve's lower slope can be caused because the foam (or more precisely the cell wall) becomes more brittle than ductile.

Figure 7.11 shows the foam microstructure for the highest alloying conditions after compression testing. Intermetallics are homogeneously distributed through the cell wall. From the crushed microstructures, it can be observed that cell wall failure happens in the thinnest area, where a higher concentration of intermetallics exists. During the compression tests, it was noticed that Mn and Ti alloyed foams showed more brittle fracture behavior than other foams; the microstructures provided corroboration of the hypothesis that these alloys failed along a series of large intermetallic particles. In the case of Ni-containing foams, Al_3Ni precipitates in the grain boundary in a Chinese script structure. Intermetallics are finely distributed in the cell wall; therefore the fracture mode for 5wt.%Ni foam, while brittle, is not clearly observed. Mg alloyed foams present a ductile fracture for all Mg contents.

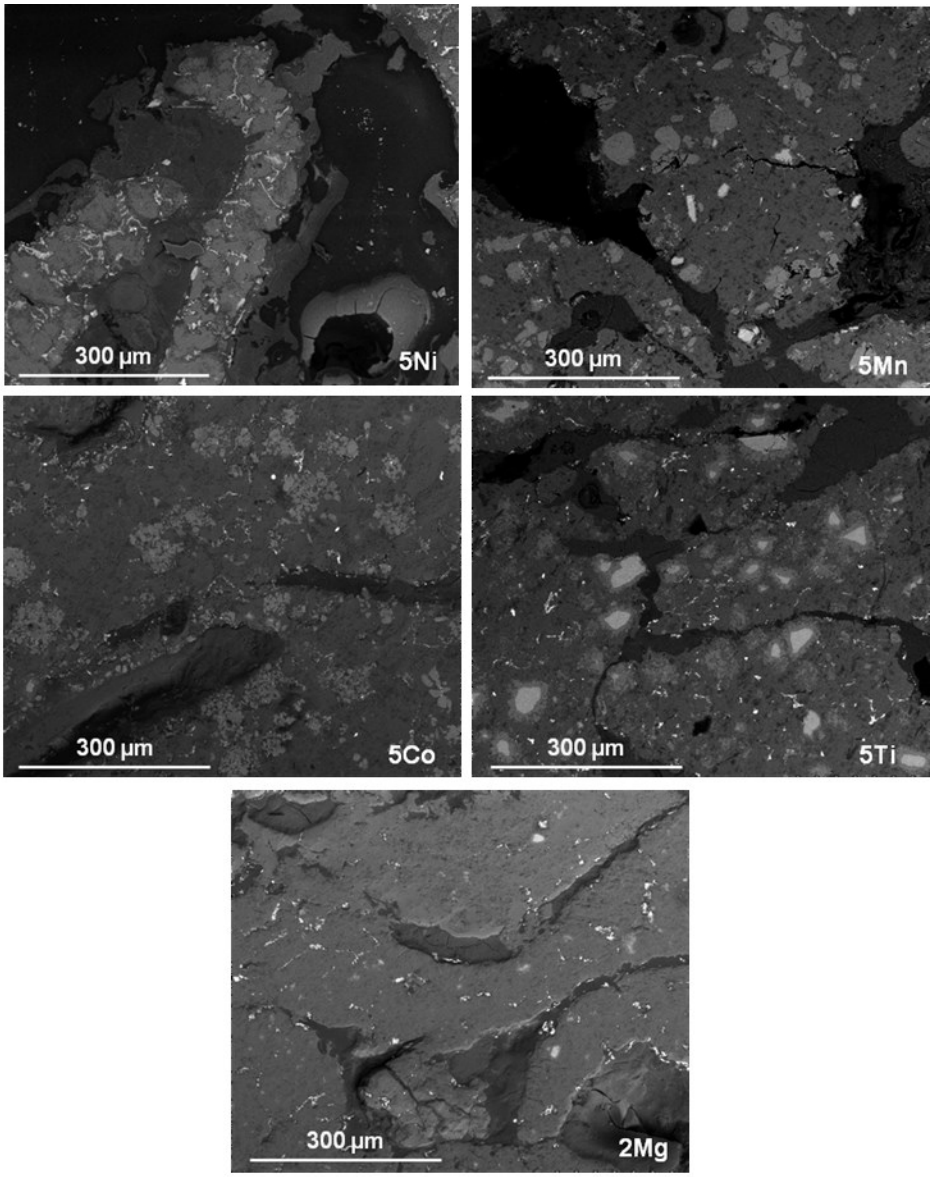

Figure 7.11. SEM BSE images of different Al-3wt.%Sn-X foam cell walls after being crushed in compression test.

Regarding the change of the fracture mechanism from ductile to brittle mode, Toda et al. [33], using characterization by synchrotron X-ray microtomography, reported that the in-situ formation of coarse micropores in the cell wall of ALPORAS [15] foams could drive brittle fracture of a cell wall. But no detailed investigation of intermetallics' effect on the fracture mode has yet been reported.

The following theory for the effect of intermetallics in foam fracture is proposed based on the cell wall microstructures and the fractured cell wall microstructures (found in Figure 7.2 and Figure 7.11). When small intermetallic particles are uniformly distributed in the cell wall, the cell wall can be strengthened, while maintaining a ductile fracture mode. However, when large irregularly shaped intermetallic phases are distributed in the cell wall, the incoherency of intermetallics and the matrix is large (as in 5wt.%Mn and 3 and 5wt.%Ti containing foams) allowing cracks to propagate easily along the particles to induce a more brittle fracture mode. Even when a large amount of eutectic phase exists in the matrix (like 5wt.%Ni containing foam), the eutectic area can be subjected to crack initiation and behave in a brittle manner. The schematic diagram of this idea is illustrated in Figure 7.12.

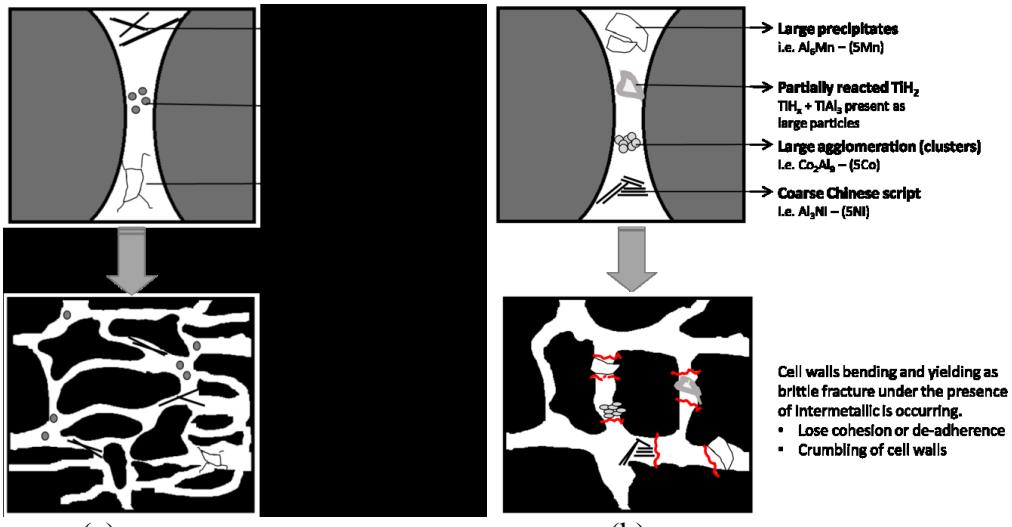

Figure 7.12. Schematic illustration of cell wall deformation due to intermetallics. (a) tensile deformation and (b) brittle fracture.

Considering the energy absorption behavior and the stress-strain curve, the optimum alloy compositions can be Al-3wt.%Sn with -5wt.%Mn, -5wt.%Ni, -

3wt.%Ti and -5wt.%Ti. Foams with these alloys show a wide range of plateau stress up to large deformations (strain up to 0.7 for Mn containing foams, 0.6 for Ni and Ti containing foams), while maintaining relatively low stress levels. In consideration foam expansion and foam stability, Ni- and Ti-containing foams can produce more than 400% expansion when foamed at 725 ^{o}C; that is a fourfold expansion compared to the original precursor size. Nevertheless, foam stability at maximum expansion is rather short (50-100 s), while Mn-containing foams can expand more than 300%, producing foams that are stable for more than 10 min [23]. Disregarding the economic aspect, all these alloys can be easily produced from the viewpoint of the metallurgical processing, and are superior to pure Al foam or other conventional Al based foams.

7.4. **Summary**

Compression tests on metallic foams of Al-3wt.%Sn alloys with alloying elements like Co, Mg, Mn, Ni and Ti were carried out to investigate the variation in energy absorption with alloy composition. In particular, the alloying elements were selected to produce various types of intermetallics. The energy absorption capacity of Al-Sn-based alloy foams is in general enhanced by the addition of alloying elements, and the enhancement increases as the amount of intermetallics increases, with the exception of Mg-containing foams. Al-3wt.%Sn alloys containing Ti (3, 5wt.%), Mn (5wt.%) or Ni (5wt.%) are found to be the most promising Al-Sn based alloys for energy absorption applications. In particular, these alloys show brittle fracture behavior in their foam cell walls, which was

explained by the morphology of intermetallics. Furthermore, it is important to remember that Mn-containing foams are very stable during the foaming process, easier to process control, and reproducibility of the foam characteristics (homogeneous pore structure and cell wall thickness) all of which helps guarantee the reproducibility of the mechanical properties.

Acknowledgements

The authors would like to thank NSERC, FQRNT, GM of Canada, and CONACyT for their financial support of this project.

References

1. Fuganti, A., et al., *Aluminium foam for automotive applications.* Advanced Engineering Materials, 2000. 2(4): p. 200-204.

2. Ito, K. and H. Kobayashi, *Production and Fabrication Technology Development of Aluminum Useful for Automobile Lightweighting*. Advanced Engineering Materials, 2006. 8(9): p. 828-835.

3. Banhart, J., *Manufacture, characterisation and application of cellular metals and metal foams.* Progress in Materials Science, 2001. 46(6): p. 559-632.

4. Gergely, V., R.L. Jones, and T.W. Clyne, *The effect of capillarity-driven melt flow and size of particles in cell faces on metal foam structure evolution.* Transactions of JWRI, 2001. 30(Special Issue): p. 371-376.

5. Ip, S.W., Y. Wang, and J.M. Toguri, *Aluminum foam stabilization by solid particles.* Canadian Metallurgical Quaterly, 1999. 38.

6. Haibel, A., A. Rack, and J. Banhart, *Why are metal foams stable?* Applied Physics Letters, 2006. 89(154102): p. 1-3.

7. Kaptay, G., *Interfacial criteria for stabilization of liquid foams by solid particles.* Colloids and Surfaces A: Physicochemical and Engineering Aspects, 2004. 230(1-3): p. 67-80.

8. Kennedy, A.R. and S. Asavavisitchai, *Effects of TiB_2 particle adddition on the expansion, structure and mechanical properties of PM Al foams.* Scripta Materialia, 2004. 50: p. 115-119.

9. Xia, X., et al., *Compressive properties of closed-cell aluminum foams with different contents of ceramic microspheres.* Materials & Design, 2014. 56(0): p. 353-358.

10. Korner, C., *Foam formation mechanisms in particle suspensions applied to metal foams.* Materials Science and Engineering: A (Structural Materials: Properties, Microstructure and Processing), 2008. 495(1-2): p. 227-35.

11. Raj, R.E. and B.S.S. Daniel, *Customization of closed-cell aluminum foam properties using design of experiments.* Materials Science and Engineering: A, 2011. 528(4-5): p. 2067-2075.

12. Raj, R.E. and B.S.S. Daniel, *Structural and compressive property correlation of closed-cell aluminum foam.* Journal of Alloys and Compounds, 2009. 467(1-2): p. 550-556.

13. Raj, R.E. and B.S.S. Daniel, *Manufacturing challenges in obtaining tailor-made closed-cell structures in metallic foams.* International Journal of Advanced Manufacturing Technologies, 2008. 38: p. 505-512.

14. Xia, X., et al., *The compressive properties of closed-cell aluminum foams with different Mn additions.* Materials & Design, 2013. 51(0): p. 797-802.

15. Miyoshi, T., et al., *ALPORAS Aluminium Foam: Production Process, Properties and Applications.* Advanced Engineering Materials, 2002. 2(4): p. 179-183.

16. Nosko, M., et al., *Stabilizing intermetallic phases within aluminum foam.* Materials Letters, 2011. 65(9): p. 1378-1380.

17. Kim, A., S.-S. Cho, and H.-J. Lee, *Foaming behaviour of Al-Si-Cu-Mg alloys.* Materials Science and Technology, 2004. 20(12): p. 1615-1620.

18. Lehmhus, D. and M. Busse, *Potential new matrix alloys for production of PM aluminium foams.* Advanced Engineering Materials, 2004. 6(6): p. 391-396.

19. Helwig, H.M., F. Garcia-Moreno, and J. Banhart, *A study of Mg and Cu additions on the foaming behaviour of Al–Si alloys.* Journal of Materials Science, 2011. 46(15): p. 5227-5236.

20. Degishcher, H.-P. and B. Kriszt, eds. *Handbook of Cellular Metals: Production, Processing and Applications*. 2002, WILEY-VCH Verlag Gmbh.

21. Jeenager, V.K. and V. Pancholi, *Influence of cell wall microstructure on the energy absorption capability of aluminium foam.* Materials & Design, 2014. 56(0): p. 454-459.

22. Campana, F. and D. Pilone, *Effect of wall microstructure and morphometric parameters on the crush behaviour of Al alloy foams.* Materials Science and Engineering: A, 2008. 479(1-2): p. 58-64.

23. Aguirre-Perales, L.Y., I.-H. Jung, and R.A.L. Drew, *Foaming behavior of powder metallurgical Al-Sn foams.* Acta Materialia, 2012. 60(2): p. 759-769.

24. Aguirre-Perales, L., I.-H. Jung, and R. Drew, *Effect of Sn on the Dehydrogenation Process of TiH_2 in Al Foams.* Metallurgical and Materials Transactions A, 2012. 43(1): p. 1-5.

25. Aguirre-Perales, L., R.A.L. Drew, and I.-H. Jung, *The Effect of In Situ Intermetallic Formation on Al-Sn Foaming Behavior.* Metallurgical and Materials Transactions A, 2014. 45(9): p. 3714-3727.

26. Bale, C.W., et al., *FactSage thermochemical software and databases.* Calphad, 2002. 26(2): p. 189-228.

27. Beals, J.T. and M.S. Thompson, *Density gradient effects on aluminium foam compression behaviour.* Journal of Materials Science, 1997. 32(13): p. 3595-600.

28. Kennedy, A.R. and S. Asavavisithchai, *Effect of ceramic particle additions on foam expansion and stability in compacted Al-TiH2 powder precursors.* Advanced Engineering Materials, 2004. 6(6): p. 400-2.

29. Baumeister, J., J. Banhart, and M. Weber, *Aluminum Foams for Transport Industry.* Materials and Design, 1997. 18(4/6): p. 217-220.

30. *Mechanical testing of metals— Ductility testing— Compression test for porous and cellular metals*, in *ISO 13314*2011, International Standards: Switzerland. p. 7.

31. Kennedy, A.R., *Effect of foaming configuration on expansion.* Journal of Materials Science, 2004. 39(3): p. 1143-1145.

32. Kennedy, A.R., *Aspects of the reproducibility of mechanical properties in Al based foams.* Journal of Materials Science, 2004. 39(9): p. 3085-3088.

33. Toda, H., et al., *Quantitative assessment of microstructure and its effects on compression behavior of aluminum foams <i>via high-resolution synchrotron X-ray tomography.* Metallurgical and Materials Transactions A, 2006. 37(4): p. 1211-1219.

Chapter 8

Conclusions

In the powder metallurgy route, titanium hydride (TiH_2) is the most commonly used blowing agent for the Al foaming process. However, the mismatch between the temperatures at which Al reaches its melting point and TiH_2 begins to dehydrogenate is this technique's main drawback. This mismatch leads to the formation of crack-like pores, hydrogen loss prior to foaming, and inferior metallic foam. This study's purpose is to develop new Al foam alloys, producing more stable, higher foam expansion with superior mechanical properties.

In this study, thermodynamic calculations with the FactSage FTlite database have been thoroughly applied to design the alloy composition. Differential scanning calorimetry (DSC) and scanning electron microscopy (SEM) were employed to understand the details of foaming behavior and microstructural changes during the foaming. A custom-made mechanical expandometer was used to perform a foaming test on metal powder compacts. A non-destructive X-ray tomography technique was used to examine the foam structure. Compression tests for foam materials were performed to characterize the mechanical response (particularly the energy absorption capacity) of the foams produced in this work.

This study's most important contribution to alloy design is the selection of Sn as a major alloying element of Al foam. This is the major finding of this thesis, since works suggesting foaming of Al alloyed with Sn have never been carried out in

the field. This may be due to Sn's lower melting temperature compared to Al. In the foaming experiments, it was found that Sn can play a key role in TiH_2 dissociation, and modification of liquid Al's surface tension. Compared to pure Al foam, Al-Sn ($1 \leq$ wt.%Sn ≤ 5) foam can expand earlier, due to the formation of liquid Sn (Sn's melting temperature is 232 ^{o}C) between solid Al powder particles. Liquid Sn can accelerate the TiH_2's dissociation by the dissolved Al in liquid Sn at a temperature much lower than pure Al melting: Al (in liquid Sn) + $TiH_2(s)$ = $TiAl_3(s)$ + $H_2(g)$. This early liquid formation can also help retain $H_2(g)$ bubbles and enhance foam expansion. Moreover, due to liquid Al's decreased surface tension by the addition of Sn, the foam becomes thermally stable, compared to pure Al foam. Al–3wt.% Sn foam can expand up to 350% at 725 ^{o}C and retain an average expansion of 325% for more than 12 min, without foam collapse. Although Sn can be added to Al up to 5 wt.% with sound foaming results, Al-3wt.%Sn was selected as a base Al-Sn alloy as the span time at maximum expansion is reasonably long rendering the process control more efficient.

Alloying elements could be added to further improve Al-3wt.%Sn foam's foaming behavior and mechanical properties,. The alloy design concept was to form in-situ intermetallics during the Al–3wt.%Sn alloy's foaming process. Co, Mg, Mn, Ni and Ti were chosen from many abundant and inexpensive metallic elements based on comprehensive thermodynamic calculations, as these alloying elements produce intermetallic phases with Al and Sn. It was found that the foaming behavior and foam stability of Al–3wt.%Sn alloys could be actively controlled by the chosen alloying elements. The formation of in-situ intermetallic

phases can produce exothermic heat and result in the acceleration of TiH_2's decomposition and local melting of the Al matrix, which helps foam expansion. Foam stabilization can be achieved by the formation of intermetallic particles, and the introduction of alloying elements responsible for the decrease in cell wall surface tension. The maximum expansion of Al-3wt.%Sn foam increased after Ni- or Ti-addition. However, the foam collapsed back immediately to the level of the Al–3wt.%Sn base alloy. Only the foam containing 3wt.%Ni retained a maximum expansion plateau for few minutes before collapsing. The alloys with Co and Mn showed the same maximum expansion as the base alloy, but with much more stable foam structure than the Al-Sn-based alloy.

The compression tests for the Al-3wt.%Sn-X foams (X representing an additional alloying element) containing Co, Mg, Mn, Ni and Ti as alloying elements were carried out to investigate the variation of energy absorption with alloy composition. The energy absorption capacity of Al-Sn-based alloy foams are in general enhanced by adding alloying elements as the amount of intermetallics increase, except for Mg containing foams. It was found that Al-3wt.%Sn-X alloys containing Ti (3, 5wt.%), Mn (5wt.%) or Ni (5wt.%) are the most promising foamable alloys for energy absorption applications. In particular, these alloys show the brittle fracture behavior of their foam cell walls, which was explained by the amount and morphology of intermetallics. Furthermore, it is important to remember that Mn-containing foams are very stable during the foaming process, leading to a more easily controlled process, and reproducibility of the foam's

characteristics (homogeneous pore structure and cell wall thickness), which guarantees reproducibility of the foam's mechanical properties.

In conclusion, new Al-Sn based alloys were developed in this study. The best alloys designed in this study for stable and highly expanding foams with superior mechanical properties are Al-3wt.%Sn alloys containing Ti (3, 5wt.%), Mn (5wt.%) or Ni (5wt.%).